Technical Report
TR-16-11
January 2017

Clay erosion – impact of flocculation and gravitation

Ivars Neretnieks
Luis Moreno
Longcheng Liu

SVENSK KÄRNBRÄNSLEHANTERING AB

SWEDISH NUCLEAR FUEL
AND WASTE MANAGEMENT CO

Box 250, SE-101 24 Stockholm
Phone +46 8 459 84 00
skb.se

SVENSK KÄRNBRÄNSLEHANTERING

ISSN 1404-0344
SKB TR-16-11
ID 1549847
January 2017

Clay erosion – impact of flocculation and gravitation

Ivars Neretnieks, Luis Moreno, Longcheng Liu
Department of Chemical Engineering and Technology
Royal Institute of Technology, KTH

Foreword

This report summarises the main findings of the work at KTH, department of Chemical Engineering and Technology in the BELBaR project under the auspices of European Atomic Energy Community's Seventh Framework Programme (FP7/2007-2011). The aim of the report is to present the results in a way that can be used to predict the rate of loss of bentonite clay in buffer and backfill in nuclear waste repositories of KBS-3 type in crystalline rock.

Three self-sustained reports were submitted to the BELBaR project:

1) Bentonite expansion and erosion – Development of a two-region model.
2) Evaluation of some erosion experiments by the two-region model.
3) Release and sedimentation of smectite agglomerates from bentonite gel/sol.

These reports are, with some modifications, appended to the present report as Appendices 1–3. They give the necessary background and details to the present report, which tries to highlight the central findings and presents simple equations in suitable form for practical use. We also try to assess, describe and quantify the uncertainties and suggest ways that could reduce the uncertainties.

Summary

Previous erosion modelling of bentonite clays surrounding copper canisters in KBS-3 type repositories have been revisited in the light of recent experiments in narrow artificial fractures. It was found that the numerical accuracy in earlier modelling was not sufficient to resolve important details in the very narrow rim zone where the smectite turns from an expanding clay to a viscous sol. A two-region model was developed that considerably improves the solution accuracy. This model was tested against experiments and it was found to strongly underestimate the erosion loss. Floc formation and flow as seen in the experiments was not included in the earlier models, because floc formation had not been expected. Introducing rapid floc formation in the two-region model gave excellent agreement at the cost of adjusting one parameter. However, the adjustment was only on the order of a factor of two from the values expected for a non-floc forming sol and is deemed acceptable considering the uncertainties in describing the diffusive properties of smectite particles in expanding clays. This adjusted model, surprisingly, gives erosive losses that differ at most a factor five from earlier modelling results based on other mechanisms.

The observed floc formation led to an additional insight, namely that the flocs sediment rapidly in sloping and vertical fractures. Erosion by floc sedimentation is as rapid or more rapid than that caused by flowing water that carries away flocs in horizontal fractures. The rate of loss of clay by sedimenting flocs in large aperture fractures (> 0.1 mm) seems to be set by the primary release rate of particles from the rim of the clay. In narrow aperture fractures, modelling suggests that the flocs will behave as a fluid, which exerts friction against the fracture walls. Under such circumstances the rate of mass loss will be proportional to the fracture aperture to the power of three. This is expected to strongly limit the loss in fractures narrower than about 0.1 mm. There is a need for additional experimental confirmation of these predictions.

Sammanfattning

Den modellering som tidigare använts for att beskriva erosion av bentonitleran som omger kopparkapslarna i KBS-3 slutförvaret har reviderats baserat på experiment utförda i tunna spalter. Den numeriska noggrannheten för att beskriva processerna i den expanderande tunna övergångszonen mellan lera och vatten var inte tillräcklig bra i föregående modell. En ny metod att lösa ekvationerna baserad på att dela området i två zoner utvecklades och befanns kunna uppnå nödvändig noggrannhet. Denna modell underskattade dock väsentligt erosionen i experimenten. Noggrannare analys av dessa visade att ett fenomen som tidigare inte var känt kraftigt bidrog till att öka erosionshastigheten. De eroderade smektitpartiklarna slår efter att ha frigjorts från leran mycket snart ihop sig i flockar vilka snabbt transporteras med vattnet som strömmar i spalten. När denna oväntade process infördes i modellen erhölls en god överensstämmelse mellan modell och experiment. Detta erhölls dock till priset av att en parameter i modellen måste empiriskt anpassas. I den tidigare modellen erhölls denna parameter från oberoende information. Parametern ändras med upp till storleksordningen en faktor två, vilket bedöms vara acceptabelt i jämförelse med andra osäkerheter. Den modifierade modellen ger förvånansvärt nog inte större skillnader i erosionsförlust än en faktor 5 jämfört med den ursprungliga modellen, trots att modellerna delvis basers på olika processer.

Flockbildning visar sig leda till en ytterligare oväntad effekt, nämligen att flockarna sedimenterar i sluttande sprickor. Erosionen som förorsakas av detta kan vara större än den som förorsakas av strömmande vatten. Erosionsförlust i sprickor med större apertur än 0.1 mm verkar bestämmas av hur snabbt flockar frigörs från leran. I trängre spalter torde flockarna då inte kunna sedimentera så snabbt som de frigörs om de blir så stora att de är i kontakt med väggarna då deras rörelse påverkas av friktion mot dessa. Modellering av detta tyder på att flödet av flocksuspensionen då bör vara omvänt proportionellt mot sprickvidden i kubik. Detta skulle kunna begränsa förlusten kraftigt. Det behöver ytterligare bekräftad av experiment.

Contents

1 Introduction and background

In KBS-3 type repositories at depths of around 500 m in crystalline rock, compacted bentonite clay surrounds copper canisters with high level radioactive spent fuel. Water from the rock is taken up by the clay, which swells and expands to fill any voids in the deposition hole and tunnel. The clay also swells out into any open fractures that intersect the holes and tunnels in the repository. In one of the variants considered the 5 m tall canisters are placed in about 8 m deep deposition holes drilled downward from the floor of the tunnels. In the other variant the canisters are placed horizontally in tunnels. The tunnels are also filled with swelling clay. Should low salinity water with less than a few mM sodium or calcium invade the rock and clay, as can happen during the time glaciers melt and recede, colloidal size smectite particles in the clay can form a sol and flow away. Clay can be lost and the clay buffer's protecting properties can decrease.

Smectite makes up the largest part of the clay mass. This clay mineral is negatively charged and surrounded by cations to assure that the overall charge always is neutral. The smectite particles are very thin coin like sheets, 1 nm thick and 50 to 500 nm large. The cations that are bound by electrostatic forces attract water and force the particles apart as water is sucked in by osmotic forces to dilute the ion concentration between sheets. Very large, many MPa, repulsive forces develop. The smectite clay swells into fractures taking up more water and forcing the particles further and further apart until they form a stable sol. When the ion concentration is larger than a few mM the smectite particles do not form a sol but form a gel from which no particles are released. In low ionic strength sodium-dominated water such clays can expand forever in horizontal fractures where they are not impeded by gravity in upward expansion or potentially pulled down by gravity, increasing loss.

For calcium dominated clays agglomerates with typically 10–20 sheets are found (Segad et al. 2010). The lengths and widths of the agglomerates may also be larger and can be more than 1 000 nm (1 micrometre). These particles still have colloidal or near colloidal size and do not readily form sol so particles are not released to seeping water by sol formation. The above description gives a simplified overview of some of the most important properties that will be treated in the following. More detailed descriptions can be found in Birgersson et al. (2009) and Neretnieks et al. (2009).

In earlier studies a dynamic clay expansion model was developed by which the rate of expansion can be predicted. It accounts for how the swelling pressure depends on particle charge, size, volume fraction smectite, ion concentration and on how the velocity of the particles that are forced apart are restrained by friction against the water into which they expand. The sol that forms has a much higher viscosity than water. The viscosity is strongly influenced by the volume fraction smectite in the sol. The expansion/solubilisation/flow model is also coupled to a model that accounts for the ion exchange between the pore water in the clay and that in the seeping water in the fractures. This model was used to simulate the expansion and solubilisation of smectite in fractures with seeping water. The model simultaneously solves a number of coupled partial differential equations, PDE's by a finite element solver (Moreno et al. 2010, 2011). It was found that the continuous ion exchange could be neglected because at the rim, where the expanding clay turns to sol, the ion concentration becomes essentially the same as that of the approaching water. Even so, the very nonlinear PDE is difficult to solve with high accuracy with finite element or other discretization methods because the location of the rim constantly moves and the rim-zone, i.e. where the solubilisation and onset of sol flow occurs is very thin compared to the region that needs to be modelled to follow the expanding clay. It was realised that large and even very large errors in the expansion and loss of clay could result.

Therefore another solution method was developed which divided the entire region into two, the expanding clay region and the rim region. The latter was, using some simplifying assumptions, solved by a technique that can resolve the details in the rim zone with very high accuracy. The rim region model is then used as a boundary condition to the expanding clay region. The latter is solved using a technique that starts with a very small region, which is allowed to expand depending on how much clay enters from the deposition hole and how much is simultaneously lost at the rim region. It can be visualised as an expanding system in which nothing exists beyond the rim zone. This model gave quite different results from the original one, Appendix 1. This model was used to simulate a

series of laboratory experiments in which a compacted clay tablet was allowed to expand into a 1 mm aperture slot in a transparent equipment where the expanding clay could be observed and where the loss of clay by erosion could be measured over time and at different chemical and hydrodynamic conditions. The model predicted the expansion of clay well into stagnant water but grossly underestimated the rate of erosion under flow conditions. Inspection of the pictures taken of the expanding and eroding clay showed that the sol that formed at the rim very quickly formed agglomerates (flocs) that flowed downstream with the same velocity as water. There seemed to be no viscosity increase of the water containing the flocs as would be the case if the sol were stable and did not agglomerate. The flowrate and velocity of the agglomerate fluid (AF) is thus much larger than what the sol model predicts.

The flocs are voluminous and contain a low volume fraction of smectite particles. Although such behaviour has been observed earlier and speculation about the reasons have been discussed, only recently it has been firmly established that the edges of smectite particles, even at near neutral pH, are positively charged (Hedström et al. 2016). This leads to edge to face attraction and formation of loose, space filling structures. The formation of such flocs is promoted by the presence of velocity gradients, such as exist in narrow fractures, which make the flat particles rotate and come in contact with each other. These observations lead to a modification of the model. As the small flocs flow with the water the impact on AF viscosity was assumed to be negligible. This implies that when the particles are released from the rim the sol quickly turns to AF and carries the particles away with the velocity of water. The two-region model was modified accordingly. The model then is simplified but an important questions arises, namely how does the rapid floc formation influence the preceding sol formation, i.e. the release rate of particles at the rim. In the rim model without floc formation the release rate is determined by the smectite expansion model, which is formulated as a diffusion model with a diffusivity that is strongly influenced by the volume fraction of smectite and by the ion concentration. The diffusivity spans over three orders of magnitudes at least in the region of interest. When the sol is stable the smectite particle diffusivity can be calculated by the model, which at the same time gives the volume fraction at which the sol can start to flow according to the viscosity model. This volume fraction lies in a range about 0.3 to 1 volume % smectite in water depending on the ion concentration. Simulations with these data did not give a sufficient increase in erosion compared to the experiments. However, using a volume fraction of 1.5 % for all experiments irrespective of flow velocity and ion concentrations gave a surprisingly good agreement (Appendix 2). In addition it results in a very simple expression for determining the loss at the rim. This is presented in Section 2.1 and will be the basis for simulation of smectite loss for PA conditions later in this report.

In the above description and modelling no account is taken of gravity effects. This is because it was found that in stable sols gravity has a negligible effect (Neretnieks et al. 2009). However in the simulated fracture experiments mentioned above it was seen that when the fracture was turned vertical the flocs sedimented and new flocs were released from the expanding clay. The erosive loss was comparable to or larger than that in the horizontal fractures (Schatz et al. 2013). These observations led us to do an explorative study of the fate of sedimenting flocs and a study of the maximum rate of the transport of smectite by flocs in narrow fractures (Appendix 3). A simple model was devised that accounts for the sedimentation rate of small floc particles in a fluid in a fracture. The model also gives the sedimentation velocity of large flocs in contact with the wall. This applies to cases with sodium-dominated clays that form flocs. In calcium dominated clays, even in deionised water, flocs are not observed. Instead it seems that heavy stacks form that may in turn agglomerate to even larger dense particles of up to a few tenths of mm size, which rapidly sediment. These particles can also be released from expanding calcium dominated clay and they sediment rapidly in inclined or vertical 1 mm aperture fractures. These phenomena are described in Chapter 3.

Questions have been raised about how wall friction in the fractures is accounted for. Below is a short description about how this is done.

Wall friction is accounted for by not allowing the *paste* in the deposition hole to be pressed into the fracture more than the short distance determined by the balance between wall friction and intrusion force. The intrusion distance is about 2-3 times the aperture of the fracture.

The clay expansion into the water starts at the tip of the extruded paste. This expansion is modelled by the expansion of the clay by the extremely strong osmotic forces sucking water in between the particles that drive them apart. The size of the colloid particles is much smaller than the aperture of fractures. The "swelling" of the montmorillonite, MMt, can be conceived as a diffusional mixing between the MMt and water, although the forces are partly different. There is no *net* movement of the fluid (the mixture of smectite and water). It is only a dilution process. Where an MMt particle vacates a space an identical volume of water replaces it *moving in the other direction*. No pressure gradient driving the fluid into the fracture results. The appendix in Neretnieks et al. (2009) describes the difference between forcing slurry/paste flow through a narrow conduit by a pressure gradient and the dilution of the MMt slurry.

Friction is again accounted for to determine the flow resistance of the expanded clay in the fractures, which is subject to a hydraulic gradient driving the water seepage in the fracture. Flow of the expanded clay essentially stops where the volume fraction of smectite is above about 1 %. Below 1% the viscosity of the sol drops from very high to that of water with decreasing volume fraction smectite.

The floc slurry viscosity immediately after formation is the same as that of water based on observations of its flow. However, as flocs grow the sedimented and compacting agglomerate is *expected* to become increasingly more viscous with time. At present its viscosity is unknown. It is, however, shown that a high viscosity of the aging floc agglomerate can strongly reduce the rate of erosion. Flocculation has not been observed in the expansion experiments without water.

2 Expansion and erosion without gravity effects

2.1 Modelling loss at rim accounting for flocculation

In Appendix 1 it is shown that when the sol or slurry viscosity is not influenced by the presence of colloid particles and when the volume fraction of smectite at the border of the rim ϕ_R is known the smectite loss at the rim can be calculated by the simple expression

$$N_{rim} = \rho_s \, \delta \, \phi_R \frac{2}{\sqrt{\pi}} \sqrt{D_R \, x \, u_o} \tag{2-1}$$

D_R is the diffusion coefficient for smectite particles *at the rim*, u_o is the approaching water velocity, ρ_s the smectite particle density. For flow past one side of a cylinder $x = \pi r_R$. As the water flows around both sides of the cylinder the total loss rate will be

$$N_{erosion} = 2N_{rim} = \rho_s \delta \, \phi_R \frac{4}{\sqrt{\pi}} \sqrt{D_R \, \pi r_R \, u_o} \tag{2-2}$$

D_R is obtained from the diffusivity function for smectites and depends on particle size, surface charge density and ion concentration. When there is floc formation ϕ_R was found to be around 0.015 by comparison with a number of laboratory experiments. This is thus an empirical parameter and is somewhat larger than what is expected for stable sols. Values slightly below 1 % are predicted when there is no floc formation Appendix 1.

This very simple expression has previously been used to assess the loss of solutes such as radionuclides from the interface between seeping water at the water/ clay interface (Neretnieks et al. 2010). In those cases neither the water velocity nor the diffusivity is influenced by the solute concentration. ϕ_R in those cases represents the solute concentration at the interface.

Note that the length of the rim changes with time as the clay expands out into the fracture. The above relation must therefore be coupled to the expansion model. This is described in Section 2.4. First, however, in the following section we briefly discuss how the diffusion coefficient D in general and at the rim D_R especially is influenced by the smectite volume fraction and the (sodium) ion concentration.

2.2 Diffusivity

The smectite clay expansion and sol formation can be described by a diffusivity function that can be used to model expansion of the clay as if it were molecular diffusion. For details please consult Liu et al. (2009a) and Neretnieks et al. (2009). The diffusivity function plays an important role in the modelling. Note in Figures 2-1 and 2-2, that at low sodium ion concentrations the diffusivity is essentially constant and around 0.3×10^{-9} m^2/s for all volume fractions in the region of the plot. For concentration c_{ion} = 1 mM at a volume fraction 0.015 it drops by about a factor of 5. For c_{ion} = 10 mM it drops by more than 3 orders of magnitude. This implies that the loss at the rim will drop very much with increasing ion concentration according to Equation (2-2). In practice, gel forms at around 4 mM and no particles are then released (Birgersson et al. 2009, Neretnieks et al. 2009, Hedström et al. 2016, Schatz and Akhanoba 2016).

For volume fractions above 0.1 the diffusivity remains constant at around 0.3×10^{-9} m^2/s. In the source i.e. the deposition hole the volume fraction is around 0.6. In the expansion model of the clay in the fracture the diffusion coefficient is essentially constant from volume fraction 0.1 to 0.6 for the entire range of ion concentrations considered here. It will be shown later that using a constant value for the entire range 0.015 to 0.6 for *expansion* modelling gives negligible errors. However, for the *rim loss modelling* it is essential that the diffusion coefficient for the condition at the rim as influenced by ion concentration is accounted for at a volume fraction 0.015.

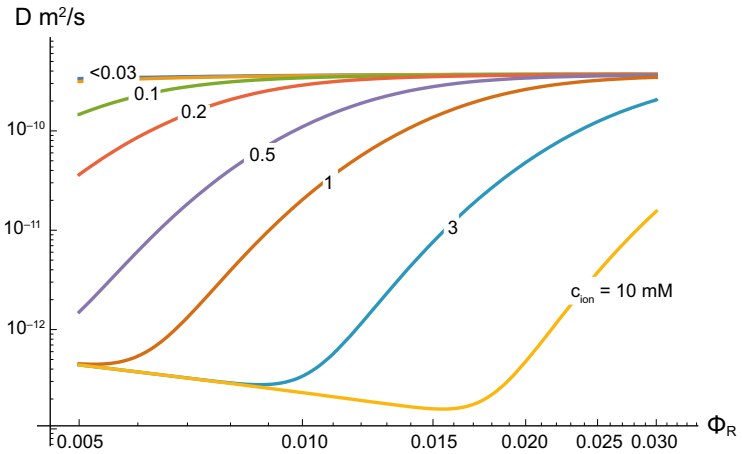

Figure 2-1. *Diffusivity function influenced by volume fraction and sodium ion concentration. Smectite diam. 200 nm*

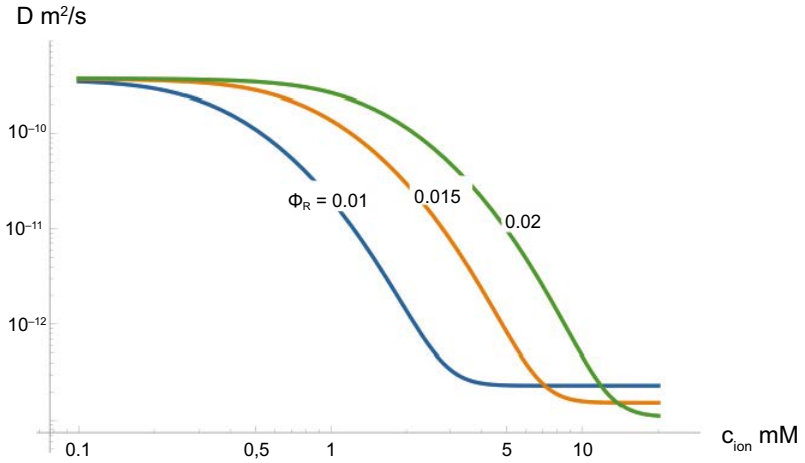

Figure 2-2. *Diffusivity function influenced by sodium ion concentration and smectite volume fraction around ϕ = 0.015. Smectite diam. 200 nm.*

2.3 Modelling expansion of clay accounting for loss at rim

The clay paste that expands into the fractures is extremely viscous and is not mobilised by the pressure difference (hydraulic gradient) from one side to the other of the extruded clay in the fracture. In a fracture that intersects the deposition hole or tunnel perpendicularly the expanding clay has a circular section with an inner radius r_i equal to that of the hole or tunnel and an outer radius $r_R(t)$, which grows with time. The latter is called the rim. At the rim the smectite particles diffuse out into the water seeping past the rim and are carried away. The rate of loss at the rim is described by Equation (2-2). The rate of expansion is calculated by solving the diffusion equation accounting for the diffusion coefficient that changes as the volume fraction decreases with the radius. All the time, the changing (increasing) loss at the rim is accounted for when solving the diffusion equation, which is a partial differential equation. This is the essence of the two-region model described in detail in Appendix 1. The rigorous solution of these coupled equations is done by a numerical technique that can be time consuming. Therefore, in addition to the numerical solution a simplified technique was also developed. This results in an analytical expression for the time derivative of $r_R(t)$. This ordinary differential equation, although nonlinear is readily integrated numerically to obtain $r_R(t)$. The solution also gives information on the rate of loss at the rim over time and of the smectite mass that resides in the fracture. Thus also the rate of loss from the source over time is obtained. This model is called the pseudo steady state, PSS, model because it uses the approximation that the smectite volume fraction profile in the expanding clay does not change shape and can be described by the profile that will be attained at steady state, SS, i.e. when the influx from the source (hole) is equal to the loss at the rim.

2.4 Examples

The main issue in this report is when the ion concentration in the seeping water is below the critical coagulation concentration CCC of sodium, which is the most common ion in the clay as well as in the groundwater. The CCC is about 4 mM (Birgersson et al. 2009, Neretnieks et al. 2009, Hedström et al. 2015, Schatz and Akhanoba 2016).

We chose 1 mM as a central case as this is around the observed value for glacial melt-water at Grimsel in Switzerland. More dilute water, 0.1 mM, is also used. The range of water velocities spans three orders of magnitude from 10^{-7} to 10^{-4} m/s. The fracture aperture is taken to be 0.1 mm in the examples.

In these examples gravity effects are not accounted for. That will be discussed in Chapter 3.

First, for illustration, some results for a case with 1 mM sodium and water velocity 10^{-5} m/s (315 m/year) is presented. Figure 2-3 shows how the radius to the rim expands over time for a deposition hole with radius $r_i = 0.925$ m where the volume fraction of solids, modelled as smectite, is $\phi_i = 0.574$. After about 200 years steady state would be reached with $r_R = 2.4$ m. The dashed line is used for the PSS solution and the full line for the considerably more complicated numerical solution.

The loss rate at the rim is shown in Figure 2-4. It stabilizes at 30 g/year.

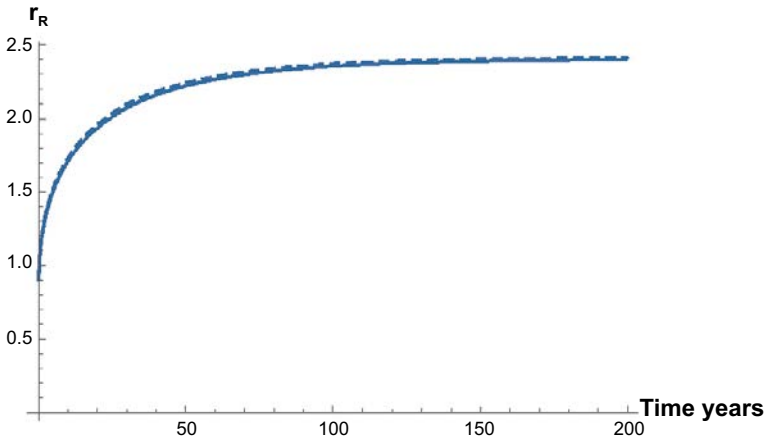

Figure 2-3. *Expansion of rim over time. $u_o = 10^{-5}$ m/s, $c_{ion} = 1$ mM. Full line numerical solution, dashed line PSS solution.*

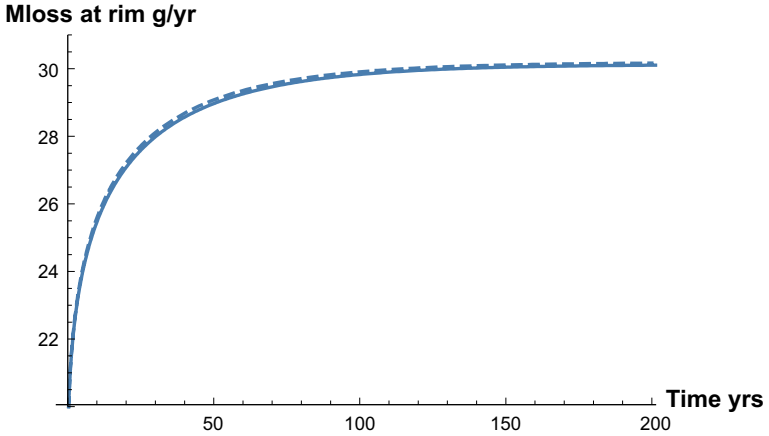

Figure 2-4. *Loss rate at rim as function of time. $u_o = 10^{-5}$ m/s, $c_{ion} = 1$ mM. Full line numerical solution, dashed line PSS solution.*

Table 2-1 summarises the results for the central case with c_{ion} = 1 mM for the entire velocity range and exemplifies results for velocity 10^{-4} m/s and c_{ion} = 0.1 mM and 4 mM. The table also shows the approximate time to reach SS, the radius at SS and how the PSS and the numeric solution differ. The entity N_{Rim}^{DL} is a dimensionless number describing the loss. It depends on ion concentration and smectite properties but is independent of water velocity and length of rim $N_{rim}^{DL} = \int_0^\infty \frac{\phi(z)}{\eta_r(\phi(z))} dz$. See Equation A1-42 in Appendix 1. It accounts for the combined change of volume fraction $\phi(z)$ and viscosity η_r ($\phi(z)$) in the rim zone as functions of dimensionless distance z from the rim. A case for c_{ion} = 10 mM and 10^{-7} m/s is included to show that the clay expansion and thus the loss of clay from the hole would continue "forever" also when there is very low flow and very small loss at the rim. The results show that the simple PSS solution is quite accurate compared to the "exact" numerical solution. More results are given in Table 2-2 for c_{ion} = 0.1 mM when a comparison is made with earlier results.

Table 2-1. Overview of results influenced by ion concentration and water velocity in 0.1 mm aperture fracture.

c_{ion} mM	u_o m/s	$N_{Rim}^{DL} \times 10^5$	t_{SS} year PSS and Num	r_{SS} m PSS/Num	N_{SS} g/year PSS/Num
0.1	10^{-4}	510	10	1.2/1.2	108/107
1	10^{-4}	314	20	1.4/1.4	71/71
1	10^{-5}	314	200	2.4/2.4	30/30
1	10^{-6}	314	5000	6.3/6.1	15/15
1	10^{-7}	314	40000	23/22	9/9
4	10^{-4}	41	1000	4.9/4.8	18/17
10	10^{-7}	10.7	Extremely long	3200/–	Extremely small

Table 2-2. Comparison with earlier results from Table 9-2 in Moreno et al. (2010). Old values reduced by factor 10 to represent results for 0.1 mm aperture fracture. c_{ion} = 0.1 mM.

Water velocity m/s	Smectite loss by erosion g/year at SS New/Old	Penetration distance into fracture (r_R–r_i) m at SS New/Old
10^{-8}	7.4/1.6	55/18.5
10^{-7}	11.4/4.3	10.6/7.0
10^{-6}	20.3/11.7	3.1/2.1
10^{-5}	55/29.2	0.9/0.5

Figure 2-5 shows how the loss rate at the rim would increase with water velocity for a given rim radius if the clay had expanded to a certain radius before water started to flow. The circles indicate the SS radius of expansion for a given velocity. If the starting radius is smaller than that at SS when water starts to flow, the clay would expand. Otherwise the radius would decrease to the SS radius. The latter could occur under conditions where clay has expanded into a fracture under low-flow or more saline conditions with small erosion, followed by high flow and low salinity during e.g. a receding ice age.

Figure 2-6 shows the accumulated mass loss over time at the rim, the dashed line, and that lost from the hole including the mass that resides in the fracture, the full line. At high velocity (left frame) they are very similar but differ considerably at low velocity (the right frame), which is expected because steady state has not been attained yet.

Figure 2-7 shows that over very long times, 100000 years, considerable amounts of clay is lost by intrusion into the fracture even at ion concentrations above the CCC in which case there is (practically) no erosion at the rim.

Considering the differences in the underlying physics, flocculation was not invoked in the old model, and that the old model did not resolve the details of the conditions in the rim zone accurately the differences are surprisingly small.

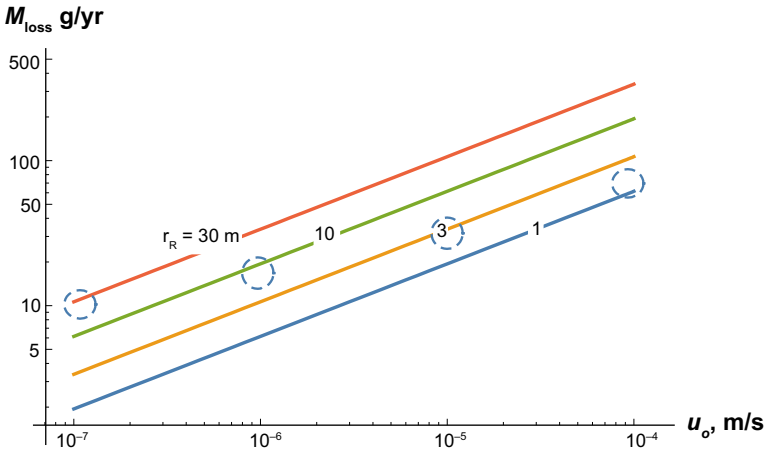

Figure 2-5. *Loss rate at rim at SS as a function of water velocity for different rim radii for c_{ion} = 1 mM. Circles show SS conditions.*

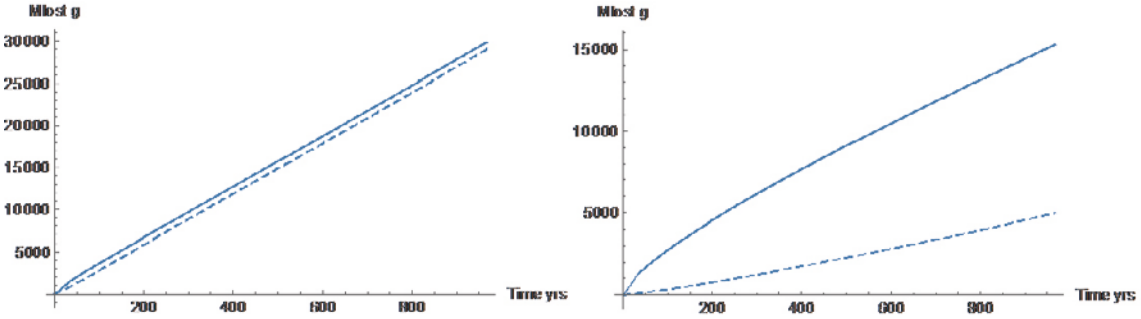

Figure 2-6. *Accumulated loss as function of time. c_{ion} = 1 mM. Dashed line lost at rim, full line lost from deposition hole i.e. including mass residing in fracture. Left figure $u_o = 10^{-5}$ m/s, right figure $u_o = 10^{-7}$ m/s*

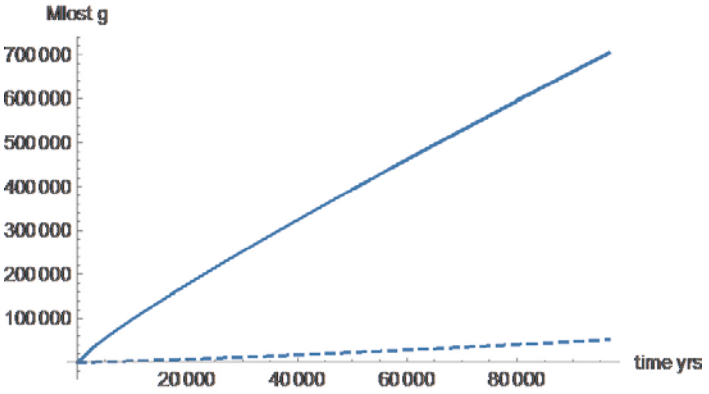

Figure 2-7. *Loss from deposition hole as a function of time. c_{ion} = 10 mM. $u_o = 10^{-7}$ m/s. Dashed line lost at rim, full line lost from deposition hole i.e. including mass residing in fracture.*

2.5 Sensitivity to some key parameters

One of the key entities in the model is the value of the volume fraction at the rim at which smectite colloids are released. The value $\phi_R = 0.015$ was obtained as a fitted parameter to laboratory experiment. It cannot be assumed that it will be independent of the type of clay used. Should ϕ_R be 0.01 instead, it will influence the loss at the rim as shown in Equation (2-2) by lowering it by one third.

A lower value for ϕ_R will also for c_{ion} = 1 mM decrease the diffusivity at the rim by nearly an order of magnitude as can be seen in Figure 2-1. Again, using Equation (2-2) this will further decrease the loss by the square root of 0.1, i.e. by 0.3. In total this would decrease the loss by 80 % for a given length of rim. This is partly counteracted by the increase of the rim length, which increased the loss at SS. For a lower ion concentration the decrease will be less. Other factors that influence the results stem from the model that generated the diffusivity function itself. In that model the surface charge density and smectite particle size (side length) enters and these differ between different bentonites. An additional uncertainty lies in the choice of fracture aperture. In all there may be considerable uncertainties in predicting what loss to expect. A further uncertainty lies in assessing the fate of the lost material and the impact of gravity. This is discussed next.

3 Impact of gravity

3.1 Some observations

Floc formation and sedimentation in test tubes as well as in narrow slots was described in Neretnieks et al. (2009). Schatz et al. (2013) in a series of systematic experiments on erosion in horizontal fractures documented floc formation in sodium dominated systems with ion concentrations below CCC. When the fractures were turned vertical very soon generation and sedimentation of flocs occurred. They settled at the bottom of the fracture. Figure 3-1 shows an example of release and sedimentation of flocs. This figure also shows the release of streams of particles in a vertical fracture. It is also seen that somewhat below the source the particles seem to form a denser phase, from which again streams of particles are released. Further details can be found in Appendix 3.

Figure 3-2 shows other examples, in this case in a fracture with 45-degree slope for purified smectite as well as for a natural bentonite.

One interesting observation is that the sediments settle at the bottom of the slit in the form of triangular heaps with an angle of repose of 15 to 45 degrees (possible friction angle). The settled sediments seem to widen as seen by the changing angle of the slope. This indicates that a friction angle of the sediment has not been reached, if there even is one. It cannot be ruled out from the present information that the sediment behaves like fluid and that the heaps would flow out sideways, given time.

The loss rates were determined to be in the range 850 and 1 550 kg/m^2/year in different experiments where the area is the aperture times the circumference of the source. A 2 m diameter source in a 0.1 mm aperture fracture would give a loss rate of 50 to 100 g/year. The experiments in 0.1 mm and 1 mm aperture fractures suggest that the loss is proportional to the aperture in this range of fracture apertures. Such experiments are shown in Figure 3-3. It may be noted that in the 1 mm aperture fracture the flocs seem too small to touch both walls but there are many of them. In the 0.1 mm aperture fracture the flocs are larger and fewer and seem to tough the walls very soon after they have formed. We interpret this to be caused by agglomeration of the smaller to larger flocs that are in contact with fracture walls in the narrow fracture and cannot move as independently as they can in the 1 mm fracture. This can have an important impact on the rate of release and sedimentation of flocs especially in narrow fractures.

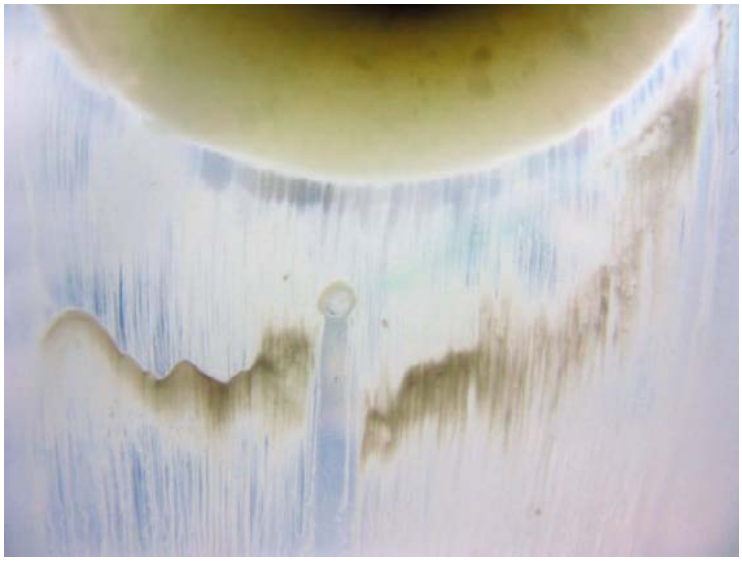

Figure 3-1. *Close-up picture of sedimenting agglomerates in de-ionised water. The cylindrical region is 2 cm in diameter. Figure 59 in Schatz et al. (2013).*

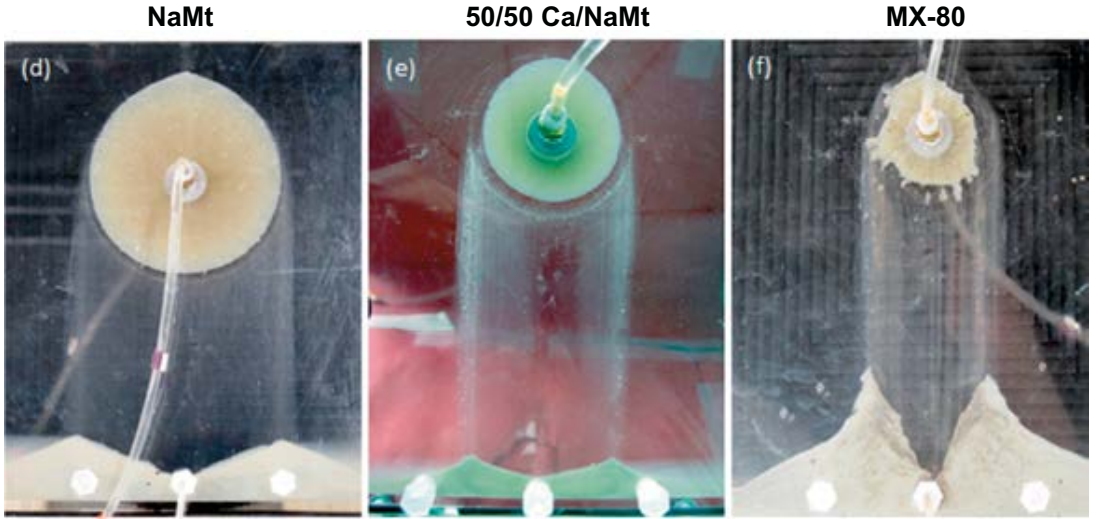

Figure 3-2. *Sedimentation and settling of flocs in a 45-degree sloping fracture of three different clays in 1 mm aperture fractures. Figure 3-3 in Schatz and Akhanoba (2016).*

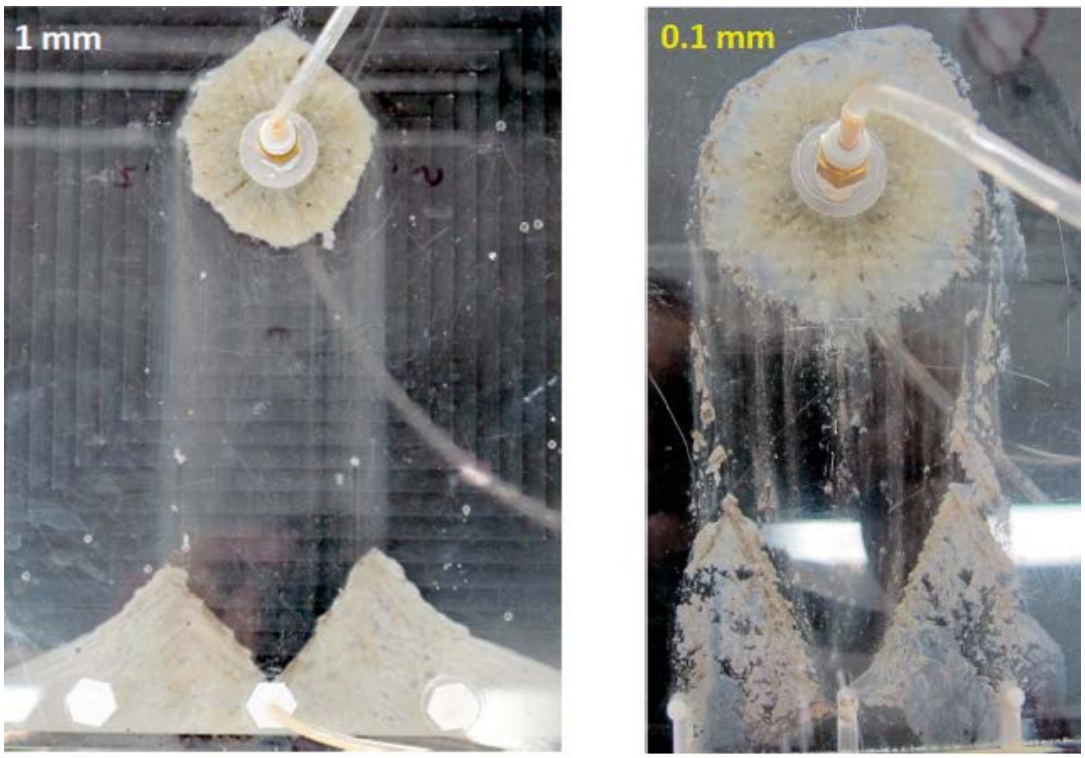

Figure 3-3. *Impact of fracture aperture on sedimentation. Figure 3-23 in Schatz and Akhanoba (2016).*

3.2 Estimation of maximum loss rate

The maximum rate of loss from the source will depend on the rate of release of smectite at the clay water interface on the one hand and on the rate at which the primary release can be transported away in the fracture.

It is assumed in our model that the flocs when released from the expanding clay are small spherical particles with density ϱ_{sph} and radius that is less than or equal to half the fracture aperture and that they form "strings of pearls". See Figures 3-1 and 3-3, left frame. These "strings of pearls" can be close together so that the water is well filled with spheres. The spheres are pulled downward by gravity. For laminar flow the sphere velocity can be approximated by Stokes law if they are far apart.

We use this approximation also when the water is well filled with spheres, accepting the errors, for these bounding calculations. The maximum rate of mass loss $N_{release}$ from a source that has expanded the gel/sol to a width W_{AF} in a sloping fracture is attained when the diameter of the sphere is equal to the fracture aperture (Appendix 3). Note that this is the maximum rate of release as it is assumed that the next sphere is released as soon as the previous has moved away and that the streams of spheres are touching each other. Furthermore, in this maximum release case it is assumed that the diameter of the released spherical agglomerate is the same as the fracture aperture. Then the maximum release rate is given by

$$N_{release} = \frac{\pi\delta^3}{108\mu_W}\left(\varrho_{sph} - \varrho_W\right)g\phi_R\varrho_S Sin(\alpha)W_{AF} \quad (3\text{-}1)$$

δ is fracture aperture, μ_W water viscosity, ϱ_{sph} and ϱ_W density of the spherical agglomerate and water, respectively, g is the gravitation constant, ϕ_R is the volume fraction of smectite in the agglomerate, ϱ_s density of smectite mineral and W_{AF} the width of the source. α is the slope of the fracture from horizontal. Equation (3-1) is probably quite conservative because the number density (number per m^3) of the released spherical agglomerates as well as the size of the spheres is taken to give the largest release rate. As soon as a particle is released and has moved one diameter, a new particle can be released. This probably considerably over-estimates the rate of release from the rim. In Chapter 4 it is shown that the assumptions of the temporal release frequency (how rapidly a new sphere" can be released after the previous) and the spatial density of release locations strongly influence the maximum rate of release of smectite. We have found no method to estimate this from first principles. It must be assessed from experiments.

If it is assumed that the released agglomerates have a constant size, smaller than the aperture, the mass release rate would be proportional to the fracture aperture and to the diameter of the agglomerate to the second power.

$$N_{release} \propto r_{sph}^2\, Sin(\alpha)\delta W_{AF} \quad (3\text{-}2)$$

We anticipate that it is difficult to quantify the release frequency and the size of the primary released flocs from first principles. So far only overall release rates N_{Exp} have been measured in sloping fractures (Schatz and Akhanoba 2016). The results suggest that the release rate is proportional to the area of interface between the clay and the water, i.e. proportional to $\delta \times W_{AF}$ as in Equation (3-2).

Should the released agglomerates join to form larger flocs and these touch the wall and sediment as an agglomerate fluid, AF, restrained by friction against the walls of the fracture. It is seen in Figures 3-1 and 3-3, right frame that in a narrow fracture the small flocs agglomerate to large sheets that are in contact with the fracture walls. Then the largest transport rate away from the source is

$$N_{sed} = \frac{\delta^3}{12\mu_{agg}}\left(\varrho_{agg} - \varrho_W\right)g\phi_R\varrho_S W_{AF} \quad (3\text{-}3)$$

μ_{agg} and ϱ_{agg} are the viscosity and density of the AF respectively

The width of the source W_{AF} will depend on how far the rim expands before it stabilises. The rate of supply of clay into the fracture at steady state, SS, i.e. when the rate of loss at the rim is equal to the rate of intrusion is (Appendix 1)

$$N_{in} = D_i 2\pi\varrho_s\delta\frac{\phi_i - \phi_R}{ln(\frac{r_R}{r_i})} \quad (3\text{-}4)$$

At SS, when $N_{in} = N_{release}$ the radius to the rim $r_R = W_{AF}/2$ can be determined.

The maximum rate of transport *away* of the smectite is proportional to the width of the source and to the third power of the aperture according to Equation (3-3). The results from the two experiments in Figure 3-3, however, suggest only a linear dependence on the aperture. We speculate that this may be due to that in the 1 mm experiment the primary release rate is limiting and that the restrictions by the presence of the wall will only begin to act at apertures around and below 0.1 mm. The pictures are suggestive in the sense that in the narrow aperture the "blobs" are much larger than the aperture.

3.3 Limitations of smectite loss due to wall friction of agglomerate fluid

When the smaller flocs have joined to form the AF the sedimentation rate is restrained by the friction against the walls of the fracture. Equation (3-3) can be used to assess the loss rate. This is discussed in more detail in Appendix 3. Should the mass sedimentation rate of the AF be smaller than the rate at which the primary flocs can form the AF would build up to the level to the source and set a limit to the loss rate. It is then straightforward to estimate how the expansion of the clay from the source will eventually be balanced by the loss by sedimentation. The expansion is modelled in the same way as was described in Section 2.3 and can be determined by Equation (3-4). Figure 3-4 illustrates the expansion of the source and loss in the rim zone by sedimentation. It also illustrates that larger sedimenting particles can catch up with smaller and form larger particles that touch the walls of the fracture

Figure 3-5 illustrates at what rate the smectite, once it has formed agglomerate fluid "blobs" could be transported away according to Equation (3-3). The transport rate is very sensitive to the aperture and it is inversely proportional to viscosity of the agglomerate fluid. It was found earlier that when flocs formed under flowing conditions they seemed to move as readily by the water as the water itself. It was then concluded that at very early times after agglomeration the viscosity was essentially as that of water. However, it is likely that the viscosity of the agglomerate fluid will increase with time (Angelini et al. 2014). If the viscosity increase is large the transport rate will decrease considerably. The migration rate of the AF will put an upper bound on the loss of smectite from the deposition hole. Clearly, narrow fractures and narrow portions in variable aperture fractures will strongly impede the flow of the agglomerate fluid. Figure 3-5 illustrates how the loss rate is influenced by aperture and agglomerate viscosity for a case when the volume fraction in the flocs is $\phi = 0.01$, which gives the density of the flocs $\varrho_{agg} = 1\,017$ kg/m^3.

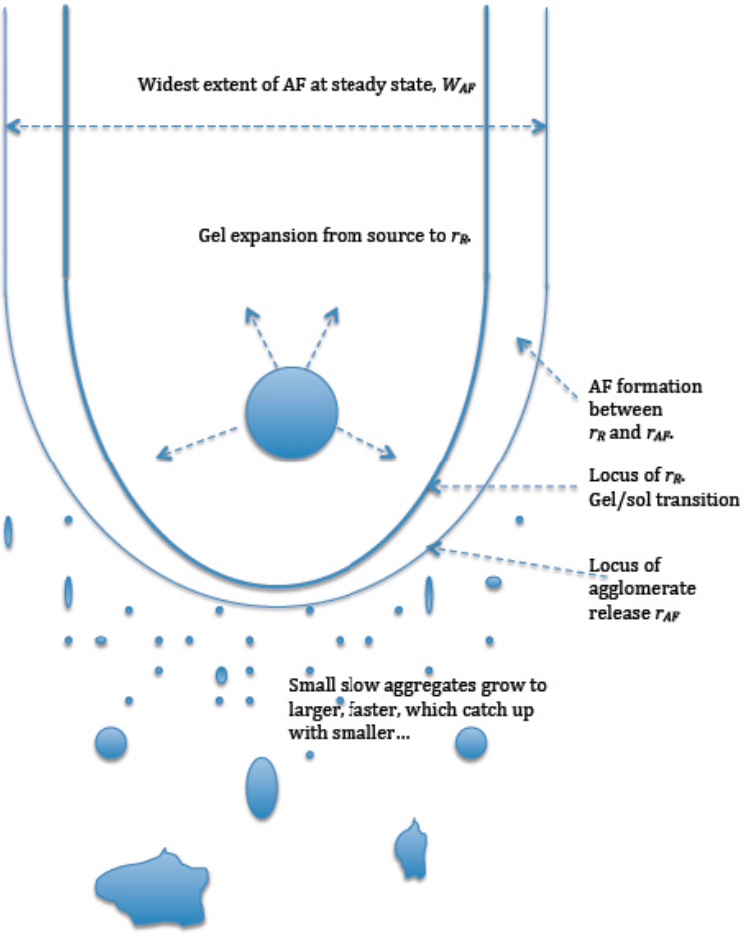

Figure 3-4. *Smectite gel expands in all directions in a vertical fracture and releases agglomerates, which sediment from a boundary at r_{AF}.*

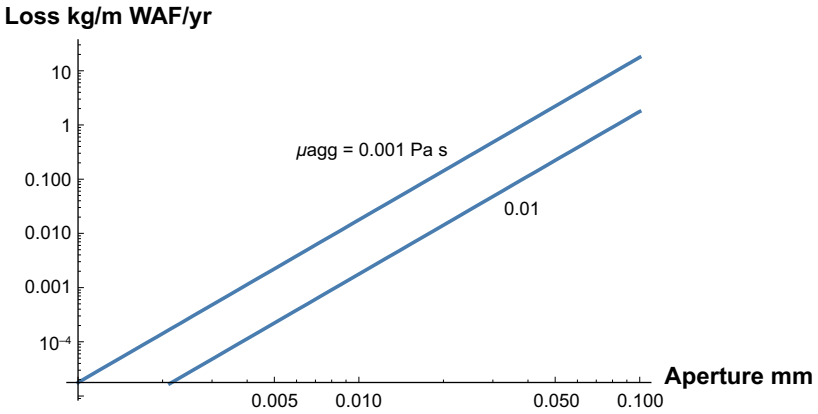

Figure 3-5. *Rate of loss per m width of source N_{smec}/W_{AF} for agglomerate viscosity as water (0.001 Pa s) and for a 10 times higher value.*

The above-described loss is for flocs formed from sodium-dominated clay at ion concentrations below CCC. Calcium dominated clays even in deionized water do not flocculate in the same way. They form denser particles that sediment rapidly. In fact in attempts to measure calcium bentonite slurry viscosity the particles sedimented out of the slurry and viscosity measurements of the slurry were not possible (Birgersson et al. 2009). The particles are released from expanding clay in the same fashion as the above-described sodium dominated clays however (Schatz and Akhanoba 2016).

3.4 Fate of the sediments

It is seen in Figures 3-2 and 3-3 that the sediments form triangular heaps at the bottom of the fractures. The slope decreases with the width as the sediment heaps grow. This suggests that a final constant slope has not yet been attained and that the sediment so far may behave as a viscous fluid. The sediments contain smectite as well as accessory minerals, which are uncharged particles larger than those of the smectite. It is anticipated that in real variable aperture fractures the accessory minerals will clog the narrow parts of the fractures. This can potentially build up a filter of the accessory mineral particles, which will increasingly hinder the escape of the smaller smectite particles. This has been observed in experiments in replicas of variable aperture fractures (Reid et al. 2015).

In contrast, calcium dominated sediments seem to stabilize at a friction angle of about 45-degrees as is shown in Figure 3-6.

Figure 3-6. *Artificial fracture test with calcium montmorillonite sample using deionized water flowing at ~ 0.09 ml/min; fracture aperture was 1 mm and fracture slope angle was 90°. Image taken 644 h after start of test. Part of Figure 3-10 in Schatz and Akhanoba (2016).*

When there is a friction angle, any fracture in a fracture network, which has a smaller angle than the friction angle cannot carry the sediment further. In a rock with random orientation of fractures further transport would tend to stop after not very many intersections. Furthermore real fractures in rock have variable aperture and the particles in the sediment will have to negotiate their way in complex paths that widen and close and move left and right in channels that often have lower slopes that the friction angle because the winding channels in a sloping fracture will have at most the slope of the fracture itself, like that of a slalom trail on a slope.

For sodium dominated AF that could continue to move, the volume of rock affected would be considerable as the following example shows. If we consider a rock with a fracture network with a porosity 10^{-4}, 100 kg of clay slurry with a volume fraction of 0.01 smectite will fill 38 000 m^3 rock. A cone section of rock with 45° slope below the deposition hole would be 33 m tall and have a bottom radius of 33 m.

Experiments are needed to further explore the mobility of slurries and agglomerate fluids in variable aperture fractures.

4 Simple analytic expressions to estimate smectite loss for PA purposes

4.1 Overview

In PA calculations fast and simple expressions that can be used in stochastic simulations are desired. In SR-Site a simple expression was used that gave the steady state loss from the time when low ionic strength water intrudes. This was deemed reasonable as the model predicted extrusion into the fracture to be quite limited and would reach a steady state loss rapidly. Intrusion into fractures under non-glacial conditions was not accounted for. Flocculation and loss by sedimentation was not addressed in the model.

The present model predicts that the clay can expand far into the fractures also when the groundwater has higher ion concentration than glacial waters do. During this period no erosion occurs at the rim, i.e. the water-clay interface. The loss over time can be expressed by a simple expression. When glacial water intrudes erosion at the rim starts. The distance to the rim can continue to increase or it can recede. Eventually a SS loss rate is reached when the rate of intrusion into the fracture and the rate of erosion become equal. The SS loss rate during this period can be described by two simple expressions. One erosion mechanism is that caused by flow and one for erosion caused by floc formation and sedimentation. The total loss from the deposition hole after the glacial cycle is the sum of that during the non-glacial period and those caused by flow and sedimentation.

The simplifications used in deriving the two simple equations and in applying them as described above introduce some errors, mainly because the changes during the transient periods are neglected. These are discussed when describing the simple expressions.

The following procedure is proposed. For a given scenario when the duration of the non-glacial and the glacial water periods are set, for each canister position where the fracture aperture, water velocity, fracture angle, and ion concentration are known

1. Calculate the loss of clay by expansion into the fracture for the non-glacial period, Equation (4-3).
2. Calculate the loss due to erosion by flow Equations (4-4, 4-5, 4-6 and 4-7).
3. Calculate the loss due to erosion by sedimentation, Equations (4-11, 4-10 and 4-8).
4. Total loss is sum of those above for the entire glacial cycle.
5. The procedure can be repeated for following glacial cycles.

4.2 Derivation of approximate expressions for clay loss

We first revisit the most important equations and show how they are further simplified for use in PA calculations. Some discussion on errors induced is also presented. The core of the present expansion and erosion model accounts for loss from the deposition hole by clay intrusion into the fracture and by loss of smectite by erosion at the rim of intruded clay at the outer boundary at radius r_R.

4.2.1 Non-glacial period

In the section below we consider a scenario where, at first, after closing and resaturation of the repository the groundwater has salinity c_{ion} larger than 4 mM. Then, no erosion takes place either by flow or by floc sedimentation. There is, however, loss from the deposition hole because clay intrudes into the fractures constantly and the rim expands. The expansion continues until glacial melt-water intrudes and erosion at the rim starts.

The rate of expansion of clay into the fracture, i.e. the rate of growth of, r_R, $\frac{dr_R}{d_t}$ is given by Equation (A1-25)[1] in Appendix 1. It depends on r_R and a number of parameters that are clay specific and specific to the case studied i.e. initial volume fraction of smectite in deposition hole ϕ_i, radius of hole r_i, etc. The equations needed to solve Equation (A1-25) are given in Equation (A1-17) to (A1-24) in the same reference.

The rate of rim expansion r_R (t), is obtained by numerical integration of

$$\frac{dr_R}{dt} = \frac{\frac{N_{in}-2N_{rim}}{\varrho_S \delta \pi} - (r_R^2 - r_i^2)\frac{\partial \phi_{mean}}{\partial \phi_i}\frac{d\phi_i}{dt}}{2r_R\phi_{mean} + \frac{\partial \phi_{mean}}{\partial r_R}(r_R^2 - r_i^2)} \qquad (4\text{-}1)$$

The derivation and use of these equations to model the instationary phase has been described in detail in Section 2.3.1 in Appendix 1 and is not repeated here.

During the non-glacial phase, Equation (4-1) only depends on time as the loss at the rim $2N_{rim}$ is zero. Furthermore we assume that the loss is small compared to the total amount of clay in the deposition hole so that the volume fraction of clay in the deposition hole is essentially constant, $\frac{d\phi_i}{d_t} = 0$. The integration gives the following results illustrated in Figure 4-1. The curve is well fitted by the following expression

$$r_R(t) = 1.300 + 0.3428\sqrt{t} - 0.0000335\, t \qquad (4\text{-}2)$$

with t in years for time from 0 to 10^5 years. The fitted full line fits the model results, points, very well as the line can hardly be distinguished from the points. The modelling results do not depend on other parameters than those defining the clay properties defined essentially by particle size and surface charge density. The clay type does not seem to have a strong impact on the swelling pressure. Liu (2013) was able to describe the swelling pressure of the smectite in several different clay types, with and without admixture of sand with the same model and model parameter values. The swelling pressure only depends on the density of the smectite fraction in the sand-smectite mixture. It may be noted that the square root term in (4-2) dominates the results also for quite long times. This is typical for instationary diffusion processes for linear expansion but also is expected for the early phase of radial expansion when the source concentration is constant, which is the case in these examples.

Similarly, the accumulated mass loss is obtained and illustrated in Figure 4-2 for a fracture aperture 0.1 mm. The mass lost is directly proportional to the aperture. The curve is well fitted by the following expression for times from 0 to 10^5 years.

$$M(t) = \delta(93.74\,\mathrm{t} - 0.0004521\,\mathrm{t}^2 + 2.236 * 10^{-9}\mathrm{t}^3) \qquad (4\text{-}3)$$

with t in years and δ in m.

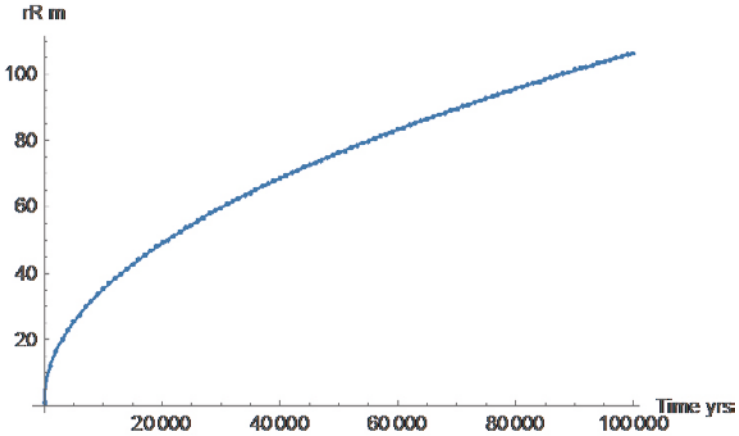

Figure 4-1. *Radius to rim as function of time for c_{ion} > 4 mM. Points are calculated values and line is a fit to the points. The fitted full line can hardly be distinguished from the simulated results, the points.*

[1] Ax-yy refer to number yy of equation, figure or table in appendix number x.

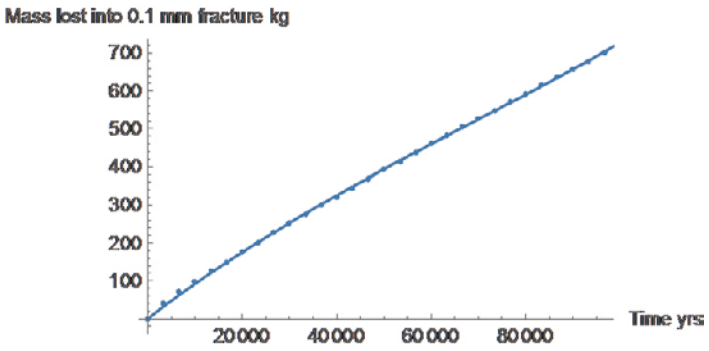

Figure 4-2. *Mass loss as function of time for c_{ion} > 4 mM. The fitted full line can hardly be distinguished from the simulated results, the points.*

The loss from a deposition hole during the non-glacial period can thus be obtained by Equation (4-3) for time from 0 to 10^5 years. It should be noted that very few individual fractures, if any with a radius of 100 m or more are expected to be present. It is more realistic to model the rock as a fracture network for the longer times. This was done by approximating the network by a 3-dimensional porous medium with a porosity of 2.1×10^{-5} with spherically radial diffusion, using the same method as was used to devise the PSS solution for the individual fracture with cylindrically radial diffusion. The porosity used was derived assuming that the area for diffusion into the rock through a fracture intersecting the cylindrical deposition hole should be equal to the area available for diffusion from a sphere with the same clay volume as in the cylindrical deposition hole. The rim radius after one million years in this case is about 110 m and the loss nearly 7 000 kg. For spherical diffusion the loss is always slightly larger than for cylindrical diffusion but the rim radius expands less rapidly. Figure 4-3 shows the radius of the spherical region as function of time and Figure 4-4 shows the mass loss over time.

When the non-glacial period is much longer, order of magnitude or more, than the duration of the glacial water intrusion, the erosion will have little impact on the loss from deposition hole and the total loss after the end of the glacial water period can be approximate by the loss according to (4-3) using the sum of the time for non-glacial and glacial period. The error introduced by this very simple approach is marginal compared to other uncertainties. However, when the non-glacial period is not much larger than the glacial period, the loss during glacial periods should be assessed separately and added. This is treated next.

We wish to emphasize that any effects of the presence of the accessory minerals are neglected in the above modelling, which only considers the migration of the colloidal size highly charged smectite particles. There is strong experimental evidence that real, variable aperture fractures, will be clogged by the larger, non-charged accessory mineral crystals. The clay expansion is expected to be strongly influenced by clogging.

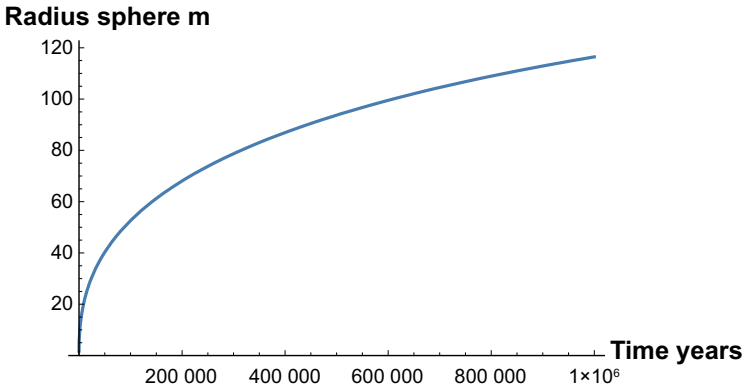

Figure 4-3. *Radius to the spherical rim as function of time for c_{ion} > 4 mM.*

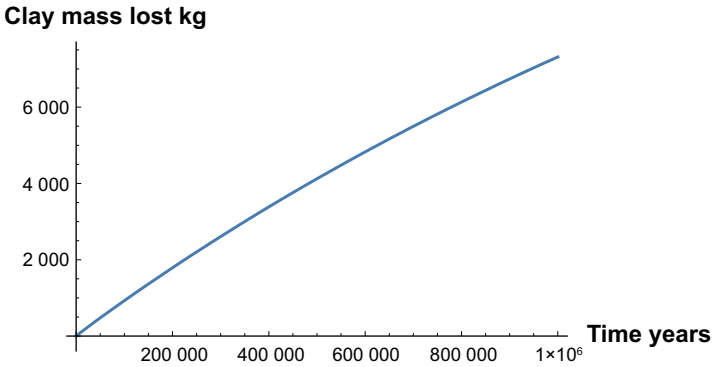

Figure 4-4. *Mass loss as function of time for c_{ion} > 4 mM for spherical expansion.*

4.2.2 Glacial water period

Erosion by seeping water

When the groundwater has an ion concentration below 4 mM there is erosion at the rim caused by both flow and floc sedimentation. During this period the intrusion into the fracture continues but the rate is influenced by the rate of loss at the rim. The radius to the rim can recede if the erosion loss rate is large, or it can continue to grow if the loss rate is small. This makes it difficult to derive a simple and accurate expression for the loss from the deposition hole. However, it has been found in the simulations that a steady state loss is rapidly attained when the erosion rate at the rim is large. Then the steady state loss can be used as if it were constant over time, neglecting the initial instationary period. The erosion rate at the rim depends on water velocity, aperture, radius to the rim and ion concentration. It can be determined by Equation (4-4). For details see Equation (A1-45) in Appendix 1.

$$N_{erosion} = \rho_s \delta \phi_R 4 \sqrt{D_R(c_{ion})\, \pi r_R\, u_o} \tag{4-4}$$

D_R (c_{ion}) is obtained by solving the equations for clay diffusion properties illustrated in Figure 2-2. The value of the volume fraction at the rim $\phi_R = 0.015$, the volume fraction found to give the best fit to experiments, see Appendix 2.

The solution for $D_R(c_{ion})$ for a given clay, in this case MX-80, when fitted gives the following equation where $x = Log10(c_{ion})$ in mM and D_R in m^2/s. It is valid for $0.1 < c_{ion} < 4$, which is within the region in which erosion occurs by flow and by floc sedimentation.

$$D_R(c_{ion}) = 10^{-9.42911 - 1.5309\, x - 1.88737\, x\text{^}2 - 0.783596\, x\text{^}3} \tag{4-5}$$

D_R is practically constant below $c_{ion} = 0.5$ and it can be set to D_R(0.1 mM) for $c_{ion} < 0.1$, but drops considerably approaching 4 mM. Above this value it can be set zero.

A transition period starts after glacial water intrusion. After some time a steady state is reached where the intrusion rate from the deposition hole is equal to the erosion rate at the rim. The distance to the rim, r_R stabilises at r_{RSS} and the loss rate from the deposition hole becomes constant. The time to reach this SS is short when erosion is large. This happens for high velocity for horizontal fractures and for large apertures for inclined fractures with floc sedimentation. For $c_{ion} < 0.5$ mM it can be illustrated by the following. For $u_o > 10^{-5}$ m/s steady state conditions are reached in less than 20 years in horizontal fractures. For $u_o = 10^{-6}$ m/s it takes about 200 years and for $u_o = 10^{-7}$ m/s it takes about 2 000 years. For low water velocities the loss rate will be small and it is reasonable to neglect the higher loss rate during the initial period and use the SS loss rate also for the entire period to avoid the need to solve the time dependent equations. For $u_o = 10^{-7}$ m/s this would underestimate the loss during 1 000 years by less than 10 % and increasingly less for longer times. With this approximation a very simple expression results that can be used to calculate the SS loss rate for apertures, velocities and ion concentrations in the ranges expected.

The procedure is as follows. When SS is reached the intrusion rate into the fracture is equal to the erosion rate at the rim. This is obtained by equating the loss rate by erosion with the intrusion rate $N_{erosion} = 2N_{rim} = N_{in}$. The equation to solve becomes, Equation (A1-26) in Appendix 1.

$$G = \frac{\varrho_s D_i \pi \delta(\phi_i - \phi_R)}{N_{rim}(r_i)} = \frac{D_i \pi(\phi_i - \phi_R)}{2\phi_R \sqrt{D_R(c_{ion})\, r_i u_o}} = ln(\frac{r_{RSS}}{r_i}) \sqrt{\frac{r_{RSS}}{r_i}} \tag{4-6}$$

Noting that G contains only known entities G is constant for a given case it has the solution

$$\frac{r_{RSS}}{r_i} = (\frac{G/2}{ProductLog(\frac{G}{2})})^2 \tag{4-7}$$

ProductLog(z) gives the principal solution for w in $z = w\, e^w$. It is also called the Lambert W function $z = \frac{G}{2}$. in this case

This gives the solution of r_{RSS} at steady state when D_i and ϕ_i are constant. D_i and ϕ_i are the smectite diffusivity and the volume fraction at the conditions in the deposition hole respectively.

With the radius to the rim from Equation (4-7) the SS rate of loss is obtained by Equation (4-4).

Figure 4-5 shows loss rate as function of water velocity for different ion concentrations for a 0.1 mm aperture fracture. Steady state is well reached for $u_o > 10^{-7}$ m/s in 1 000 years. The dashed line shows the old model results from Neretnieks et al. (2009).

Figure 4-6 shows the SS radius to the rim as function of velocity and ion concentration,

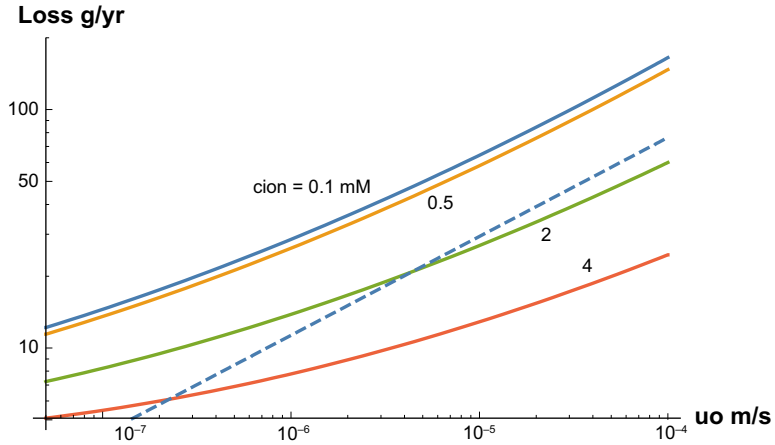

Figure 4-5. *Loss rate as function of water velocity for different ion concentrations in mM for a 0.1 mm aperture fracture. Dashed line shows the old model results from TR-09-35.*

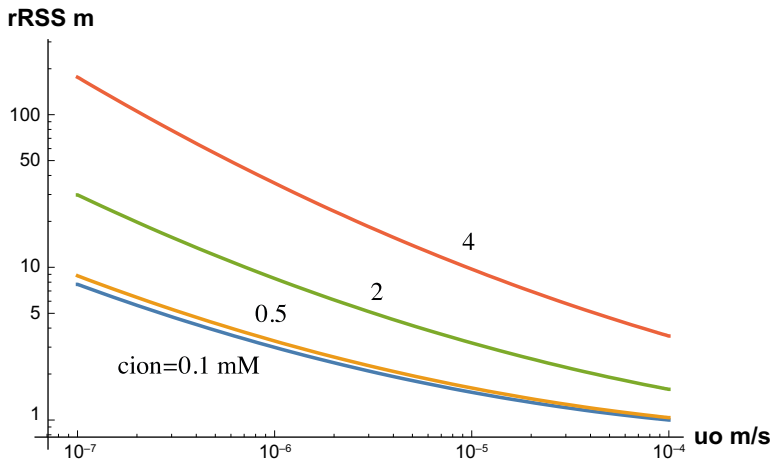

Figure 4-6. *r_R at steady state for different ion concentrations.*

Erosion by sedimentation

It was shown in Section 3.3 that one can find an upper bound on the formation and release of agglomerates but that this is probably very conservative. At present we must use direct experimental results on the loss rate from small cylindrical sources and assume that these results can be extrapolated to much larger dimensions. Experiments in sloping fractures show that in low ionic strength waters tiny smectite agglomerates are constantly released and they sediment in the fracture (Schatz et al. 2013, Schatz and Akhanoba 2016). Examples were shown in Figures 3-1 to 3-3. The results can be summarised as follows for 45 and 90° slopes from the horizontal, Equation (4-8). The release rate is proportional to the circumference of the extruded clay times the aperture.

$$N_{Exp} = J_{Exp}\ \delta\ 2\pi r_{RSS} Sin(\alpha)\ ^{2} \qquad (4\text{-}8)$$

J_{Exp} was found to be 850 and 1 550 kg/m^2/year by Schatz and Akhanoba (2016) for different clays in fractures with slopes of 90 and 45° from horizontal. The SS radius to the rim r_{RSS} is obtained by solving

$$N_{Exp} = N_{in} \qquad (4\text{-}9)$$

With N_{in} from (3-4) this has an analytical solution

$$r_{RSS} = \frac{F_{Exp}}{ProductLog(\frac{F_{Exp}}{r_i})} \qquad (4\text{-}10)$$

where $F_{Exp} = \frac{D_i \varrho_s (\phi_i - \phi_R)}{J_{Exp} Sin(\alpha)} t_y$ (4-11)

$t_y = 3.15 \times 10^7$ s/year

The rate of loss is then directly obtained by inserting the value in (4-8). The next step is to see if that rate of released smectite can be transported away in the fracture as an agglomerate fluid. Then Equation (3-3) with $W_{AF} = 2\ r_{RSS}$ is used to calculate N_{sed}.

Figure 4-7, left frame, shows how the loss would increase with increasing aperture based on the experiment according to Equation (4-8) for a vertical fracture and with J_{Exp} = 1 000 kg/m^2/year, the full line. The dashed line shows the maximum rate of sedimentation of the AF according to (3-3). For fractures narrower than 0.016 mm the sedimentation rate is not sufficient to carry away the released smectite. The right frame shows the maximum loss from the source accounting for these limitations. The maximum loss in a 0.1 mm aperture is 0.61 kg/year.

From Equations (4-10) and (4-11) it is found that the rim only expands from the radius of the deposition hole 0.925 to 0.972 m. i.e. 4.7 cm to reach steady state conditions in a vertical fracture when the loss is not limited by AF flow.

As the release rate according to Equation (4-8) is based directly on experiments without a firm theoretical understanding and the viscosity of the agglomerate fluid may well be underestimated, a simple sensitivity analysis is presented below. Table 4-1 shows the loss rate in a 0.1 mm aperture fracture for different combinations of C_{Exp} and μ_{agg}. In the examples the lowest μ_{agg} is taken to be as that of water without any particles. This may well underestimate the viscosity of the AF when it has had time to "mature", i.e. arrange its internal structure to find the lowest energy configuration. The larger the fracture aperture is the less chance will the sedimentation rate have to set an upper bound on the loss because of the third power of aperture influence.

[2] Schatz and Akhanoba do not account for the angle in their summary of results. Until we have access to the detailed data we no include the effect of slope in Equation (4-8) as it is expected that there should be such an influence.

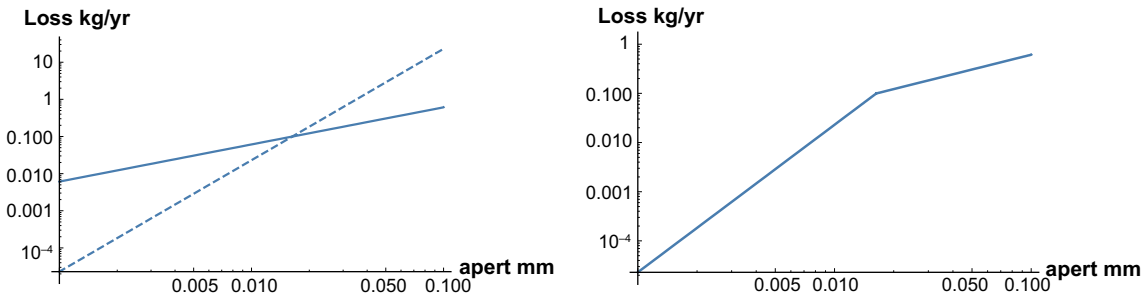

Figure 4-7. *Left frame, Maximum possible release rate of smectite, full line and possible sedimentation rate of the agglomerate fluid, dashed line. Right frame, maximum loss from source taken from left frame.*

Table 4-1. Smectite loss by sedimentation in a vertical fracture for different combinations of C_{Exp} and μ_{agg}. The figures in parentheses show what the loss would be if it were not limited by the rate at which the sediments can move away.

C_{Exp} kg/m²/year	μ_{agg} mPa s	N_{loss} kg/year
1 000	1	0.61
10 000	1	6.1
1 000	10	0.61
10 000	10	2.3 (6.1)
1 000	100	0.23 (0.61)
10 000	100	0.23 (6.1)

It is seen that the loss is very sensitive to the release rate and that the increase in agglomerate viscosity only starts to matter when the agglomerate fluid viscosity is very large as seen in the last three rows in Table 4-1. The loss by sedimentation in the central case (row 1) is about two to three times higher than for horizontal fracture with flow for the highest considered water velocities in horizontal fractures. This loss occurs even without any flow in the sloping fractures, provided the sediments can move away continuously. Such further movement may not be assured if the sediments have a non-zero friction angle and cannot move on at intersections with fractures with slopes less than the friction angle.

5 Discussion and conclusions

The most recent “erosion by flow” model (2016) quantitatively agrees well with laboratory scale experiments. This model accounts for rapid flocculation in the sol. This process was not included in previous models. The new model is very simple and is founded on simple well-established physics. The new model predicts larger losses than the original model (2009). However, it should be emphasized that we now have introduced an adjustable parameter, which must be obtained directly from experiments in fractures. The old model was based on using only independently determined parameter values in the rim modelling. The above findings therefore should be used with caution for predictions under conditions that differ from those in Schatz et al. (2013) experiments”.

In addition to flow, erosion experiments have shown that flocs sediment in sloping fractures. This can cause smectite loss larger than that caused by flow. Upper bounds of loss by gravity were established by determining maximum flowrate of a denser liquid (the floc slurry) in a less dense fluid, water. The maximum rate of transport away from the source under such conditions is predicted to be proportional to the aperture to the third power. This suggests that in fractures narrower than 0.1 mm the gravity induced floc migration can limit the loss rate. It is suggested that this is verified experimentally, especially considering how the floc viscosity evolves over time, which cannot be quantified at present. The agglomerate fluid viscosity may well become very large at the low shear rates expected in narrow fractures.

A reasonably limited release of flocs will fill very large volumes of rock and it is not obvious that so much rock would become available, even over long times. This may be of special importance for calcium-dominated clays that seem to form strong aggregates in contrast to sodium-dominated clays that form loose floc slurries that flow. Aggregate heaps of calcium dominated clays seem to attain approximately a 45-degree slope of repose (friction angle). This will limit the agglomerates to move in less than 45-degree slope fractures. Also here further studies are needed to verify these tentative observations.

It is to be noted that all the above modelling and experiments have modelled the clay as containing only the mineral smectite mineral montmorillonite. Smectite particles are extremely small thin sheets, 1 nm thick and some 100 nm in the other dimensions. They have a strong inbuilt negative charge which gives rise to the strong swelling pressure and to sol formation in low ionic strength waters. The natural bentonites considered as buffer and backfill materials contain noticeable amounts of other mineral particles, typically on the order of 10 % by weight. These mineral particles on average are tens to hundreds or more times larger than the smectite particles and have been seen to clog filters and replicas of natural variable fractures. These particles have a good potential of slowing down or even strongly impeding the expansion of the clay in natural fractures. In the recently finished EC project BELBaR several such observations have been reported. (European Atomic Energy Community’s Seventh Framework Programme (FP7/2007-2011)). Investigations of the clogging of fractures may reveal a potentially important mechanism that will limit clay loss.

6 Notation and data used

Table 6-1. Notation and data used.

c_{ion}	Ion concentration mM	Unless otherwise stated in text.
D_I	Smectite diffusion coefficient in deposition hole, m^2/s.	10^{-9}
D_R	Smectite diffusion coefficient at rim, m^2/s.	10^{-9}
g	Gravitational constant, m/s^2.	9.81
G	Entity defined in Equation (4-6).	
J_{Exp}	Constant in Equation (4-8), defining flux of released sediments, kg/m^2/year. Exp stands for based on experiments.	1 000
r_i	Radius of deposition hole, m.	0.925
r_R	Radius to rim, m.	
t	Time, s or year.	
u_o	Water velocity, m/s.	
W_{AF}	Horizontal width of expanded clay, m.	
α	Angle of facture to horizontal.	
δ_{fr}	Fracture aperture, m.	
ρ_{agg}	Density of agglomerate fluid, kg/m^3.	1 017
ρ_s	Density of smectite mineral, kg/m^3.	2 700
ρ_{sph}	Density of spherical floc, kg/m^3.	1 017
ρ_w	Density of water, kg/m^3.	1 000
μ_{agg}	Viscosity of agglomerate fluid Pa × s.	10^{-3}, 10^{-2} and 10^{-1}
μ_w	Viscosity of water Pa × s.	10^{-3}
ϕ_i	Volume fraction smectite in deposition hole.	0.574
ϕ_{mean}	Mean volume fraction smectite in fracture.	
ϕ_R	Volume fraction smectite at rim.	0.015

Table 6-2. Summary and explanations of equations for the different flowrates N.

	Equation number	Comment
$N_{rim} = \rho_s\, \delta\, \phi_R \frac{2}{\sqrt{\pi}} \sqrt{D_R\, x\, u_o}$	2-1	N for rim of length x.
$N_{erosion} = 2N_{rim} = \rho_s \delta\, \phi_R \frac{4}{\sqrt{\pi}} \sqrt{D_R\, \pi r_R\, u_o}$	2-2	N for both half-sides of a cylinder.
$N_{release} = \frac{\pi\delta^3}{108\mu_W} \left(\varrho_{sph} - \varrho_W\right) g \phi_R \varrho_s Sin(\alpha) W_{AF}$	3-1	Maximum N for release of small sedimenting flocs with diameter equal to fracture aperture.
$N_{release} \propto r_{sph}^2\, Sin(\alpha) \delta W_{AF}$	3-2	N for release of small sedimenting flocs with radius r_{sph}.
$N_{sed} = \frac{\delta^3}{12\mu_{agg}} \left(\varrho_{agg} - \varrho_W\right) g \phi_R \varrho_s W_{AF}$	3-3	N for sedimentation of agglomerate fluid, AF.
$N_{in} = D_i 2\pi \varrho_s \delta \frac{\phi_i - \phi_R}{ln(\frac{r_R}{r_i})}$	3-4	N for transport out through concentric cylinder at SS. This is the PSS inflow from the source.
$N_{erosion} = \rho_s \delta \phi_R 4 \sqrt{D_R(c_{ion}) \pi\, r_R\, u_o}$	4-4 (and 2-2)	N for two half-sides of a cylinder. Emphasis of $D_R(c_{ion})$.
$N_{Exp} = J_{Exp}\, \delta\, 2\pi r_{RSS} Sin(\alpha)$	4-8	N from experimental data.
$N_{Exp} = N_{in}$	4-9	N for SS conditions.

References

SKB's (Svensk Kärnbränslehantering AB) publications can be found at www.skb.com/publications.

Angelini R, Zaccarelli E, de Melo Marques F A, Sztucki M, Fluerasu A, Ruocco G, Ruzicka B, 2014. Glass–glass transition during aging of a colloidal clay. Nature Communications 5. doi:10.1038/ncomms5049

Bird R B, Stewart W E, Lightfoot E N, 2002. Transport phenomena. 2nd ed. New York: Wiley.

Birgersson M, Börgesson L, Hedström M, Karnland O, Nilsson U, 2009. Bentonite erosion. Final report. SKB TR-09-34, Svensk Kärnbränslehantering AB.

Carslaw H S, Jaeger J C, 1959. Conduction of heat in solids. 2nd ed. Oxford: Clarendon.

Hedström M, Ekvy Hansen E, Nilsson U, 2016. Montmorillonite phase behaviour. Relevance for buffer erosion in dilute groundwater. SKB TR-15-07, Svensk Kärnbränslehantering AB.

Jansson M, 2009. Bentonite erosion. Laboratory studies. SKB TR-09-33, Svensk Kärnbränslehantering AB.

Liu L, 2010. Permeability and expansibility of sodium bentonite in dilute solutions. Colloids and Surfaces A: Physicochemical and Engineering Aspects 358, 68–78.

Liu L, 2011. A model for the viscosity of dilute smectite gels. Physics and Chemistry of the Earth 36, 1792–1798.

Liu L, 2013. Prediction of swelling pressures of different types of bentonite in dilute solution. Colloids and Surfaces A: Physicochemical and Engineering Aspects 434, 303–318.

Liu L, Moreno L, Neretnieks I, 2009a. A dynamic force balance model for colloidal expansion and its DLVO-based application. Langmuir 25, 679–687.

Liu L, Moreno L, Neretnieks I, 2009b. A novel approach to determine the critical coagulation concentration of a colloidal dispersion with plate-like particles. Langmuir 25, 688–697.

Liu L, Neretnieks I, Moreno L, 2011. Permeability and expansibility of natural bentonite MX-80 in distilled water. Physics and Chemistry of the Earth 36, 1783–1791.

Moreno L, Neretnieks I, Liu L, 2010. Modelling of erosion of bentonite gel by gel/sol flow. SKB TR-10-64, Svensk Kärnbränslehantering AB.

Moreno L, Neretnieks I, Liu L, 2011. Erosion of sodium bentonite by flow and colloid diffusion. Physics and Chemistry of the Earth, Parts A/B/C 36, 1600–1606.

Neretnieks I, 2009. Some scoping erosion experiments in thin slits between glass plates. Report, Chemical Engineering, KTH Royal Institute of Technology, Stockholm, Sweden.

Neretnieks I, Liu L, Moreno L, 2009. Mechanisms and models for bentonite erosion. SKB TR-09-35, Svensk Kärnbränslehantering AB.

Neretnieks I, Liu L, Moreno L, 2010. Mass transfer between waste canister and water seeping in rock fractures. Revisiting the Q-equivalent model. SKB TR-10-42, Svensk Kärnbränslehantering AB.

Reid C, Lunn R, El Mountassir G, Tarantino A, 2015. A mechanism for bentonite buffer erosion in a fracture with a naturally varying aperture. Mineralogical Magazine 79, 1485–1494.

Rhén I, Forsmark T, Hartley L, Jackson P, Roberts D, Swan D, Gylling B, 2008. Hydrogeological conceptualisation and parameterisation -Site descriptive modelling SDM-Site Laxemar. SKB R-08-78, Svensk Kärnbränslehantering AB

Richards T, Neretnieks I, 2010. Filtering of clay colloids in bentonite detritus material. Chemical Engineering & Technology 33, 1303–1310.

Schatz T, Akhanoba N, 2015. Erosion of bentonite material in sloped fracture Environments, Poster presentation at International Conference on Clays in Natural and Engineered Barriers for Radioactive Waste Containment, Brussels, 23–26 March 2015.

Schatz T, Akhanoba N, 2016. Buffer erosion in sloped fracture environments. Posiva Report 2016-13, Posiva Oy.

Schatz T, Kanerva N, Martikainen J, Sane P, Olin M, Seppälä A, Koskinen K, 2013. Buffer erosion in dilute groundwater. Posiva 2012-44, Posiva Oy, Finland.

Secor R B, Radke C J, 1985. Spillover of the diffuse double layer on montmorillonite particles. Journal of Colloid and Interface Science 103, 237–244.

Segad M, Jönsson B, Åkesson T, Cabane B, 2010. Ca/Na montmorillonite: structure, forces and swelling properties. Langmuir 26, 5782–5790.

SKB, 2011. Long-term safety for the final repository for spent nuclear fuel at Forsmark Main report of the SR-Site project. SKB TR-11-01, Svensk Kärnbränslehantering AB.

Vilks P, Miller N H, 2010. Laboratory bentonite erosion experiments in a synthetic and a natural fracture. NWMO TR-2010-16, Nuclear Waste Management Organisation, Canada.

Appendix 1

Bentonite expansion and erosion – development of a two-region model

Summary

Erosion of smectite in a fracture intersecting a deposition hole for spent nuclear fuel embedded in a clay buffer has been modelled with the dynamic clay expansion model. In previous work it was found that even sophisticated finite element methods could not resolve the details of the very sharp front in the rim-region of the expanding gel. A two-region model, which avoids some problems in earlier work was developed and tested. The model divides the region of the expanding clay in the fracture in one where the clay behaves like a Bingham solid/fluid that cannot flow but can expand by the repulsive forces between the smectite particles and another, the rim-region surrounding the former where the gel/sol, although highly viscous near the rim-border, can flow and carry away the smectite particles that diffuse into this region. This two-region model gives results that are more accurate than those obtained earlier by the fully coupled model because of a much higher resolution in the region where the erosion loss occurs was implemented by a special technique.

One novelty of the paper is the high accuracy of the rim model. Another novelty is the numeric technique with an expanding grid. A further novelty is the development of a very simple pseudo steady state model to follow the bentonite expansion.

A1.1 Introduction and background

In nuclear waste repositories of the KBS-3V type used in Sweden and Finland copper canisters, about 1 m in diameter and 5 m tall containing the spent nuclear fuel will be emplaced in vertical boreholes at the floor of tunnels in granitic rock at depths of about 500 m. The canisters are embedded in compacted bentonite clay consisting of around 80 % smectite (SKB 2011). When wetted by groundwater the smectite in bentonite swells due to the strong repulsive forces between smectite particles. The bentonite protects the copper canister from corrosive agents carried by the seeping ground water in the fractures as it has a very low hydraulic conductivity and solutes must penetrate this barrier by molecular diffusion only, which is a slow process. Should the canister somehow be breached, leaking radionuclides must diffuse through this barrier to reach seeping groundwater. The plastic bentonite barrier also protects the canister from minor rock movements. If in contact with low ionic strength water, which could reach repository depth during e.g. an ice age when melting glacier water penetrates the rock, the bentonite can release colloidal smectite particles to the seeping water forming a sol. The water can carry away the sol. The main concern is that much bentonite is lost impacting important barrier functions. A secondary concern is that eroded smectite colloids could carry attached radionuclides away from a breached canister.

A bentonite erosion model was developed to estimate the loss of smectite from bentonite used as buffer and backfill in the Swedish KBS-3 repository concept. The model was used in performance assessment calculations for the Swedish and Finnish repositories. The model is based on a dynamic force balance model and a gel/sol viscosity model summarised in Neretnieks et al. (2009) and described in more detail in a number of publications (Liu 2010, 2011, 2013, Liu et al. 2009a, b, 2011, Moreno et al. 2010, 2011).

The central idea is that swelling of the smectite in the bentonite clay into the fractures with seeping water and the further transport as gel/sol with the water is influenced by the pore water concentration of primarily mono-and divalent cations. The swelling and erosion can be quantitatively described by a set of partial differential equations, PDE's. The system of PDE's is nonlinear and sometimes difficult to solve numerically because of the mutual influence of the evolving chemistry in the

smectite gel/sol, the forces acting on the smectite particles and on the viscosity of the gel/sol[3], which determines when and how it can flow. The numerical difficulties and complex interaction between the various mechanisms involved have led us to explore which mechanisms have a dominating impact on the erosion and how simplifications could be made that will lead to more transparent, faster and stable calculations.

It is found that water chemistry has the largest influence in the outer regions of the gel/sol and that the composition in the approaching groundwater essentially determines the smectite properties in the region where the gel/sol flows with the water. This allows the chemical transport model to be decoupled from the smectite expansion model, which eliminates the need for continuous coupling of the migration of ions in the expanding gel between the seeping water and interior of bentonite bulk.

In earlier studies it was also found that the flow of the gel/sol occurs in a thin rim-region where the smectite volume fraction changes from a few percent by volume to essentially smectite free water. This led us to explore if it is possible to decouple the swelling of the gel/sol in the region where it expands by the swelling forces from the thin rim-region[4] where the gel/sol both swells and flows.

One aim of this study is to gain better insights into the complex and intertwined mechanisms that cause swelling and erosion of the smectite clay. A further aim is to generate transparent, fast and stable calculation procedures suited for calculations of bentonite loss from a deposition hole. The study addresses smectite clays dominated by monovalent ion chemistry over a wide range of salinity.

The paper is structured as follows. The concept of a two-region model is introduced. Then an inner region where the gel expands radially by a diffusion-like process, although it does not flow by the prevailing hydraulic gradient, is modelled. At the rim-border the second, mobile, region commences into which smectite particles diffuse. In this region the gel/sol can flow and carry away the smectite particles it contains. The two regions are then coupled and solved simultaneously. This is called the numeric solution. In addition, a simple pseudo steady state model, PSS, is developed to test the numeric model and to gain further insights. Various tests are used to ensure that the models give reasonable results. Examples are presented and compared to previous results.

A1.2 Modelling expansion of gel and smectite loss to seeping water

A1.2.1 Concept of a two-region model

In this paper the concentration of bentonite in the gel/sol is expressed as volume fraction of smectite particles.

Figure A1-1 illustrates how the clay expands from a source radially into a fracture with flowing water. The rigid gel, the white region, releases particles to the seeping water, which carries them away downstream. The gel with a volume fraction above a certain value does not flow because it behaves as Bingham body and the expanding clay retains the circular shape up till a point where the volume fraction has dropped to ϕ_R where the gel/sol suddenly attains a finite viscosity η_R and can start to flow, albeit with a low velocity set by the viscosity. The expanding clay continuously releases particles by diffusion into the rim-region in which ϕ and η decrease in the outward radial direction. The velocity increases gradually as η drops.

It was found in previous modelling by Moreno et al. (2010, 2011) that the escape and flow of smectite takes place in a very narrow region, where the smectite volume fraction very rapidly drops from some value ϕ_R at the rim-border to zero. Below ϕ_R, roughly in the region $0.005 < \phi < 0.015$, depending on ion concentration, the viscosity of the gel/sol decreases very strongly with decreasing ϕ. The gel/sol velocity where $\phi > \phi_R$ is negligible compared to that in the rim-region. This is supported by the experiments presented in Schatz et al. (2013) where it was found that the gel was rigid and did not flow, or even deform, by the seeping water. The rim-region can be very thin compared to the radius of the expanded gel.

[3] The term gel/sol is used because in the region of interest in this report there is a gradual transition from gel to sol. When it is clearly a gel or a sol these terms are used.

[4] We use the term rim-border or sometimes rim to denote the border between the expanding rigid gel-region and the region in which the gel/sol flows. The latter is called the rim-region.

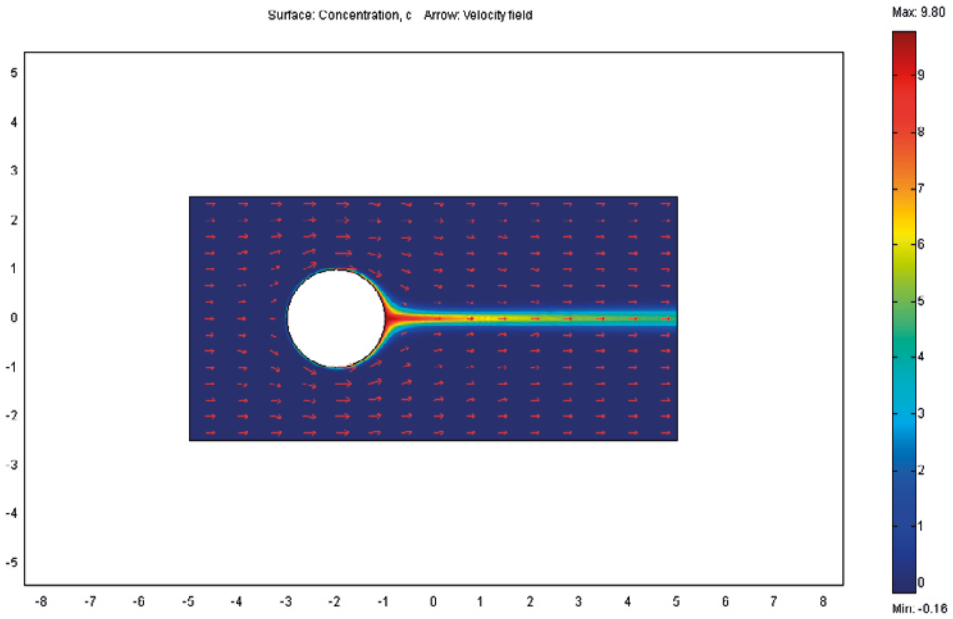

Figure A1-1. *Water flows around a bentonite gel/sol that has expanded into a fracture from a circular deposition hole. The smectite particles in the bentonite diffuse into the seeping water and are swept downstream.*

When using conventional finite element, volume or difference methods with a *fixed grid* the inner region, which constantly expands, pushes the rim-region outward. If the thickness of the rim-region is small compared to the grid size the resolution in the very thin rim-region may not be sufficient to accurately compute the details of smectite diffusion and flowrate in this region. To exemplify this, consider a two-dimensional grid, 1 000 elements long and 1 000 elements wide. The diameter of the source is taken to be 20 elements and the rim-border has expanded radially ten times the source diameter to 200 elements. At some point in time the thickness of the rim can be much less than one percent of the radius of the expanded gel, i.e. $0.01 \times 100 = 1$ element. The resolution of the details in the zone will be very poor as the rim-border moves past one element to the next. The problem could in principle be resolved by discretizing only the rim-region much finer, but as its location constantly changes, adaptive grid methods must be used. Discussions with knowledgeable numerical analysis colleagues discouraged us to at present implement such techniques. Instead we chose the approach described below which is simple in principle and encourages us to seek insights in the underlying physics.

As the rim-region makes up only a small fraction of the whole region, it seems reasonable to assume that an acceptable error will be introduced if one neglects the slight difference in length between the inside and outside borders of the curved rim-region. The rim-border around a circular region can be placed at the circle with radius $r = r_R$. Other shapes than a circle can also be used to define the location of the rim-border. An extension to this idea is that when the curvature of the rim-region is small it can be approximated by a straight "ribbon" with a length $\pi r_R \times r_R$ is the outer radius of the expanding rigid gel. Under these conditions the expansion and flow of the particles in the rim-region can be modelled in Cartesian coordinates with ϕ_R located at y = 0 along the x-axis. The particles in the rim-region move by diffusion in the y-direction and flow in the x-direction. Particles that have penetrated some distance into the rim-region are carried downstream by a velocity that is influenced by the local viscosity of the gel/sol. At a location $x = \pi r_R$ downstream the flowing gel/sol leaves the contact with the rigid gel. The flowrate of the mass of smectite particles past this location is N_{rim}, which is the loss by erosion. We seek a way to quantify N_{rim} as function of chemical conditions, water velocity and length of rim-border, x.

A1.2.2 Diffusivity and viscosity of a gel/sol

Diffusivity

Expansion of a smectite gel/sol can be modelled as a diffusion process analogous to diffusion of a solute in water. There is, however, a major difference between the smectite particles and most other solute molecules and ions. The smectite particles are highly charged and surrounded by counterions that form a cloud of diffuse ions near the surface of each smectite particle. The diffuse layer of counterions generates repulsive forces between nearby particles. At high particle concentrations this causes the particles to disperse much more strongly than if only Brownian forces disperse the particles. At low volume fractions only the latter act on the particles. Another difference to large molecules and ions is that at higher ionic strengths the diffuse counterion layer can become so thin that the attractive van der Waals forces become larger than the repulsive forces and the system collapses to a cohesive gel. No particles can then be released from the cohesive gel by just thermal movement of the particles (Brownian movement).

The repulsive forces between the particles cause the particles to move away from each other. The friction of the particles against the water in which they move counteracts the expansion. The balance between expansion and friction forces can be described by a diffusion coefficient for smectite particles. The rate of expansion can then be modelled as a diffusion process. This is the essence of the dynamic gel expansion model in Neretnieks et al. (2009). Figure A1-2 shows the diffusion coefficient $D(\phi)$ for the smectite particles in water as function of the volume fraction ϕ for different concentrations of monovalent ions for smectite particle diameter 200 nm and thickness 1 nm. The dashed line does not include crystalline swelling. Crystalline swelling was not used in earlier simulations.

It is seen that for ion concentrations above 1 mM the diffusion coefficient is approximately constant around 10^{-9} m^2/s in the volume fraction range $0.02 < \phi < 0.6$. At even lower ion concentration the volume fraction range for constant diffusivity is extended to ϕ down to 0.002 or less. Then, rather abruptly, note the logarithmic scale, the diffusion coefficient drops by two to three orders of magnitude. The viscosity of the gel/sol also changes very strongly in the region around $\phi = 0.01$ for the ion concentrations of interest here.

For high ionic concentrations the critical coagulation concentration CCC is predicted to be around 50 mM monovalent ions at which the gel becomes cohesive at around $\phi_{CCC} = 0.05$. The CCC can be deduced from the information in Figure A1-2. It is between 30 and 100, where D becomes negative. A compact gel in free swelling will expand only to ϕ_{CCC} (Liu et al. 2009b). In this paper we discuss only ion concentrations below the CCC but it may be noted that also a gel that finally will be cohesive, swells strongly when above $\phi > \phi_{CCC}$.

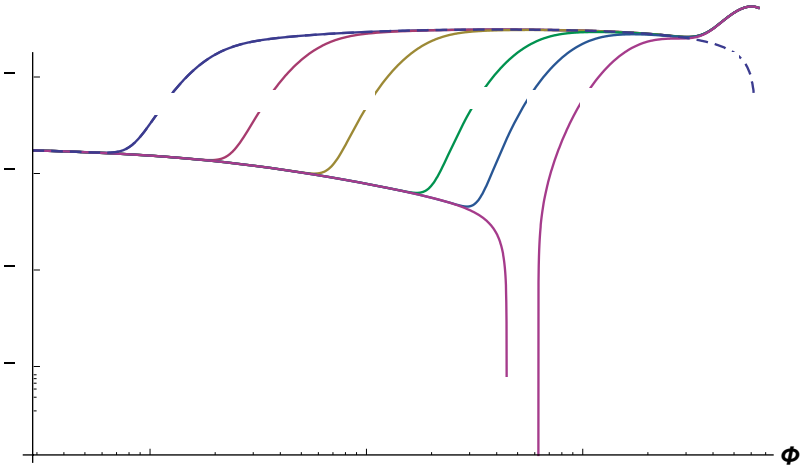

Figure A1-2. *Diffusion coefficient D(ϕ) for the gel/sol as function of the volume fraction ϕ for different concentrations of monovalent ions, 200 nm particle diameter. Dashed line, without accounting for crystalline swelling.*

Viscosity of gel/sol

The gel/sol viscosity increases with increasing ϕ. It also changes with ion concentration and particle dimensions as does D. The viscosity of very dilute sols approaches that of water. With increasing volume fraction of smectite the viscosity increases and at higher volume fractions the gel viscosity becomes larger and increasingly more non-Newtonian. This means that the shear force is no longer proportional to shear rate. In a narrow region of volume fractions the gel abruptly starts to behave like a Bingham fluid/body. A minimum shear force is then needed to make the gel/sol flow. However, it may be noted that an expanding gel will "expand", decreasing the particle concentration, unimpeded by the gel viscosity. This is because in the "expansion" there is no *net flow of gel*. The gel is a mixture of smectite particle and water. Smectite particles that move are replaced by an *identical* volume of water. There is thus no net movement of the smectite-water mixture making up the gel when it expands by becoming more dilute. It can be compared to the diffusional mixing of two mutually soluble liquids A and B. They mix by diffusion and a concentration profile evolves. The location of a given concentration of species A in B can be followed as it moves but there is no net fluid movement of the mixture due to diffusion.

The shear force that the water exerts on the gel/sol with $\phi > \phi_R$ cannot mobilise it. Just outside this region $\phi < \phi_R$ and the gel/sol can suddenly flow with a finite velocity. A sharp front will develop between the expanding gel and the seeping sol. The front expands continuously and the smectite particles at the front are released by the repulsive double layer forces. They diffuse outward into the flowing sol as illustrated in Figure A1-1.

We use Liu's model (2011) to describe the gel/sol viscosity. It is based on the notion of co-volume and fitted to available experimental data, which covers volume fractions up to nearly 0.01 where the co-volume fraction for the underlying data is about 1.6. The co-volume is the volume of "would be" sphere with the diameter of the smectite sheets extended by the Debye length divided by the gel/sol volume. The idea is that when the smectite sheets no longer can rotate freely, the gel viscosity dramatically increases. This abrupt increase in viscosity has been observed in experiments where water flows past an expanding gel (Schatz et al. 2013). This is also supported by a number of rheological experiments reported in Birgersson et al. (2009).

The largest increase in the viscosity is about 10 times that of water before the gel becomes "rigid". Liu's model summarises experimental data in the following expression.

$$\eta_r = \frac{\eta}{\eta_w} = 1 + 1.022\phi_{cov} + 1.358(\phi_{cov})^3 \qquad \text{(A1-1)}$$

η is the gel viscosity, η_w that of water and η_r is the relative viscosity. The co-volume fraction ϕ_{cov} (ϕ) depends on the particle dimensions, the charge of the cations and their concentration. These relations are not shown here. The reader is referred to Liu (2011).

In Figure A1-3 the relative viscosity is shown for three different ionic strengths. The maximum viscosity is just below 10 before becoming "infinite". Finite discretisation methods have considerable difficulties handling so abrupt changes.

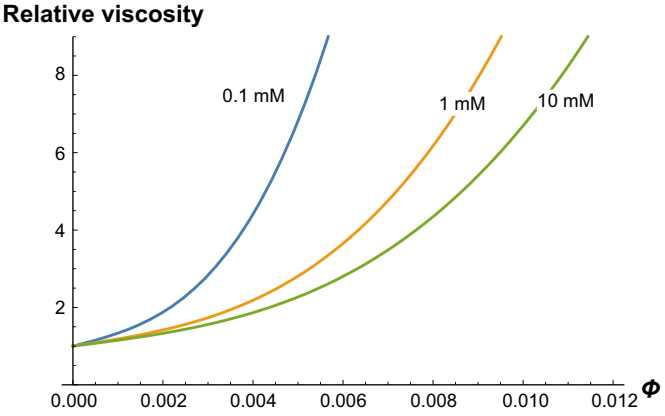

Figure A1-3. *Relative viscosity for the gel/sol as function of the volume fraction ϕ for different concentrations of monovalent ions. 200 nm particle diameter.*

A1.2.3 Mathematical model for expansion of the rim-border

First the expansion model of the gel subject to smectite loss at the rim-border is developed. Thereafter the rim-region model, which is treated as a boundary condition to the expanding inner region is developed. For the inner expanding region we use an expanding grid in the finite difference method when solving the equations. This is described below. In the rim-region, in contrast, no discretisation is needed as will be described in the rim-region model section.

Consider a fracture that intersects a circular hole of radius r_i filled with compacted bentonite where the smectite volume fraction is ϕ_i at r_i, from which the gel expands radially outward to a radius r_R where the volume fraction is ϕ_R. The rim-region starts there. In that region the gel/sol can flow. From the deposition hole at r_i there is a supply of smectite that intrudes into the fracture. At r_R there is loss due to the flowing gel/sol. The rate of accumulation of smectite mass in the fracture is

$$\frac{dM}{dt} = N_{in} - 2N_{rim} \tag{A1-2}$$

N_{in} is the rate of transport of smectite from the deposition hole into the fracture and N_{rim} the rate of loss at the rim-border. The "2" in $2N_{rim}$ is introduced because later N_{rim} will be used to denote the loss of smectite into water symmetrically flowing past one side of the cylinder. The mass in the fracture between r_R and r_i is

$$M = \varrho_s \delta_{fr} \pi \phi_{mean} (r_R^2 - r_i^2) \tag{A1-3}$$

ϕ_{mean} is the mean volume fraction in the gel-region between r_R and r_i. The rate of mass accumulation in the fracture is

$$\frac{dM}{dt} = \varrho_s \delta_{fr} \pi \left(\frac{d\phi_{mean}}{dt} (r_R^2 - r_i^2) + \phi_{mean} 2 r_R \frac{dr_R}{dt} \right) = N_{in} - 2N_{rim} \tag{A1-4}$$

N_{in} can be obtained knowing the gradient of ϕ at the inlet to the fracture and ϕ_{mean} from the solution of the diffusion equation in time and space $\phi(t,r)$ and integrating as described later.

$$N_{in} = -D_{r_i} 2\pi r_i \varrho_s \delta_{fr} \left. \frac{\partial \phi}{\partial r} \right|_{r=r_i} \tag{A1-5}$$

We will in a later section develop an expression for N_{rim} as function of r_R and ϕ_R, pore water chemistry and water velocity in the fracture. At present it is sufficient to note that N_{rim} depends on the radius to the rim-border, r_R. From (A1-4) we have

$$\frac{dr_R}{dt} = \frac{N_{in} - 2N_{rim}(r_R)}{\varrho_s \delta_{fr} \pi 2 \phi_{mean} r_R} - \frac{d\phi_{mean}}{dt} \frac{(r_R^2 - r_i^2)}{r_R 2 \phi_{mean}} \tag{A1-6}$$

An alternative way of determining $\frac{dr_R}{dt}$ can be derived based on the conditions at the rim-border where transport to the rim will cause accumulation with concentration ϕ_R in the rim-region that expands outward from $r_R\,(t)^2$ to $r_R\,(t + dt)^2$ during the time interval dt. The mass balance is

$$\phi_R \varrho_s \delta_{fr}\, \pi \frac{dr_R^2}{dt} = \phi_R \varrho_s \delta_{fr}\, 2\pi r_R \frac{dr_R}{dt} = -2\pi \varrho_s \delta_{fr} r_i D_{r_i} \left. \frac{d\phi}{dr} \right|_{r=r_i} - 2N_{rim} \tag{A1-7}$$

and

$$\frac{dr_R}{dt} = \frac{-\pi \varrho_s \delta_{fr} r_i D_i \left. \frac{d\phi}{dr} \right|_{r=r_i} - N_{rim}}{\varrho_s \phi_R \delta_{fr}\, \pi r_R} \tag{A1-8}$$

Both expressions for $\frac{dr_R}{dt}$ (A1-6) and (A1-8) have been used in the technique described below, and were found to give the same results.

$\phi(t,r)$ in the expanding grid can be obtained by solving the instationary diffusion equation in the region $r_i < r < r_R\,(t)$. This equation is derived below.

A mass balance of a solute that enters a control volume at r through cross section area A_r and partly leaves at $r+dr$ through A_{r+dr} can be formulated. The difference of mass in and out accumulates in the volume $A_r dr$. The thickness of the thin slice dr is allowed to change with time in the expanding grid. We will allow it to be a constant fraction of the region $r_R(t)–r_i$, which expands with time. It is seen in (A1-6) that the accumulation depends on the change of mean concentration as well as on the changing distance to the rim-border. The rate of change of the smectite volume in a small control volume, which changes with time as the volume expands, is the difference between what enters and what leaves by diffusion.

$$\frac{\partial(A\,dr\,\phi)}{\partial t} = -D_r A_r \frac{\partial \phi}{\partial r}\Big|_r + D_{r+dr} A_{r+dr} \frac{\partial \phi}{\partial r}\Big|_{r+dr} = \frac{\partial}{\partial r}\left(DA\frac{\partial \phi}{\partial r}\right) dr \quad \text{(A1-9)}$$

The left hand side of (A1-9) is expanded

$$\frac{\partial(A\,dr\,\phi)}{\partial t} = A\,dr\frac{\partial\,\phi}{\partial t} + A\,\phi\frac{\partial(dr)}{\partial t} + dr\,\phi\frac{\partial A}{\partial t} = A\,dr\frac{\partial\,\phi}{\partial t} + A\,\phi\frac{\partial(dr)}{\partial t} + dr\,\phi\frac{dA}{dr}\frac{\partial r}{\partial t} \quad \text{(A1-10)}$$

The grid expands proportionally to the rate of movement of the front, so every point beyond r_i in r-space is "stretched" in proportion to the expansion of r_R . This implies that the "independent" variable $r = r(r_R(t))$ is a function of t because the entire space increases with time. r_R is only function f time and

$$\frac{\partial r}{\partial t} = \frac{dr_R}{dt}\frac{r-r_i}{r_R-r_i} \quad \text{(A1-11)}$$

dr is chosen as a small fraction of $r_R–r_i$ in the subsequent discretisation schemes with N_j discrete volumes. Note that r_i remains constant in time.

$$dr = (r_R - r_i)/N_j \text{ and } d(dr) = dr_R/N_j \quad \text{(A1-12)}$$

(A1-11) and (A1-12) inserted in (A1-10) gives

$$\frac{\partial(A\,dr\,\phi)}{\partial t} = A\,dr\frac{\partial\,\phi}{\partial t} + A\,\phi\frac{dr_R}{dt}/N_j + dr\,\phi\frac{dA}{dr}\frac{dr_R}{dt}\frac{r-r_i}{r_R-r_i} =$$
$$A\,dr\left(\frac{\partial\,\phi}{\partial t} + \frac{dr_R}{dt}\phi\left(\frac{1}{N_j dr} + \frac{1}{A}\frac{dA}{dr}\frac{r-r_i}{r_R-r_i}\right)\right) \quad \text{(A1-13)}$$

$Njdr = r_R–r_i$ and we have the equation for the expanding grid, which together with the rate of movement of r_R from Equation (A1-6) defines the equations to solve. For cylindrically radial expansion

$$A(r) = 2\pi\delta_{fr} r \quad \text{(A1-14)}$$

(A1-13) and (A1-14) in (A1-9) finally gives

$$\frac{\partial\,\phi}{\partial t} = \frac{1}{r}\frac{\partial}{\partial r}\left(Dr\frac{\partial \phi}{\partial r}\right) - \frac{dr_R}{dt}\frac{\phi}{r_R-r_i}\left(1 + \frac{r-r_i}{r}\right) \quad \text{(A1-15)}$$

When $\frac{dr_R}{d_t} = 0$ this reduces to the well known instationary diffusion equation for cylindrically symmetry.

The two coupled equations (A1-15) and (A1-6 or A1-8) were solved numerically using the implicit Crank-Nicolson, CN, method for (A1-15) combined with explicit forward stepping to update r_R from (A1-6 or A1-8). In the computation for the next time step the $\frac{dr_R}{d_t}$ term in (A1-15) is calculated using data from the previous time step and is thus constant when solving (A1-15) by the implicit CN method. This avoids the need to solve, what would be a non-linear system if also (A1-6 or A1-8) were used directly in the CN method.

Time steps are made to increase geometrically as the region expands. The discretisation of the radial region can be made finer nearer the rim-border to ensure that the resolution where D changes rapidly is determined accurately. On the order 200 space steps and several hundreds but up to 100 000 time steps are used when the loss at the rim is small and when the rim-border expands to very large distances. The solution could need up to tens of minutes for the more time consuming cases on a desk computer. Mostly it is much faster. To test the accuracy of the numerical solver several test were made. One was to use a very small value of ϕ_R. This implies that there is a negligible loss at the rim, $N_{rim} \rightarrow 0$, and the location of the rim-border will expand "forever". During the expansion the concentration profile should be practically the same as that obtained from the analytical solution of Equation (A1-15) without the expansion term. This was found to be the case for $\phi_R = 0.0001$and small values for N_{rim}.

When the volume fraction in the source changes due to the expansion into the fracture this is readily accounted for by depleting the source with a rate equal to N_{in} assuming that the entire source is depleted evenly

$$V_{source}\varrho_s \frac{d\phi_i}{dt} = -N_{in} \tag{A1-16}$$

Also (A1-16) is updated by explicit forward stepping.

A simplified model based on the pseudo steady state, PSS, assumption

To gain further insights and to further test the numerical solution, a pseudo steady state (PSS) approach was used to assess the rate of expansion of the gel/sol. It had been found from the numerical simulations with constant D that the shape of the concentration profile does not change very much even when the rim moves further out with time. The shape of the front is identical to the steady state, SS, profile when SS is reached finally, Equation (A1-17) below. The influx at SS, from the source becomes equal to the loss at the rim. The PSS model needs constant D. With also constant ϕ_i a further simplification is possible. The main assumption for the PSS model is that the shape for the profile throughout the expansion is that which will be reached at steady state. With these simplifications the gradient at r_i is only a function of r_R. Also the mean concentration ϕ_{mean} has an analytical expression. Then $\frac{dr_R}{dt}$ (Equation (A1-6)) can also be expressed with known entities and there is no need to solve the partial differential Equation (A1-15) because only an ordinary differential equation remains.

When there is no depletion of the source, i.e. ϕ_i is constant, a steady state will be reached and then the steady state profile is (Carslaw and Jaeger 1959, p 189)

$$\phi(r) = \phi_i - (\phi_i - \phi_R)\frac{\ln\left(\frac{r}{r_i}\right)}{\ln(\frac{r_R}{r_i})} \text{ for } r_i < r < r_R \tag{A1-17}$$

From this

$$N_{in} = -D2\pi r_i \varrho_s \delta_{fr} \left.\frac{\partial\phi}{dr}\right|_{r=r_i} \tag{A1-18}$$

where

$$\left.\frac{d\phi}{dr}\right|_{r=r_i} = -\frac{\phi_i - \phi_R}{r_i\, ln(\frac{r_R}{r_i})} \tag{A1-19}$$

and

$$\phi_{mean} = \frac{(r_i^2 - r_R^2)(\phi_i - \phi_R) + 2(r_i^2\phi_i - r_R^2\phi_R)ln(\frac{r_R}{r_i})}{2(r_i^2 - r_R^2)ln(\frac{r_R}{r_i})} \tag{A1-20}$$

Further for use in Equation (A1-6) we expand

$$\frac{d\phi_{mean}}{dt} = \frac{\partial\phi_{mean}}{\partial r_R}\frac{dr_R}{dt} + \frac{\partial\phi_{mean}}{\partial\phi_i}\frac{d\phi_i}{dt} \tag{A1-21}$$

where in the PSS case we have analytical expressions for the two partial derivatives

$$\frac{\partial\phi_{mean}}{\partial r_R} = -\frac{(\phi_i-\phi_R)((r_i^2-r_R^2)^2 - 4\ln\left(\frac{r_R}{r_i}\right)^2 r_i^2 r_R^2)}{2r_R\ln\left(\frac{r_R}{r_i}\right)^2(r_i^2-r_R^2)^2} \tag{A1-22}$$

$$\frac{\partial\phi_{mean}}{\partial\phi_i} = \frac{(r_i^2-r_R^2)+2r_i^2 ln(\frac{r_R}{r_i})}{2(r_i^2-r_R^2)ln(\frac{r_R}{r_i})} \tag{A1-23}$$

then

$$\frac{dM}{dt} = \varrho_s\delta_{fr}\pi\left(\phi_{mean}2r_R\frac{dr_R}{dt} + \frac{\partial\phi_{mean}}{\partial r_R}\frac{dr_R}{dt}(r_R^2 - r_i^2)\right. \tag{A1-24}$$
$$\left. + (r_R^2 - r_i^2)\frac{\partial\phi_{mean}}{\partial\phi_i}\frac{d\phi_i}{dt}\right) = N_{in} - 2N_{rim}$$

and

$$\frac{dr_R}{dt} = \frac{\frac{N_{in}-2N_{rim}}{\varrho_s\delta_{fr}\pi} - (r_R^2-r_i^2)\frac{\partial\phi_{mean}}{\partial\phi_i}\frac{d\phi_i}{dt}}{r_R 2\phi_{mean} + \frac{\partial\phi_{mean}}{\partial r_R}(r_R^2-r_i^2)} \tag{A1-25}$$

It may be noted that in this case when the concentration profile is known Equations (A1-22) and (A1-23) also have simple analytical expressions. This makes it possible to approximately take in account changes in the concentration at the inlet boundary ϕ_i caused for example by the depletion of the mass in the deposition hole by the intrusion into the fracture, at least for slow changes in ϕ_i.

If one knows how N_{rim} depends on r_R this ordinary differential equation can be integrated with the initial value that $r_R = r_i$ at time zero. It will be shown later that the difference between the simple PSS and numerical solutions is quite small.

It may be noted that at steady state when ϕ_i is constant $N_{in} = 2N_{rim}$ (r_R) and with $N_{rim} \propto \sqrt{r_R}$, as will be shown later to be the case, Equation (A1-41), gives

$$G = \frac{\varrho_s D\pi\delta_{fr}(\phi_i-\phi_R)}{N_{rim}(r_i)} = ln(\frac{r_{RSS}}{r_i})\sqrt{\frac{r_{RSS}}{r_i}} \tag{A1-26}$$

from which the steady state r_{RSS} can be obtained.

Noting from the second expression in (A1-26) that as G, contains only known entities G is constant for a given case and (A1-26) has the solution (Wolfram Mathematica®, Version 10)

$$\frac{r_{RSS}}{r_i} = (\frac{G/2}{ProductLog(\frac{G}{2})})^2 \tag{A1-27}$$

ProductLog(z) gives the principal solution for w in $z = w\,e^w$. It is also called the Lambert W function.

This gives the *exact* solution of r_{RSS} at steady state when D and ϕ_i are constant. It can be used to test the numerical scheme and to get a first impression the magnitude of the expansion. It may also be noted that for the time evolution of the expansion a comparison shows that if ϕ_R approaches zero, which implies that there is no loss at the rim and ϕ_i is constant, the exact solution (Carslaw and Jaeger 1959) of the radial diffusion function (A1-15) without the last term predicts 13 % larger mass influx into the fracture than the PSS solution over all times. This suggests that the PSS solution gives reasonably accurate results when ϕ_R is small. This is the case for the conditions of interest in this paper.

It remains to determine how the flowrate N_{rim} depends on geometry, water velocity, fracture aperture, gel viscosity and gel expansion properties. This is done in the following section.

A1.2.4 Modelling loss at the rim-border

It is expected that the rapid decrease of diffusivity with decreasing ϕ in the rim-region can have a strong impact on the rate of transport into the seeping water. Similarly the decrease of viscosity with decreasing ϕ can have a considerable impact on the local gel/sol velocity. The impact of these combined effects is explored below. It was found in earlier simulations with finite discretisation methods that the rim-region can be very thin compared to the length of the travel path (Moreno et al. 2010). It seems reasonable to assume that the curvature of the rim-border will not much influence the conditions in the rim-region. It is therefore "unwound" from the circular border, straightened and aligned along the x-axis in Cartesian coordinates, starting at $y = 0$.

The flowrate of smectite at a given flow distance x along the rim-border can be determined by integrating the product of velocity and smectite concentration (flux), from the rim-border $y = 0$ to infinity.

$$N_{rim} = \rho_s \delta_{fr} \int_0^\infty u_x(y)\phi(y)dy = \rho_s \delta_{fr} u_o \int_0^\infty \frac{\phi(y)}{\eta_r(\phi(y))} dy \qquad \text{(A1-28)}$$

In the narrow slot the flow velocity is proportional to the hydraulic gradient and the proportionality factor is inversely proportional to the viscosity of the fluid. We therefore approximate the local velocity to be inversely proportional to the local viscosity.

Then the right-most term in Equation (A1-28) is obtained. The relative viscosity $\eta r = \eta(\phi(y))/\eta_w$ where η_w is the viscosity of the water without smectite, $\eta(\phi(y))$ is the viscosity of gel/sol with smectite volume fraction ϕ and u_o is the approaching pure water velocity.

The change in sol velocity in x-direction generates a movement in the y-direction to maintain the mass balance. The equation of continuity describes this.

$$\frac{\partial u_x}{\partial x} + \frac{\partial u_y}{\partial y} = 0 \qquad \text{(A1-29)}$$

The equation that describes the evolution of the smectite concentration in the gel/sol is

$$\frac{\partial \phi}{\partial t} = \frac{\partial}{\partial x}\left(D(\phi)\frac{\partial \phi}{\partial x}\right) + \frac{\partial}{\partial y}\left(D(\phi)\frac{\partial \phi}{\partial y}\right) - u_x\frac{\partial \phi}{\partial x} - u_y\frac{\partial \phi}{\partial y} \qquad \text{(A1-30)}$$

In the thin rim-region the rate of diffusion in the x-direction is much smaller than in the y-direction and can be neglected. The velocity in the y-direction is much smaller than in the x-direction but $u_y\frac{\partial \phi}{\partial y}$ can be of the same order of magnitude as $u_x\frac{\partial \phi}{\partial x}$ because the concentration gradient in the y-direction is much larger than in the x-direction. However, $u_y\frac{\partial \phi}{\partial y}$ is set zero. It is expected and shown later that the impact of this simplification underestimates N_{rim}. A further important simplification is that $\frac{\partial \phi}{\partial t}$ can be neglected and pseudo steady state conditions, PSS, can be used. This is based on the observation that the gel/sol expands very much slower in the y-direction than it travels in the x-direction. Then Equation (A1-30) reduces to

$$\frac{\partial}{\partial y}\left(D(\phi)\frac{\partial \phi}{\partial y}\right) = \frac{u_o}{\eta_r}\frac{\partial \phi}{\partial x} \qquad \text{(A1-31)}$$

The boundary conditions to solve this equation are

for $x \leq 0$, $\phi = 0$ (A1-32)

at $y = 0$, $\phi = \phi_R$ (A1-33)

for $y \rightarrow \infty$, $\phi = 0$ (A1-34)

The model of Liu (2009) and Liu at al. (2009a) for smectite diffusion coefficient is used for $D\phi$. It is lengthy and is not reproduced here but Figure A1-2 shows an example of D as function of ϕ and ion concentration.

The equations to solve are strongly non-linear and will have to be solved with high resolution in the rim-region. When the diffusivity and viscosity are constant, or do not vary very much, ordinary finite difference, finite element methods or the method of lines give rapid and accurate solutions. For more non-linear conditions errors increase and strong non-linearities can result in considerable errors. We therefore make a variable transform that circumvents this problem.

Transform of model from 2D to 1D

Differentiating the L.H.S. of (A1-31) and introducing a dimensionless diffusion coefficient $D_r(\phi) = D(\phi)/D_o$ gives

$$D_r(\phi)\frac{\partial^2\phi}{\partial y^2} + \frac{dD_{rel}(\phi)}{d\phi}\left(\frac{\partial\phi}{\partial y}\right)^2 = \frac{u_o}{D_o\eta_r(\phi)}\frac{\partial\phi}{\partial x} \tag{A1-35}$$

By introducing a dimensionless variable z, Equation (A1-31) can be transformed to an ordinary differential equation (Bird et al. 2002, p 116).

$$z = \frac{y}{2\sqrt{D_o x/u_o}} \tag{A1-36}$$

(A1-35) becomes

$$\eta_r(\phi)D_r(\phi)\frac{d^2\phi}{dz^2} + \eta_r(\phi)\frac{dD_r(\phi)}{d\phi}\left(\frac{d\phi}{dz}\right)^2 = -2z\frac{d\phi}{dz} \tag{A1-37}$$

The transform applied to the boundary conditions gives at

$$z = 0,\ \ \phi = \phi_R \tag{A1-38}$$

and when

$$z \to \infty,\ \ \phi = 0 \tag{A1-39}$$

Attempts to solve this boundary value problem by a finite difference method did not result in sufficiently good resolution because of the very sharp front. (A1-37) is therefore solved by the shooting method. In the shooting method the problem is redefined from a boundary value problem to an initial value problem. The second boundary condition (A1-39) is exchanged for

$$z = 0 \quad \frac{d\phi}{dz} = k \tag{A1-40}$$

The value of k is not known so the problem is solved iteratively for different k's in a systematic way until (A1-39) is satisfied. This is called the shooting method and is automated. Some reasonable starting value for k must be supplied. This method of solving boundary value problems has the advantage that the step-length can be adapted locally so that it can be decreased to extremely short steps in locations where the front is very steep. Also special stiffness handling methods are available in many ODE solvers for initial value problems. The reference D_o can be any value. We chose a value of 10^{-9} m^2/s in the present calculations. This is near the largest D-value in the range of interest. The loss at the rim-borderthen becomes

$$N_{rim} = \rho_s\delta_{fr}u_o\frac{dy}{dz}\int_0^\infty \frac{\phi(z)}{\eta_r(\phi(z))}dz = \rho_s\delta_{fr}2\sqrt{D_o x u_o}\int_0^\infty \frac{\phi(z)}{\eta_r(\phi(z))}dz = \rho_s\delta_{fr}2\sqrt{D_o x u_o} \times N_{rim}^{DL} \tag{A1-41}$$

where

$$N_{rim}^{DL} = \int_0^{\infty} \frac{\phi(z)}{\eta_r(\phi(z))} dz \quad \text{(A1-42)}$$

N_{rim}^{DL} is dimensionless and incorporates the effects of water chemistry, particle size, variable viscosity and diffusivity. It is independent of water velocity u_o and rim-border length x. It is a constant for a given ion concentration and particle dimensions. Integrating from $y = 0$ to infinity covers the volume fraction range from ϕ_R to zero.

It may be noted that when gel viscosity and diffusivity are constant the second term in (A1-37) is zero, and then the solution to the concentration profile becomes (Neretnieks et al. 2010)

$$\phi(z) = \phi_R Erfc(z) \quad \text{(A1-43)}$$

$$N_{rim}^{DL} = \frac{\phi_R}{\sqrt{\pi}} \sqrt{\frac{D_R}{D_o \eta_r}} \quad \text{(A1-44)}$$

and

$$N_{rim} = \rho_s \delta_{fr} \phi_R \frac{2}{\sqrt{\pi}} \sqrt{D_R \, x \, u_o} \quad \text{(Reminder to reader that D and } \eta_r = 1 \text{ are constant)} \quad \text{(A1-45)}$$

This very simple expression has previously been used to assess the loss of solutes such as radionuclides from the interface between seeping water at the water/ clay interface (Neretnieks et al. 2010). In these cases neither the water velocity nor the diffusivity is influenced by the solute concentration and furthermore the diffusion coefficient of different ions and small solutes are within a range of a factor four.

Examples from 1D rim-region model

Figure A1-4 shows the concentration profile in the rim-region for 200 nm particle diameter, $\phi_{Cov} = 1.6$ and $c = 0.1$ mM monovalent ions. With these data, with η_r from (A1-1) and the solution of (A1-37 to A1-39) to obtain $\phi(z)$ and (A1-42), $N_{rim}^{DL} = 27.3 \times 10^{-5}$ and $\eta_r = 8.2$ at $y = 0$.

The drawn out curve in the left frame shows the profile for constant D and viscosity. The volume fraction at the border of the rigid gel is 0.0054 for $\phi_{Cov} = 1.6$. The other curve shows that the concentration profile drops sharply to zero at z around 0.35. Figure A1-4b shows an entity proportional to the flux of smectite as function z. It increases slowly with z as the viscosity decreases and the volume fraction decreases and then abruptly drops to essentially zero at $z = 0.35$. It is used to calculate the smectite flowrate a locus x by integration from y = 0 to infinity, Equation A1-41.

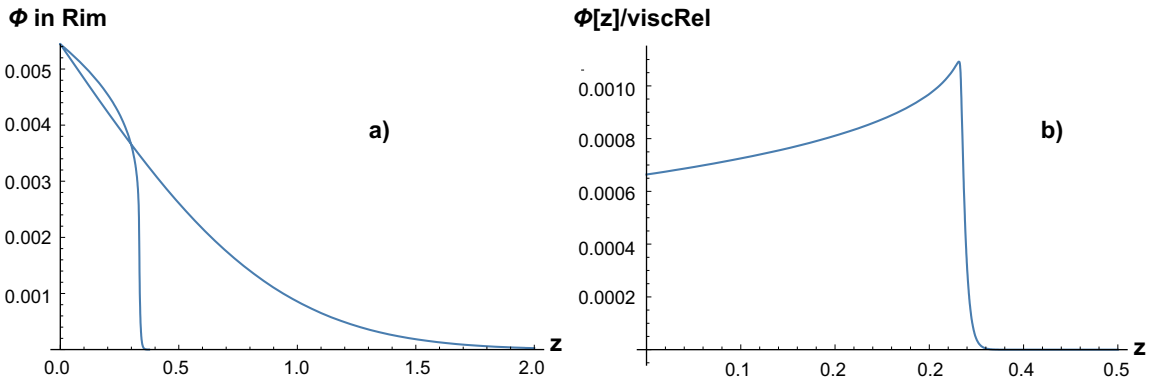

Figure A1-4. *a) left, Concentration profile in the rim-region, $\phi_{Cov} = 1.6$ and c = 0.1 mM monovalent ions. The drawn out curve is for constant D and viscosity. The other curve is for variable diffusivity. b) shows a measure proportional to the smectite flux in rim-region.*

Table A1-1. Dimensionless N_{rim}^{DL} for different concentrations of monovalent ion in water, different particle diameters and co-volume fractions. $D_o = 10^{-9}$ m²/s.

	d_p = 200 nm, ϕ_{Cov} = 1.6		d_p = 200 nm, ϕ_{Cov} = 2	
c mM	ϕ_R %	N_{rim}^{DL}	ϕ_R %	N_{rim}^{DL}
0.1	0.54	27.3×10^{-5}	0.68	34.7×10^{-5}
1	0.91	11.3×10^{-5}	1.14	9.7×10^{-5}
10	1.10	9.6×10^{-5}	1.37	9.7×10^{-5}

In Table A1-2 it is seen that the diffusion coefficient in the rim-region drops by three orders of magnitude when the ion concentration in the approaching water increases from 0.1 to 10 mM. Table A1-2 shows a comparison between N_{rim}^{DL} obtained by Equation (A1-42), which accounts for variable diffusivity and viscosity and that by Equation (A1-44), which is based on the diffusivity at the rim-border $D(\phi_R)$.

It is somewhat unexpected that the simple formula (A1-44) using only the values ϕ_R and η_r at the rim-border does not give larger differences than a factor four at most when it neglects the sharp viscosity and diffusivity changes in the rim-region.

Table A1-2. Dimensionless N_{rim}^{DL} for different concentrations of monovalent ion in water, $D_o = 10^{-9}$ m²/s, 4th column and for constant diffusivity and viscosity at rim-border conditions, 5th column. d_p = 200 nm, ϕ_{Cov} = 1.6.

c mM	ϕ_R %	$D(\phi_R)$ % m²/s	N_{rim}^{DL} by Equation (A1-42)	N_{rim}^{DL} by Equation (A1-44)
0.1	0.54	1.25×10^{-10}	27.3×10^{-5}	108.8×10^{-5}
1	0.91	4.46×10^{-12}	11.3×10^{-5}	34.4×10^{-5}
10	1.10	2.11×10^{-13}	9.6×10^{-5}	9.0×10^{-5}

Errors introduced by neglecting the y-velocity component

Neglecting the term $u_y \frac{\partial \phi}{\partial y}$ in (A1-30) introduces some error. The error was explored by solving Equation (A1-30), without neglecting this term, using a finite element method, Comsol Multiphysics®. It was then necessary to adjust the location and width of the rim-region by trial and error so that the thin rim-region could be discretised with an extremely dense net of elements. Another run was made in which u_y was neglected. The square root dependence of N_{rim}^{DL} with distance, see (A1-41), in both cases was accurately reproduced. Table A1-3 shows the difference between N_{rim}^{DL} obtained using the correct formulation of the flow equation. i.e. accounting for u_y and the approximation where it is neglected. Neglecting the velocity y-component underestimates the N_{rim}^{DL} by a factor of up to 2.4. The Comsol Multiphysics results are deemed to be reasonably correct for 1 and 10 mM. For 0.1 mM it was difficult even with repeated "manual" adjustments of the region where the discretisation was extremely dense to obtain smooth concentration ϕ-profile where the flux drops so sharply at z ≈ 0 35, as shown in Figure A1-4b.

Table A1-3. Ratio N_{rim}^{DL} with/without y-component of velocity for three different ion concentrations and results from (A1-44), which assumes D and η_r to be constant .

c mM	N_{rim}^{DL} with y-component of velocity	Ratio N_{rim}^{DL} with/without y-component of velocity	N_{rim}^{DL} by Equation (A1-44)
0.1	65.1×10^{-5}	2.4	108.8×10^{-5}
1	23.1×10^{-5}	2.0	34.4×10^{-5}
10	11.9×10^{-5}	1.25	9.0×10^{-5}

The difference decreases with increasing ion concentration because the front sharpness decreases with increasing ion concentration. It is surprising that the simple Equation (A1-44) gives results that deviate less than a factor of two from the results obtained by the quite elaborate calculations accounting for up to three order of magnitude changes in diffusivity and one order of magnitude change in viscosity in the rim-region by using the constant values of both diffusivity and the viscosity at the border of the rim-region.

A1.3 Solving the expansion model coupled to the rim model

Equations (A1-41) and (A1-42) for the loss at the rim-border are used in the numerical solution of equation (A1-15) using (A1-6) for the rate of expansion of the rim-border. Some examples are presented below that test the accuracy of the numeric model. The examples are based on the conditions for a deposition hole 0.875 m in radius and 8 m deep with an original volume fraction of smectite of 0.574. These conditions are very similar to those used in earlier simulations (Moreno et al. 2010). The numerical solution and the PSS solution give practically identical results for the expansion of the rim-border when the diffusivity is constant and when the volume fraction in the source is constant. This shows that the numerical solution with the expanding grid correctly handles the expanding grid. In the PSS examples the diffusivity is taken to be the mean value between the conditions in the deposition hole and that at the rim-border. Figure A1-5 shows that the numerical model and the PSS model give quite similar, but not identical results for the expansion of the rim-border when the diffusivity in both models is constant and when the source, i.e. the volume fraction in the deposition hole is depleted, Equation (A1-16). After 100 000 years the source has been depleted by about 1 120 kg or 4 % of the source. About 970 kg has been lost at the rim-border by erosion. 150 kg remain in the 0.1 mm aperture fracture. The PSS solution gives somewhat faster expansion of the gel than the numeric solution with variable diffusion coefficient. The slight decline in the distance to the rim-border after about 10 000 years is due to the depletion of the source. The rim-border recedes at longer times.

N_{rim}^{DL} in this case is underestimated by a factor of 2.4. Using the much higher value for N_{rim}^{DL} *of* 65×10^{-5} to repeat the calculations in Figure A1-5 gives the results in Figure A1-6. The largest expansion distance reduces by a factor of 3 and loss after 100 000 years increases 50 %.

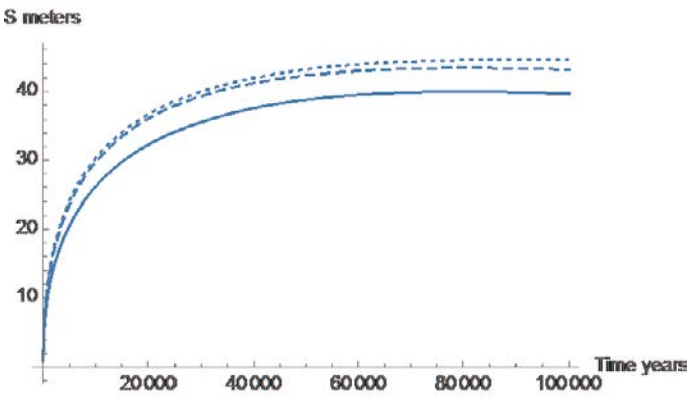

Figure A1-5. *Expansion of the rim-border for c = 0.1 mM and* $u_o = 10^{-5}$ *m/s, initial* $\phi_i = 0.574$, $d_p = 200$ *nm.* $N_{rim}^{DL} = 27.3 \times 10^{-5}$. *Full line is the numeric solution with variable diffusion coefficient. The dashed line shows the numeric solution with constant diffusion coefficient* 1.47×10^{-9} m^2/s. *The dotted line is the PSS solution for the same diffusion coefficient, penetration depth* $S = r_R - r_i$.

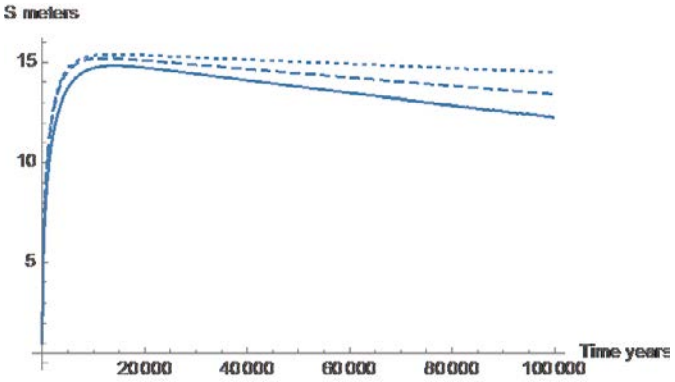

Figure A1-6. *Expansion of the rim-border for c = 0.1 mM and $u_o = 10^{-5}$ m/s, initial $\phi_i = 0.574$, $d_p = 200$ nm. $N_{rim}^{DL} = 2.4 \times 27.3 \times 10^{-5}$. Full line is the numeric solution with variable diffusion coefficient. The dashed line shows the numeric solution with constant diffusion coefficient 1.47×10^{-9} m^2/s. The dotted line is the PSS solution for the same diffusion coefficient, penetration depth $S = r_R - r_i$.*

A1.4 Comparison with earlier results

Calculations of the loss of smectite from depositions holes for spent fuel in a KBS-3 type repository have been presented in Neretnieks et al. (2009) and Moreno et al. (2010). Those results were obtained by the so-called fully coupled model, in which the flow of water and gel, expansion and erosion of bentonite and diffusion of ions between the water and in the gel were accounted for. The influence of ion concentration as well as of the volume fraction of particles on the gel/sol diffusivity and viscosity was modelled. It was found that the migration of ions in the gel/sol could be neglected and that there were considerable difficulties to attain stable solutions by the numerical method used for the lower velocities, Comsol Multiphysics®. Furthermore it was suspected that the results might have considerably overestimated the loss of smectite to the seeping water.

In the two-region model the migration of ions is neglected and the conditions in the rim-region are computed in much finer detail than before. Table A1-5 shows the results from the previous modelling and those obtained by the two-region model. In the old results the ion concentration at the rim-border is about 0.1 mM and no depletion of the source is accounted for. The mass in the fracture was not reported in the old results but is considerably smaller because the outer radius is much smaller, especially for the higher velocities. Note that in the old results a 1 mm aperture was used. We now use a more realistic 0.1 mm aperture and have scaled down the previous result by a factor of 10 in the table to be comparable to the new results.

It is seen in Table A1-5 that there are considerable differences between the old and the new results. The loss is considerably lower and the radial expansion considerably larger with the new model. It may further be noted that the mass in the fracture could be large for the low water velocities.

Table A1-6 shows the *total loss* from the source is not very sensitive to the water velocity or the ion concentration.

Table A1-5. Loss of smecite for ion concentration 0.1 mM for different water velocities in 0.1 mm aperture fracture. N_{rim}^{DL} from Table A1-3, i.e. the y-component of the velocity is accounted for.

Water velocity m/s	Mass eroded at rim at 10 000 years, kg Old	Penetration depth, S, of rim at SS m Old	Mass eroded at rim at 10 000 years, kg	Mass lost from deposition hole at 10 000 years, kg	Penetration depth S of rim at 10 000 years m
10^{-7}	43	7.0	7.6	140	34.2
10^{-6}	117	2.1	22	148	32.0
10^{-5}	292	0.5	144	172	14.7

Table A1-6. Loss of smecite for different ion concentrations in 0.1 mm aperture fracture. Water velocity 10^{-5} m/s. N_{rim}^{DL} from Table A1-3, i.e. the y-component of the velocity is accounted for.

Concentration cion mM	Mass eroded at rim at 10 000 years, kg	Mass lost from deposition hole at 10 000 years, kg	Mass in fracture at 10 000 years, kg	Penetration depth of rim at 10 000 years m
0.1	144	172	28	14.7
1	63	148	85	27.0
10	59	146	87	24.3

A1.5 Discussion and conclusions

Modelling of the loss of smectite caused by seeping water that comes in contact with the expanding bentonite clay has previously been modelled by finite element methods. There have been concerns that the discretization may have to be much more detailed in order to obtain accurate results than what available finite element or similar methods can handle. This is because there is a moving boundary zone, the rim-zone that must be followed in its movement and in which the discretisation must be very much finer that in the rest of the region. In the present two-region method this problem is avoided at the penalty of introducing some other errors. The rim model neglecting the y-component of velocity underestimates the loss at the rim-border by up to a factor 2.4 in the studied cases. This can underestimate the expansion of the rim-border and also underestimate the loss from the deposition hole.

A simplified analytical rim model was found to give results that agree surprisingly well with the full rim model, considering the uncertainties of the rim model. This, especially when combined with the simplified pseudo steady state, PSS, for the gel expansion, which obviates the need for numerically solving the expanding gel region model as the PSS model has an analytical solution. The combination of the PSS model and the simplified rim model can be a valuable tool for making scoping calculations, which can show if there is a need to do the more complex calculations.

Sample calculations show that the there are two major differences between the earlier results and those obtained by the new two-region model. The latter predicts considerably smaller loss of smectite to the seeping water. This in turn causes the bentonite to expand much further out into the fracture because less is lost to the seeping water. The loss from the source, however, being the sum of how much smectite is lost to the water and how much has intruded and still resides in the fracture is smaller but not very different from the earlier results. These differences can be quite important because when bentonite has expanded far out in the fractures this adds considerably to the resistance to diffusional transport to and from the deposition hole of solutes such as corrosive agent and escaping radionuclides..

The model described above does not consider potential effects of gravity. Nor does it consider how the presence of other minerals than smectite in the bentonite may affect the erosion.

There is a number of observations that show that there are other mechanisms than those described above that cause erosion of smectite. In Neretnieks et al. (2009) some experiments are described that show that gel/sol subject to gravity can flocculate and sediment rapidly, hours to days, through narrow passages such as a fine net or a semi vertical fracture. The same phenomenon was observed by Schatz et al. (2013). The loss cased by gravity effects could be larger than what the models discussed above suggest. The mechanisms are not well understood. This is discussed in Appendix 3.

Appendix 2

Evaluation of some erosion experiments by the two-region model

Summary

A number for smectite erosion experiments in a narrow slit have been modelled using our two-region model. The experiments cover a range of monovalent ion concentrations and water velocities. The model successfully predicted the expansion of the gel at high ion concentrations and also predicted that there would be no erosive loss. For lower ion concentrations the erosive loss was considerably underestimated and the expansion of the gel was somewhat overestimated. It is suggested that the unsatisfactory predictions are due to the formation of smectite flocs close to the gel/sol interface. This mechanism is not included in the original two-region model. Invoking floc formation the predictions of both gel expansion and erosive loss are quite good. However, the floc formation mechanisms are not well understood and the amended model must be further validated.

A2.1 Introduction and background

A2.1.1 Background

In nuclear waste repositories of the KBS-3V type used in Sweden and Finland, copper canisters, about 1 m in diameter and 5 m tall, containing the spent nuclear fuel are emplaced in vertical boreholes at the bottom of tunnels in granitic rock at depths of about 500 m. The canisters are embedded in compacted bentonite clay consisting of around 80 % smectite. When wetted by groundwater the smectite in the bentonite swells due to the strong repulsive forces between the smectite particles. The bentonite protects the copper canister from corrosive agents carried by the seeping groundwater in the fractures as it has a very low hydraulic conductivity and solutes must penetrate the barrier by molecular diffusion, which is a slow process. Should the canister somehow be breached, leaking radionuclides must diffuse through the barrier to reach the seeping groundwater. The plastic bentonite barrier also protects the canister from minor rock movements. If in contact with low ionic strength water, which could reach repository depth e.g. during an ice age when melting glacier water penetrates the rock, the bentonite can release the colloidal smectite particles to the seeping water forming a sol. The water can carry away the sol. One concern is that much bentonite may be lost. If a large amount of bentonite is lost important barrier functions can be lost. Another concern is that eroded smectite colloids could carry attached radionuclides to the biosphere.

A bentonite erosion model was developed to estimate the loss of smectite from bentonite used as buffer and backfill in the Swedish KBS-3V repository concept. It was used in performance assessment calculations by SKB and in the modelling of the Finnish repository at Onkalo. The model is based on the dynamic force balance model and gel/sol viscosity models summarised in Neretnieks et al. (2009) and described in more detail in a number of publications (Liu, 2010, 2011, 2013, Liu et al. 2009a, b, 2011, Moreno et al. 2010, 2011) The swelling of the smectite in the bentonite clay into the fractures with seeping water and the further transport as gel/sol with properties is influenced by the pore water concentration of primarily mono-and divalent cations. The swelling and erosion can mathematically be described by a set of partial differential equations, PDE's. The system of PDE's is nonlinear and sometimes difficult to solve numerically because of the mutual influence of the evolving chemistry in the smectite gel/sol, the forces acting on the smectite particles and the viscosity of the gel/sol[5], which determines when and how it can flow. The use of standard techniques to solve the PDE's e.g. Comsol Multiphysics® need extremely fine discretisation, which results in uncomfortably computing times. Even so it was found that the results were not reliable when the gel expanded far into the fractures.

The numerical difficulties and complex interaction between the various mechanisms involved have led us to explore which mechanisms have a dominating impact on the erosion and how simplifications could be made that will lead to more transparent, faster and stable calculations. It was found that the flow of the gel/sol occurs in a very thin rim zone where the smectite volume fraction changes from less than one to a few percent by volume to essentially smectite free water. This makes it possible to decouple the swelling of the Bingham-like gel in the region where it expands by the swelling forces but does not flow, from the thin rim zone where the gel/sol both swells and flows. A new model based

[5] The term gel/sol is used because in the region of interest in this paper there is a gradual transition from gel to sol. When it is clearly a gel or a sol these terms are used.

on the two distinct regions, zones, was developed. The inner region contains the expanding but non-flowing gel surrounded by a tin rim zone into which the smectite particles diffuse from the interface between the gel-zone and the rim-zone. In the rim-zone the gel/sol flows. The viscosity in the thin rim-zone decreases strongly as the volume fraction of the smectite decreases. Also the diffusivity of the smectite particles can drop rather abruptly by orders of magnitude across the rim-zone. Both viscosity and diffusivity are strongly influenced by the ion concentration in the approaching water. As the inner zone expands the length of the rim-zone increases, which increases the rate of loss of smectite to the seeping water. The model of the inner zone of the expanding gel is solved by a modified Crank-Nicolson method using an expanding grid with the outer boundary condition based on the solution of the loss of smectite in the rim-zone. The latter is modelled as a thin strip resulting in an ordinary differential equation, which can be solved with extremely high resolution. The model is derived and described in Appendix 3.

The central relations can be summarised as follows. The diffusivity of the smectite particles in the gel/sol is illustrated in Figure A2-1. The underlying model and the rather lengthy equations can be found in Neretnieks et al. (2009), Liu (2010) and Liu et al. (2011).

The viscosity of the gel/sol is described by Liu's semi-empirical model (Liu 2011).

$$\eta_r = \frac{\eta}{\eta_w} = 1 + 1.022\phi_{cov} + 1.358(\phi_{cov})^3 \qquad \text{(A2-1)}$$

where η is the viscosity of gel/sol, and η_w the viscosity of water. The co-volume fractio ϕ_{cov} is the volume fraction of smectite particles modelled as spheres with the diameter of the smectite sheets, also accounting for the extent of the diffuse electrical double layer. The parameters in (A2-1) were obtained by fitting available experimental data. It may be noted that the largest volume fraction is 0.009 in the experiments and the largest co-volume fraction is about 1.6. The gel with a co-volume fraction above about 1.6 will not flow under the prevailing hydraulic gradients expected under repository conditions. The experiments described below used similar hydraulic gradients. The largest increase in the viscosity is around 10.

The expanding gel is modelled as being radially symmetric, as found in the experiments, by

$$\frac{\partial \phi}{\partial t} = \frac{1}{r}\frac{\partial}{\partial r}\left(Dr\frac{\partial \phi}{\partial r}\right) - \frac{dr_R}{dt}\frac{\phi}{r_R - r_i}\left(1 + \frac{r - r_i}{r}\right) \qquad \text{(A2-2)}$$

where ϕ is the volume fraction, D the diffusivity of smectite particles in gel/sol, r_i the inner radius of cylindrical source, r_R the outer radius of expanding gel in fracture. The expansion rate $\frac{dr_R}{dt}$ of the rim is accounted for and solved using an expanding grid in the numerical Crank-Nicolson scheme

$$\frac{dr_R}{dt} = \frac{N_{in} - 2N_{rim}(r_R)}{\varrho_s \delta_{fr} \pi 2 \phi_{mean}} - \frac{d\phi_{mean}}{dt}\frac{(r_R^2 - r_i^2)}{r_R 2 \phi_{mean}} \qquad \text{(A2-3)}$$

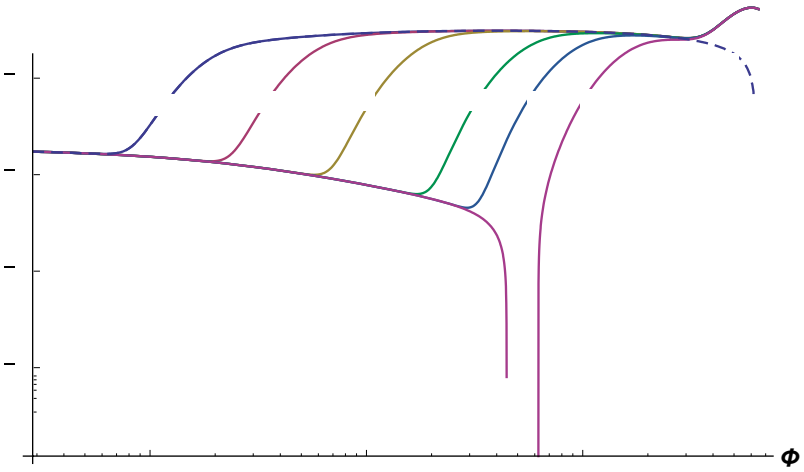

Figure A2-1. *Diffusion coefficient D(ϕ) for the gel/sol as function of the volume fraction ϕ for different concentrations of monovalent ion, 200 nm particle diameter. Dashed line without accounting for crystalline swelling.*

where N_{in} is the rate of smectite inflow into fracture from source, N_{rim} the rate of loss by erosion on one side of the circular rim, ϕ_{mean} , the mean smectite volume fraction in the volume between inner and outer radius, δ_{fr} the fracture aperture and ϱ_s the density of smectite mineral.

This avoids using a very fine grid to cover the entire region into which the gel/sol could expand. The loss at the rim is given by

$$N_{rim} = \rho_s \delta_{fr} 2\sqrt{D_o \pi r_R u_o} \times N_{rim}^{DL} \quad \text{(A2-4)}$$

where D_o is an arbitrarily chosen value of the diffusion coefficient used to calculate the entity N_{rim}^{DL}, which is obtained by solving the coupled flow and diffusion PDE's for diffusion and flow by accounting for the viscosity changes in the rim-zone. u_o is the water velocity in the fracture. Both diffusion and viscosity depend on the volume fraction.

$$N_{rim}^{DL} = \int_0^{\infty} \frac{\phi(z)}{\eta_r(\phi(z))} dz \quad \text{(A2-5)}$$

where z is the outward distance from the rim, the border between the expanding non-flowing gel and the flowing gel/sol. N_{rim}^{DL} depends mainly on the smectite particle size, the volume fraction at which the gel/sol starts to flow and the ion concentration. It has to be determined only once, given these conditions.

Some properties in the gel/sol relevant to the modelling of the experiment are described below. The gel/sol is expanding also if the ionic strength is above the critical coagulation concentration, CCC. At CCC the gel would have expanded to a certain volume fraction after which it stops expanding and does not release particles by diffusion (Brownian motion). Below the CCC it behaves as an expanding gel at all volume fractions and becomes a stable sol at low volume fractions. Below about $\phi = 0.001$ the sol viscosity is only slightly larger than that of water. Above $\phi = 0.01$ to 0.02 the gel/sol can become "rigid" and will not flow or deform, but it can expand by the repulsive forces between the charged smectite particles. Two distinct regions will exist, one inner region where the gel/sol does not flow and one outer region where it flows if subject to a hydraulic gradient. In the thin rim-zone the smectite volume fraction very rapidly drops from some value ϕ_R at the rim to zero. Below ϕ_R , roughly in the region $0.005 < \phi < 0.02$, the viscosity of the gel/sol decreases very steeply with decreasing ϕ. When $\phi \ll \phi_R$ it behaves like a Bingham body/fluid. This is supported by the experiments presented in Schatz et al. (2013) where it was found that the gel was rigid and did not flow, or even deform, by the seeping water. When the volume fraction $\phi << \phi_R$ the velocity of the water seeping in the fracture is equal to that of the water outside u_o. The process is illustrated in Figure A2-2 where it is seen that the rigid gel, the white region, releases particles to the seeping water, which carries them away downstream. The rim zone can be very thin, fraction of one percent of the radius of the expanded gel.

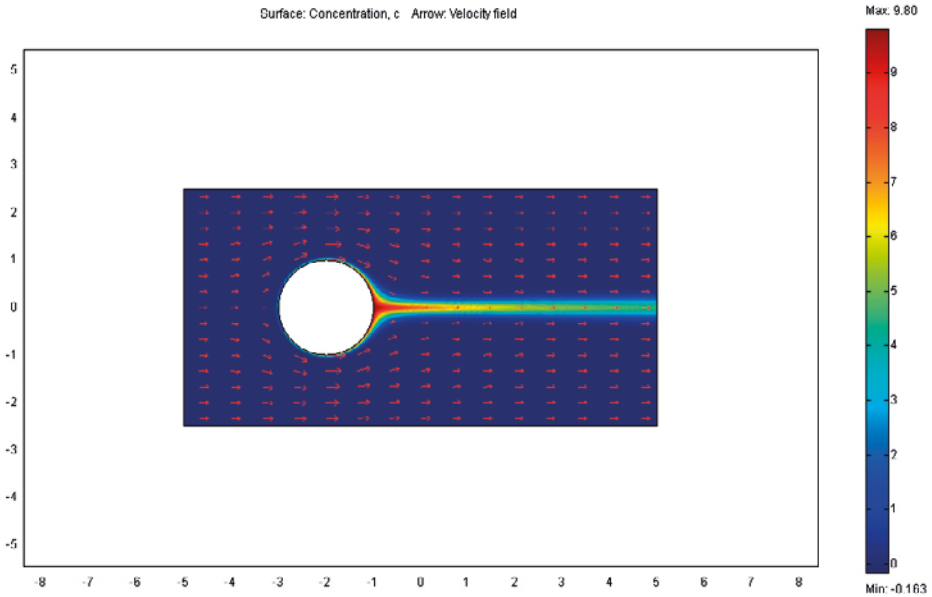

Figure A2-2. *Water flows around a bentonite gel/sol that has expanded into a fracture from a circular deposition hole. The smectite particles in the bentonite diffuse into the seeping water and are swept downstream.*

A2.1.2 Overview of the experiments

Schatz et al. (2013) performed a series of experiments with bentonite expanding in a thin slit with slowly seeping water. A cylindrical piece of compacted smectite was emplaced through a hole in a two parallel transparent acrylic blocks. The space between the blocks was 1 mm, forming the slit. The cylinder has a 2 cm diameter and is 2 cm high. Water injected at one side of the slit flows around the pre-wetted cylindrical smectite, which expands radially out into the slit. Figure A2-3 shows the arrangement.

Bentonite was carefully purified from detritus material leaving smectite, which was ion-exchanged to be homoionic with either sodium or calcium, called NaMt and CaMt respectively. 13 different experiments, where the slit was horizontal, were performed using different water compositions. In nine experiments the smectite consisted of only NaMt. In four experiments a 50/50 mixture of NaMt and CaMt was used. Water with NaCl in different concentrations and a synthetic natural groundwater simulating water from Grimsel with Na^+ and Ca^{2+}, 0.68 and 0.14 mM, respectively and also deionised water was used. With waters of 17 and 171 mM Na^+ there was very small or no release of smectite particles to the water, whereas in other experiments considerable amounts, several to many tens of %, of the emplaced smectite was carried away by the water during times ranging from 456 to 1 152 hours. The pH of the waters is not reported. The original amount of smectite in the source was considerably depleted during the experiments. In the non-eroding cases the gel expanded from 10 mm radius by 50–60 mm at the end of the experiments and on the order of 20–30 cm in the low ionic strength experiments. In the latter much was lost by erosion. Two experiments were performed where the ion concentration decreased in four steps from 8.6, to 4.3, to 2.1 mM and finally to deionised water over 2 688 hours. Water velocities in the experiments ranged from 5.6×10^{-6} to 2×10^{-4} m/s.

In all experiments the expansion was radially symmetric and a very sharp rim separating the expanding gel from the flowing gel/sol formed. Also in the low ionic strength, including deionised water experiments, the rim was sharp although released smectite agglomerates, flocs, could clearly be seen in the water seeping around the expanding cylindrical gel region. The flocs did not slow down the water carrying the flocs as found by dye injection. At the end of the experiments the slit was turned vertically around the axis in the flow direction. In the low ionic strength experiments flocs sedimented downwards in a few hours to a day.

A2.1.3 Application of the two-region model

The process is modelled in the following way for a case where a cylinder of compacted clay in a solid body is intersected by a fracture in the solid as shown in Figure A2-3.

The compacted bentonite in the source hole is fully water saturated and when the fracture is filled with water the gel starts to expand into the water. This expansion is caused by the smectite particles moving outward in the intruding water. The space vacated by a particle is replaced by an identical volume of water moving in the opposite direction. There is thus no net movement of the gel/sol as a body. It just becomes more and more dilute further out from the source.

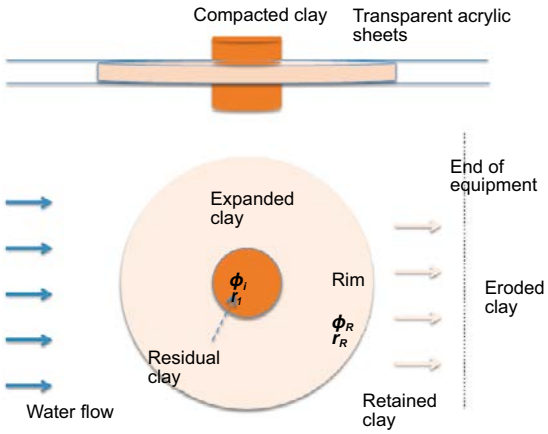

Figure A2-3. *Smectite gel expands out into a slit with flowing water.*

The gel expansion is modelled as a diffusion process of the colloidal smectite particles in the water. The diffusion coefficient depends on the concentration of the colloid particles. It is described by a diffusion function. This has three major components. Firstly, the forces between the particles caused by double layer repulsion and van der Walls attraction, which cause the smectite particles to distance themselves from each other or come closer, are described. This dominates the process at higher volume fractions. Secondly at lower volume fractions, the movement of the smectite particles as they are impacted by the randomly moving water molecules, causing Brownian movement and thirdly, the friction force between the particles and the water in which they move are described. The latter restrains the rate of expansion of the gel/sol.

Symbolically the diffusion function can be written as

$$D = \frac{1}{f_{fr}(\phi)}\left(k_B T + f_1(\phi)\frac{d}{dh}\left(F_{vdW} - F_{DDL}\right)\right) \qquad \text{(A2-6)}$$

where f_{fr} is the friction factor for the particles in the gel/sol as they move in the water. k_B is Boltzmann's constant, T the temperature $h(\phi)$, the distance between particles, $f_1(\phi)$ is a function of the volume fraction ϕ and the particle thickness. F_{vdW} is the attractive van der Waal's force and F_{DDL} is the repulsive double layer force. The latter two are well understood and reliably modelled for sodium dominated systems. The diffusion model has been successfully used to simulate smectite gel expansion of compact tablets and of migration through narrow pores (Neretnieks et al. 2009; Liu et al. 2011). In the present analysis we simulate a set of experiments of smectite expansion in a slit and erosion to seeping water. The friction factor expression is based on the theoretically well-founded Kozeny-Carman expression, which, however, contains an empirical factor that depends on smectite properties and the presence of detritus material in the bentonite clay.

In all simulations the same particle dimensions and the same co-volume fraction at which the gel becomes rigid are used. Table A2-1 shows the data used in the simulations. The entity N_{rim}^{DL} in the fourth column accounts for the impact of gel viscosity in the rim zone. In the fifth column viscosity effects are neglected to test if the observation of flocs in water do not slow down the velocity of the slurry and may increase erosion. This effect is discussed later.

Table A2-1. ϕ_R and N_{rim}^{DL} for different concentrations of monovalent ion in water for the experiments. d_p = 200 nm, ϕ_{Cov} = 1.6.

Experiment	c_{ion} mM	ϕ_R % From co-volume relation ϕ_{Cov} = 1.6	N_{rim}^{DL} with Viscosity Function Equation (A2-1)	N_{rim}^{DL} Constant visccosity
11	DI (0.03)[1]	0.32	0	0
3,5,9	DI (0.03)[2]	0.32	13.2×10^{-5}	68.5×10^{-5}
6	0.83 = GW [3]	0.95	10.1×10^{-5}	43.5×10^{-5}
10	1.66 = 2GW	0.97	9.0×10^{-5}	16.3×10^{-5}
12	2.1	0.99	9.0×10^{-5}	11.9×10^{-5}
13	4.3	1.06	9.1×10^{-5}	8.9×10^{-5}
8	4.0	1.05	9.3×10^{-5}	8.9×10^{-5}
4 and 7 Gradient	8.6	1.09	$12.9–182\times10^{-5}$	$9.0–68.5\times10^{-5}$
2	17	1.10	9.8×10^{-5}	9.1×10^{-5}
1	171	5.0 [4]	(10.0×10^{-5})	(10.0×10^{-5})

[1] DI water is outside the range of validity of gel viscosity relation, which is based on ion concentration between 0.6 an 10 mM. A value of c_{ion} = 0.03 mM is used for DI.

[2] Based on assumption that the gel/sol viscosity for DI is same as for water. Schatz et al. (2012) experiments show that smectite particles agglomerate and the slurry flows readily.

[3] GW stands for simulated Grimsel water.

[4] The ion concentration in the water is well above the critical coagulation concentration. The modelled volume fraction at the rim is about 5 % and no erosion is expected.

The experiments are listed in order of increasing ion concentration because it is expected to have the largest impact on the erosion rate in the rim. Deionised water is modelled as having properties similar to an ion concentration of 0.03 mM. Much lower values were also tested but did not improve predictions.

A2.2 Simulation results

Table A2.A-1 in the sub-appendix summarises the simulations and compares the results with the experimental data. The table is arranged in the order of increasing ionic concentration ranging from deionised water, DI, up to 171 mM.

Three sets of results are presented. The first is with model variant *a* which is the full more complex model It is based on the rim model using the co-volume fraction $\phi_{cov} = 1.6$ to determine the volume fraction at the rim border as well as to determine the viscosity of the gel/sol in the rim zone. It is noted that Equation (A2-1) is based on data in the range $c_{ion} = 0.6–10$ mM at pH = 10 (Liu 2011), and may not be valid for deionised water at neutral pH. This variant assumes that the smectite particles form a sol of individual particles at low volume fractions and that they do not aggregate to form flocs, which could lead to different viscosity behaviour of the suspension. The pH of the waters in the experiments is not reported but the preparation procedure suggests a pH of near 7. The other variants called *b* and *c* will be discussed later.

First we analyse three cases where there is no loss due to erosion. This shows if the inner zone with expanding clay is correctly predicted.

In experiment 11 with DI water there is no flow and the predicted expansion agrees well with the experimental data as can be seen in Figure A2-4

Similarly with an ion concentration of 171 mM, which is well above the CCC, see Figure A2-5 where the diffusivity drops to negative values at c_{ion} just above 30 mM, the agreement is fair and no erosion is predicted as also was found in the experiment. The dotted line is obtained by a simplified analytical pseudo steady state, PSS, solution to Equations (A2-2) and (A2-3) which was devised as a tool for scoping calculations.

Predicted expansion of Experiment 2 with flow and 17 mM, which is near the CCC is shown in Figure A2-6. The model under-predicts the expansion but correctly predicts that there is no erosion.

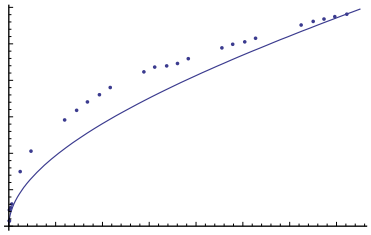

Figure A2-4. *Experiment 11, DI water and no flow. Measured, points, and simulated expansion of rim.*

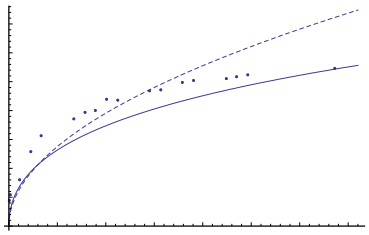

Figure A2-5. *Experiment 1. $c_{ion} = 171$ mM and $u_o = 2.0 \times 10^{-4}$. Full line is from PDE, dashed from PSS solution and points are experimental data.*

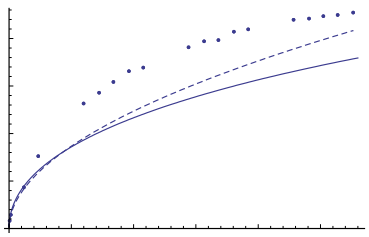

Figure A2-6. *Experiment 2. $c_{ion} = 17$ mM and $u_o = 1.9 \times 10^{-4}$. Full line is from PDE, dashed from PSS solution and points are experimental data*

The first two examples show that the expansion of the gel in the inner zone is reasonably well predicted. In the third example negligible erosion is predicted but the expansion is then not well predicted. The loss by erosion is considerably under-estimated. One important reason is that in the rim-zone model the release of smectite colloids and their transport is modelled by assuming that they stay as individual particles in the gel/sol and that this affects the viscosity of flowing gel/sol according to Equation (A2-1). In the experiments it was found that this is not the case. Also because of the under-estimation of the erosion loss the model over-predicts the expansion radius r_R of the rim and the mass of clay in the expanded zone by a factor of two to four, the larger values for the lower ion concentrations.

The smectite particles form "large" flocs that are transported downstream without noticeably impeding the flow velocity. The flocs may be in the form of complex "house of cards" or other loose arrangements caused by edge to face attraction. This has been suggested by Birgersson et al. (2009). The flocs are seen in all the pictures in the report of Schatz et al. (2013) on the expanding and eroding clay. It was also found that by tilting the slit from its original horizontal position to vertical, flocs were *released* from the rim by gravity forces and sediment "rapidly". It is therefore explored whether the floc suspension, if it has the viscosity of water and thus does not slow down its flow, could cause the erosion increase. In this variant the viscosity is kept constant equal to that of water in Equation (A2-5). However, the release is still assumed to be as individual smectite particles. They then "immediately" form flocs. This is called model variant *b* and the original model is called *a*. In *b* the simulated loss by erosion increased but still clearly under-predicted it for all experiments. This can be seen in Table A2.A-1 in the sub-appendix where details are given on how much of the 10 grams emplaced mass remains in the source (Residual), how much resides in the expanded zone (Extruded), how much is still in the equipment (Retained) and how much has eroded and was collected in the effluent water (Eroded). In Model variant b the co-volume fraction is still used to determine the volume fraction at the rim border ϕ_R It decreases with decreasing ion concentration and would become very small in DI as seen in Table A2-1.

The differences in erosion loss between the complex model *a* and the experiments are shown in Figure A2-7. Model variant *b* gives somewhat smaller differences but is still far from satisfactory.

In model variants *a* and *b* the smectite volume fraction at the rim ϕ_R is calculated from the co-volume fraction ϕ_{cov} = 1.6 at which value the gel/sol can start to flow. The ϕ_R value in the modelling strongly influences the release rate at the rim, especially for the lower ion concentrations because a small decrease in ϕ_R can give a very large decrease in the diffusion coefficient at the rim, which sets the pace for smectite particle diffusion from the rim into the rim-zone. If flocs form very close to the rim the release mechanism as used in the complex model *a* may not be valid. If they form already at the rim and are released from the rim by the shear force of the water at a higher ϕ_R the erosion will be larger. Considering the observations that gravity can pull off flocs it may not be inconceivable that this may happen in an expansive gel below the CCC. A third model variant, *c*, was tested. The differences between the three model variants are summarised in Table A2-2.

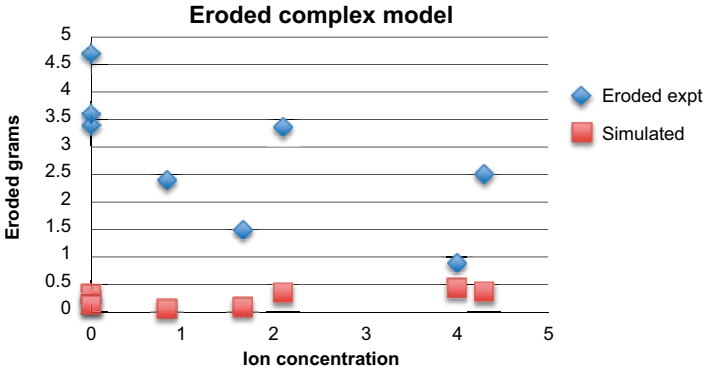

Figure A2-7. *Eroded mass from experiments and simulations Model variant a as function of ion concentration mM*

In the third model variant *c*, which introduces an empirical adjustment of ϕ_R the idea that the concentration at the rim is not governed by the co-volume fraction is explored. At the rim where the smectite particles are released, the water flows unimpeded by the presence of flocs. The volume fraction at the rim that governs the rate of release by smectite particle diffusion from the rigid boundary is used as a fitting parameter. It is called $\phi_{R,f}$. The entity governing the release rate, as given by Equation (A2-4) in this case using $\phi_{R,f}$, becomes very simple under the assumption that N_{rim}^{DL} is constant and it becomes

$$N_{rim} = \rho_s \delta_{fr} \phi_{R,f} 2 \sqrt{D_R\, r_R\, u_o} \qquad \text{(A2-7)}$$

This expression has been derived and used previously for solute diffusion from the rim of expanded clay in fractures for assessing escape of radionuclides. In that case the solute concentration would be used instead of $\rho_s \phi_{R,f}$ (Neretnieks et al. 2010).

At the rim the diffusion coefficient D_R is determined using the diffusion function for the $\phi_{R,f}$ chosen and it is different for different ion concentrations.

Table A2-2 summarises the three model variants.

Table A2-2. summarises the model variants.

Variant	Viscosity of gel/so l η	ϕ_R	D_R
a (Complex model)	Function of ϕ	From ϕ_{Cov} = 1.6 ϕ_R varies with c_{ion}	From ϕ_{Cov} = 1.6 and ϕ_R D_R varies with c_{ion}
b	As water	From ϕ_{Cov} = 1.6 ϕ_R varies with c_{ion}	From ϕ_{Cov} = 1.6 and ϕ_R D_R varies with c_{ion}
c (Simple model)	As water	0.015	From ϕ_{Cov} = 0.015 and ϕ_R D_R varies with c_{ion}

Physically model variant *c* implies that at the border of the rim, at r_R, the particle concentration is $\phi_{R,f}$ and that the release rate is set by the diffusion coefficient at the rim border. It also implies that the individual smectite particles diffuse some distance into the rim-zone without increasing the water viscosity before they form flocs. Interestingly, in experiments 3, 5 and 7 close-up pictures of the rim region shows such a phenomenon.

Simulation results with $\phi_{R,f}$ = 0.001 and 0.015 are presented in Table A2.A-2 in the sub-appendix. Only the experiments that are affected by the use of $\phi_{R,f}$ are presented.

Figure A2-8 shows the results for 0.83 mM, which is that for Grimsel groundwater. Model variants *a* and *b* over-predict the expansion of the radius to the rim and considerably under-predict the loss from the source and the eroded mass. Variant *c* predicts expansion reasonably well as well as Residual, Extruded and Retained mass.

Figure A2-9 summarises the eroded mass from experiments and simulations of the simple model *c*.

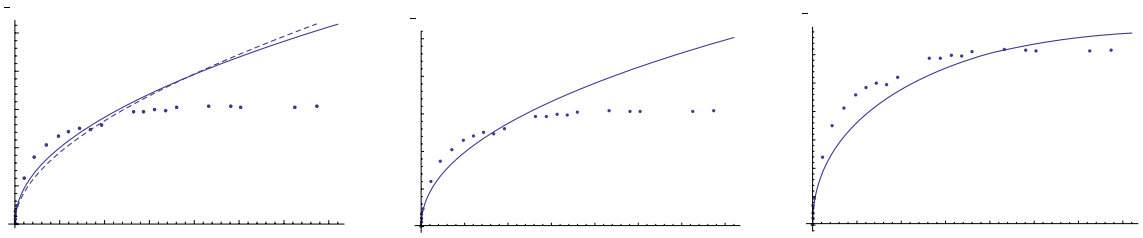

Figure A2-8a, b and c. *Experiment 6. c_{ion} = 0.83 mM and $u_o = 3.3 \times 10^{-5}$. Full line is from PDE, dashed from PSS solution and points are experimental data. 8a model variant a. 8b model variant b. 8c model variant c, $\phi_{R,f}$ = 0,015.*

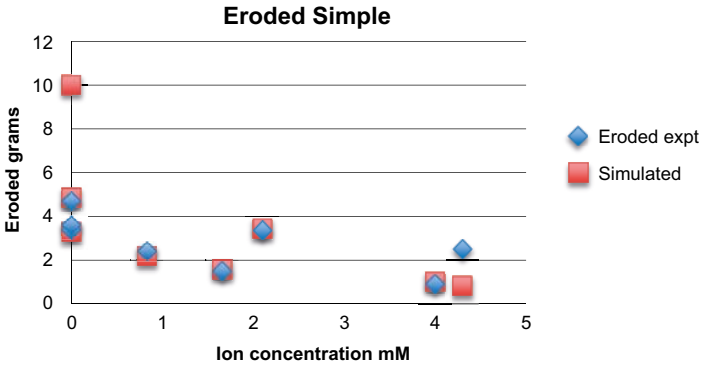

Figure A2-9. *Eroded mass from experiments and simulations of model variant c as function of ion concentration mM with* $\phi_{R,f} = 0.015$

A2.3 Discussion and conclusions

The above results are obtained using the diffusivity function derived and validated earlier for the expansion of smectite clay. It was found that when there is no flow as in example 11 the prediction is fairly good. Also the two experiments with 17 and 171 mM sodium solutions were predicted reasonably well.

However, when there is flow several other effects come into play. In the two-region model the conditions at the interface between the two regions strongly impact the rate of loss by erosion. A central idea to assess the conditions at the rim is that the smectite particles in the gel/sol remain as individual particles and that the co-volume viscosity model, which has been validated by a number of experiments (Liu 2011), is valid for the experiments discussed. That model was calibrated to data in the range of ion concentration in the range 0.6–10 mM (Liu 2011) and for pH = 10 where edge to face attraction is perhaps avoided. The pH in the Schatz et al. (2013) experiments is not reported but is probably around 7. Flocculation of the smectite particles was seen to occur in the experiments. Flocculation at near neutral pH has also been found by Jansson (2009), Neretnieks et al. (2010), Schatz et al. (2013) and references therein. The released smectite particles rapidly form loose flocs that flow away with practically the velocity of the water according to observations in Schatz et al. (2013). The flocs are clearly visible to the naked eye and can have a size of up to 5 mm. This implies that the gel/sol viscosity cannot be described by the relation used for a sol of individual particles, Equation (A2-1).

A third crucial relation in the model is that which governs the volume fraction ϕ_R at which the gel turns from rigid to mobile at the rim. This was also determined by the co-volume relation in model variants *a* and *b* and seems not to be valid when flocculation occurs.

The simulations show that the effects of flocculation on the properties of the rim zone cannot be neglected. We are not aware of any model that quantitatively describes flocculation and its impact in a way useful for the present application. However, retaining the basic idea of the two-region model and empirically adapting ϕ_R , the model "predictions" and experiments can be made to agree reasonably well. Below we explore a possible reason for this behaviour.

For the rim region the following partial differential Equation (A2-8) is solved but without the reaction term, the last term in the equation which is added for the discussion below.

$$\frac{\partial}{\partial y}\left(D(\phi)\frac{\partial \phi}{\partial y}\right) = \frac{u_o}{\eta_r}\frac{\partial \phi}{\partial x} + R_{floc}\phi \qquad \text{(A2-8)}$$

The reaction term implies that the smectite particles irreversibly form flocs and do not contribute to the impact on the sol viscosity anymore, nor do the particles in the flocs randomly diffuse back towards the gel/sol interface, the rim border. The region in which this happens is thin, on the order of a mm as seen in some experiments e.g. Figure 45 in Schatz et al. (2013). Due to the reaction the gradient at the rim border becomes steeper and the release from the gel increases. The flocs do not influence the viscosity of the floc slurry noticeably so this flows away with the velocity of the water.

The relative viscosity η_r of the floc slurry is thus unity. The flocculation rate constant can roughly be estimated as follows. The diffusion of the smectite particles carries them a short distance Δy from the rim before they form flocs. With a diffusion coefficient D_R at the rim the time for flocculation to occur is on the order of the characteristic diffusion time $t_{char} = \frac{\Delta y^2}{D_R}$, which is a measure of the time it would take to essentially fill the region Δy with the concentration at the border of the rim ϕ_R.The rate constant is then on the order of the inverse of this or larger by a factor of two to three because with a given rate constant the concentration would drop by approximately half of the original and two to three times larger R_{floc} would deplete the region by four to 8 times the starting concentration so $R_{floc} > \frac{D_R}{\Delta y^2}$. With $\Delta y = 1 \times 10^3$ m and $D_R = 10^{-10}$ m^2/s, the time $t_{char} = 1 \times 10^4$ *s* and the rate constant $R_{floc} > 1 \times 10^{-4}$ s^{-1}. $R_{floc} > 1 \times 10^{-4}$ s^{-1}. The entity that governs the gradient at the rim is $\frac{R_{floc}}{u_o}$.

With $u_o = 10^{-5}$ m/s and $R_{floc} = 1 \times 10^{-4}$ s^{-1} and 3×10^{-4} s^{-1} the gradient along the rim is shown in Figure A2-10 together with the case when there is no flocculation. The gradient increases by a factor 2 to 3 above that when no flocculation occurs. This will have the same impact as an increase in ϕ_R by the same factor.

The flocculation rate will have the expected impact on the release rate but it is not satisfactory to have to rely on an empirical value for ϕ_R from small-scale experiments for predictions of erosion loss under vastly different conditions such as those for bentonite in large deposition holes in rock. Furthermore experiments have shown that flocs are released from the gel by gravity and sediment "rapidly". The underlying mechanisms are not understood in detail nor have they been modelled in quantitative terms. It would be of considerable value to better understand and quantify flocculation during slow flow in narrow slits and floc behaviour also under gravity. Maximum erosion rates due to gravity effects have been modelled by estimating how fast released flocs could move away from the gel.

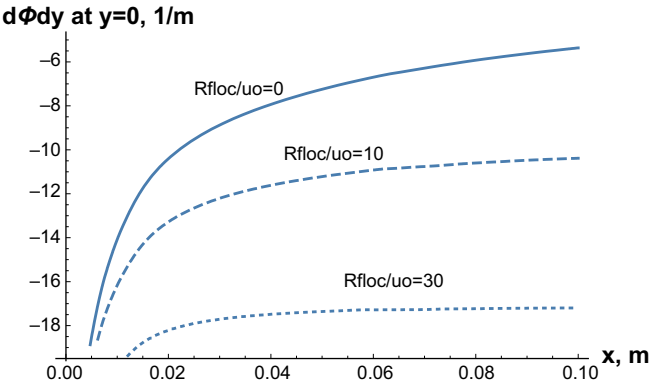

Figure A2-10. *Gradient of smectite volume fraction along the rim of the gel for different flocculation rate constants.*

Table A2.A-1. Fate of smectite in the experiments. E+R means that the sum of Extruded and Retained mass is reported.

Expt. #	Na+ concentration in water c_{ion}, mM, and u_o m/s	Smectite type, Time hrs	Extruded mass up to rim, g Variant a/b	Retained mass in rim zone, g	Residual mass in source, g Variant a/b	Eroded mass, g Variant a/b
11 Meas.	DI no flow	NaMt	E+R = 3.51	0.98	5.17	0
11 Simul.	$u_o = 0$	**720**	**E+R = 3.60**		**6.40**	**0/0**
3 Meas.	DI	NaMt	E+R = 0.68		4.61	4.7
3 Simul.	$u_o = 1.9 \times 10^{-4}$	**456**	**E+R = 2.61/1.74**		**7.05/6.78**	**0.33/1.74**
5 Meas.	DI	NaMt	0.91	0.75	4.9	3.4
5 Simul.	$u_o = 2.6 \times 10^{-5}$	**672**	**E+R = 3.18/2.52**		**6.67/6.55**	**0.15/0.91**
9 Meas.	DI	50/50 Na/CaMt	E+R = 1.08		5.28	3.6
9 Simul.	$u_o = 3.3 \times 10^{-5}$	**648**	**E+R = 2.90/2.32**		**6.96/6.85**	**0.13/.0.81**
6 Meas.	c_{ion} = 0.83 = GW	NaMt	1.31	0.57	5.74	2.4
6 Simul.	$u_o = 6.2 \times 10^{-6}$	**672**	**E+R = 3.51/3.26**		**6.42/6.38**	**0.06/0.34**
10 Meas.	c_{ion} = 1.66 = 2GW	50/50 Na/CaMt	1.28	0.51	6.66	1.5
10 Simul.	$u_o = 5.6 \times 10^{-6}$	**1152**	**E+R = 4.16/4.07**		**5.74/5.73**	**0.09/0.18**
12 Meas.	c_{ion} = 2.1	NaMt	No info.	No info.	No info.	3.37
12 Simul.	$u_o = 5.6 \times 10^{-6}$	**720**	**E+R = 3.25/3.14**		**6.38/6.37**	**0.35/0.47**
13 Meas.	c_{ion} = 4.3	NaMt	No info.	No info.	No info.	2.51
13 Simul.	$u_o = 5.6 \times 10^{-6}$	**696**	**E+R = 3.16/3.17**		**6.45/6.46**	**0.37/0.36**
8 Meas.	c_{ion} = 4.0	50/50 Na/CaMt	1.99	0.38	6.74	0.9
8 Simul.	$u_o = 2.0 \times 10^{-4}$	**864**	**E+R = 3.16/3.21**		**6.40/6.40**	**0.43/0.38**
4/7 Gradient	c_{ion} = 2.1−> 0	NaMt (4) 50/50 (7) Na/CaMt	0.13 (4) 0.13 (7)	0.10 (4) 0.35 (7)	3.23 (4) 3.17 (7)	(6.5−)
4/7 Simul.	$u_o = 1.9 \times 10^{-4}$	**2688/2016** [1]	**E+R = 4.03**		**3.54**	**2.42**
4/7 Gradient	c_{ion} = 8.6− > 0	NaMt (4) 50/50 (7) Na/CaMt	0.13 (4) 0.13 (7)	0.10(4) 0.35 (7)	3.23 (4) 3.17 (7)	(6.5−) [2]
4/7 Simul.	$u_o = 1.9 \times 10^{-4}$	**2688/2016**	**E+R = 4.00**		**3.70**	**2.30**
2	c_{ion} = 17	NaMt	E+R = 3.79		6.21	0
	$u_o = 1.9 \times 10^{-4}$	**552**	**E+R = 2.83**		**6.86**	**0.30/0.27**
1	c_{ion} = 171	NaMt	2.04	0.53	7.30	< 0.2
	$u_o = 2.0 \times 10^{-4}$	**888**	**E+R = 2.98**		**7.03**	**0/0**

[1] The entire duration of tests 4 and 7 was 2688 hrs. Deionised water was introduced after 2016 hrs.

[2] The simulated results give information up to the time when DI is introduced whereas the experiments report all eroded mass up to the end of the experiment. By far the largest erosion takes place when DI is injected.

It can be seen in Table A2.A-1 that the prediction with model variant *a* is very poor. Variant *b* gives somewhat better results for the cases with deionised water but the predictions are still far from satisfactory.

The results using variant *c* with the adjustable empirical parameter $\phi_{R,f}$ are presented in Table A2.A-2.

Table A2.A-2. Fate of smectite in the experiments. E+R means that the sum of Extruded and Retained mass is reported. Results for model variant c with $\phi_{R,f}$ = 0.010/0.015.

Expt. #	Na+ concentration in water, mM, and u_o m/s	Extruded mass, g	Retained mass, g	Residual mass, g	Eroded mass, g
3 Meas.	DI	E+R = 0.68		4.61	4.7
3 Simul.	$u_o = 1.9 \times 10^{-4}$	**E+R = 0.037/0.0**		**4.21/0.0**	**5.74/10.0**
5 Meas.	DI	0.91	0.75	4.9	3.4
5 Simul.	$u_o = 2.6 \times 10^{-5}$	**E+R = 0.57/0.18**		**5.77/4.95**	**3.65/4.86**
9 Meas.	DI	E+R = 1.08		5.28	3.6
9 Simul.	$u_o = 3.3 \times 10^{-5}$	**E+R = 0.57/0.19**		**6.15/5.39**	**4.41/3.28**
6 Meas.	0.83= GW	1.31	0.57	5.74	2.4
6 Simul.	$u_o = 6.2 \times 10^{-6}$	**E+R = 3.04/1.76**		**6.35/6.05**	**0.59/2.18**
10 Meas.	1.66 = 2GW	1.28	0.51	6.66	1.5
10 Simul.	$u_o = 5.6 \times 10^{-6}$	**E+R = 4.08/2.87**		**5.72/5.53**	**0.18/1.58**
8 Meas.	4.0	1.99	0.38	6.74	0.9
8 Simul.	$u_o = 2.0 \times 10^{-4}$	**E+R = 3.22/2.67**		**6.40/6.30**	**0.38/1.02**
12 Meas.	c_{ion} = 2.1	No info.	No info.	No info.	3.37
12 Simul.	$u_o = 5.6 \times 10^{-6}$	**E+R = 3.13/0.85**		**6.37/5.70**	**0.49/3.44**
13 Meas.	c_{ion} = 4.3	No info.	No info.	No info.	2.51
13 Simul.	$u_o = 5.6 \times 10^{-6}$	**E+R = 3.17/2.77**		**6.46/6.39**	**0.35/0.83**
2 Meas.	NaMt	E+R = 3.79		6.21	0
2 Simul.	552	**E+R = 2.87/2.81**		**6.86/6.86**	**0.26/0.32**

It is seen in Table A2.A-2 that with $\phi_{R,f} = 0.010$ the loss by erosion agrees quite well with the experimental results for DI but gives only marginal improvement for sodium containing waters over model variants *a* and *b*. With $\phi_{R,f} = 0.015$ the agreement is fair to good for all cases except for experiment 3 where total loss of the source is very over-predicted.

Appendix 3

Release and sedimentation of smectite agglomerates from bentonite gel/sol

Summary

In a number of observations it has been seen that smectite agglomerates are released by gravity from expanding bentonite gel/sols. In waste repositories in fractured rocks sub-vertical fractures that intersect deposition holes for canister with nuclear waste may loose bentonite that surrounds and protects the waste form and hinders and/or slows down the release of contaminants such as radionuclides. A number of such observations and experiments are shortly described. Some important release mechanisms are discussed. It has not been possible to quantify some of the important intertwined release mechanisms for the purposes of devising a predictive model for the possible rate of loss of smectite. Instead by modelling the rate of transport of the released smectite agglomerates in fractures, an upper bound of the loss of smectite can be defined, as there cannot be a larger loss from the source than what can be transported away in the fractures. It is found that the maximum rate of loss of smectite caused by gravity effects is comparable to both the loss caused by shearing away agglomerated by the friction force of the seeping water at high velocities as well as by individual smectite particle diffusion into seeping water under conditions in fractured granitic rocks typical for nuclear waste repositories.

A3.1 Introduction and background

In the KBS-3 design of a repository for spent nuclear fuel the waste is contained in a copper canisters about 5 m long and 1.05 m diameter. The canisters are emplaced in vertical boreholes 1.85 m diameter and about 8 m deep at 500 m depth in granitic rock. The canisters are surrounded by a compacted bentonite buffer, which, when wetted by natural groundwater, swells strongly. The buffer protects the copper canister from mechanical movement of the rock and hinders water seeping into fractures from flowing past the canister. Corrosive substances in the water can only slowly reach the canister by diffusion through the buffer. Should any canister be breached the buffer also acts as a diffusion barrier for any leaking radionuclides (SKB 2011)

The strong swelling of the buffer will cause some buffer to slowly expand into any open fractures that intersect the deposition hole. Over the very long times of interest, 10 000 years, and more, a part of the buffer mass can have penetrated into the fractures which leads to loss of swelling pressure. Should larger aperture fractures with high water seepage rates intersect the deposition hole the smectite in the bentonite buffer can be carried away from the surface of the bentonite gel. At low salinities in the water this could lead to an increase of the loss of buffer in the deposition hole. This has been discussed and quantified in previous studies (Neretnieks et al. 2009, Moreno et al. 2010).

There is another mechanism that can further increase the rate of loss of smectite, which has been observed but has not yet been addressed in more detail. Jansson (2009) and Neretnieks (2009) observed that bentonite gel that swells in downward sloping fractures could release agglomerates of clay pulled down by gravity into low salinity water. Lately Schatz et al. (2013) and Schatz and Akhanoba (2015) made similar observations. The loss by this mechanism is clearly visible by the eye and it is asked weather this loss could further increase the loss from a deposition hole. We discuss the gravity effect and try to quantify the rate of loss caused by sedimentation of agglomerates. The reader of Appendix 3 should be aware of the sparseness of quantitative information on smectite floc formation, their properties as well as means to quantify many of the mechanisms and processes that determine the release rate of flocs. Some of the mechanisms that we deem to be of importance are discussed qualitatively and speculatively, however. Due to these difficulties we instead quantify an upper bound of the smectite loss by floc formation due to gravity effects. This is done by modelling how flocs are transported in fractures by gravity using established models for sedimentation of flocs and flow of fluids in narrow fractures.

A3.2 Some experiments and observations

Jansson (2009) reported some tests where gravity effects were investigated. This is also partly reported in Neretnieks et al. (2009), from which following excerpt is taken.

"Some simple tests were made where a small amount of clay (0.2 g) was put into the bottom of test tubes. 10 ml deionised water was poured onto the clay, which was allowed to swell and expand in the water giving a volume fraction of smectite of 0.7 %. A thin very fine filter with nominal hole-size of 10 μm was fastened in the tube at the top of the gel/sol. The tubes were then filled to the rim with water with different compositions. After one day the tube was turned upside-down. The response was easy to observe visually within 5 minutes. Either the clay dispersed and started to fall through the net or else it stayed above the net. Some tubes where the clay stayed above the net were left for 1 month (for instance untreated MX-80 in deionised water) without anything happening."

Untreated MX-80 bentonite with remaining detritus material did not disperse in limited volumes of deionised water. However, when the accessory minerals were removed from MX-80 bentonite by washing twice, centrifuging and collecting the top fraction, the treated clay fell through the net into deionised water. At least two reasons for this difference were identified. The detritus material could have formed a mechanical filter and/or the gypsum in the detritus material dissolved to raise the calcium concentration above the CCC when the gel is cohesive and does not release particles

The tests with the ion exchanged and purified materials were used to determine the lowest calcium concentration needed to keep homoionic sodium smectite from dispersing. According to the tests performed, a calcium concentration of about 1 mM is needed to stop the particles from penetrating the filter. This is in agreement with observations of CCC of Ca as the dominating cation in water. It should be noted that the notion of a CCC is not well defined. For Na exchanged clay contacted with calcium containing water, ion exchange will play a role, as sodium in the smectite will exchange for calcium in the solution and then sodium would be CCC-determining ion, at least partly.

Figure A3-1 (Figure 3.8 in Neretnieks et al. 2009) shows how the clay particles (rapidly) penetrate through the filter and sediment downwards in the tube. This phenomenon was observed for Na-exchanged smectite in waters below the CCC. In these experiments, the amount expressed as charge equivalent of ion exchange sites was about the same as the total amount of calcium in the added water with 2 mM. This implies that even if most of the calcium enters the exchange sites there still is about half the calcium concentration remaining in the water.

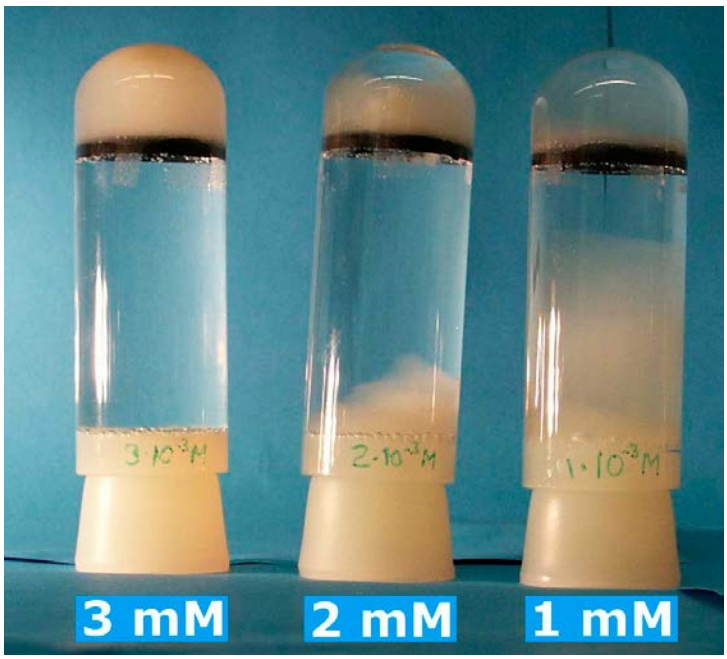

Figure A3-1. *Determination of lowest calcium concentration needed to keep homoionic sodium smectite from dispersing.*

Tests with 0.02 g of smectite were also performed. Then the smectite will have more than 90 % calcium in the exchange sites. (See Chapter 7 in Neretnieks et al. (2009) where ion exchange equilibria are discussed). The concentration at which the smectite no longer could pass the net was again about 2 mM.

When starting with fully Ca exchanged clay, no particles were released even in very low ionic strength waters. This partly supports theories stating that calcium rich smectite particles will tend to stick strongly and closely together. The experimental conditions thus influence the gel properties and it must be expected that calcium dominated clay will behave differently if it is expanding or if it is sedimenting. Some possible reasons for such behaviour are discussed in Chapter 7 of Neretnieks et al. (2009).

It should be noted that the gel particles (flocs) sediment much faster than individual smectite sheets could do it, see Section 6.3 in Neretnieks et al. (2009). Similar observations are reported by Birgersson et al. (2009). This indicates that even at ionic strengths below the CCC the smectite particles can agglomerate to form flocs that sediment much more rapidly than individual smectite sheets can do. At the same time such flocs can easily break up to pass very fine holes and recombine after passage. The underlying mechanisms are not understood sufficiently to quantify the process.

Neretnieks (2009) made a series of scoping experiments where smectite gels in about one mm wide slits between plane glass sheets were subjected to gravity. It was found that natural MX-80 bentonite as well as MX-80 washed of its gypsum content and homoionic calcium smectite could release clay flocs into initially deionised water. The water after some time in contact with the clay had acquired Na and Ca concentrations ranging form 0.42 to 2.9 and from 0.02 to 1.02 mM respectively.

Figure A3-2 shows how gel fingers form at the gel/water boundary under influence of gravity. The gel was formed from untreated MX-80 in distilled water. After the experiment the water contained the following main cat-ions: [Na] = 2.91 mM, [Ca] = 0.15 mM, [Mg] = 0.09 mM.

Figure A3-3 shows an enlargement of the gel. The small dark spots are deemed to be detritus particles. One aggregate about 1.0 mm in size has just been released and moves slowly downward.

Figure A3-4 shows a detail of the hanging gel. In both Figures A3-3 and A3-4 it can be seen that the gel/ water interface is quite distinct in most places but in Figure A3-3 right hand lower corner a diffuse velvety protuberance without detritus particles is seen. In Figure A3-4, which has a black background a number of much smaller particles are seen. These seemed to be nearly immobile and are probably tiny specs that adhered to the *dry* glass surfaces of the slit when some bentonite powder was pored into the slit prior to filling it with water.

Figure A3-2. *Enlargement of the upside down turned slit 24 hours later. Gel is slowly pulled downward by gravity. Small gel blobs are released and very slowly move downward. The whole picture is about 4 cm high.*

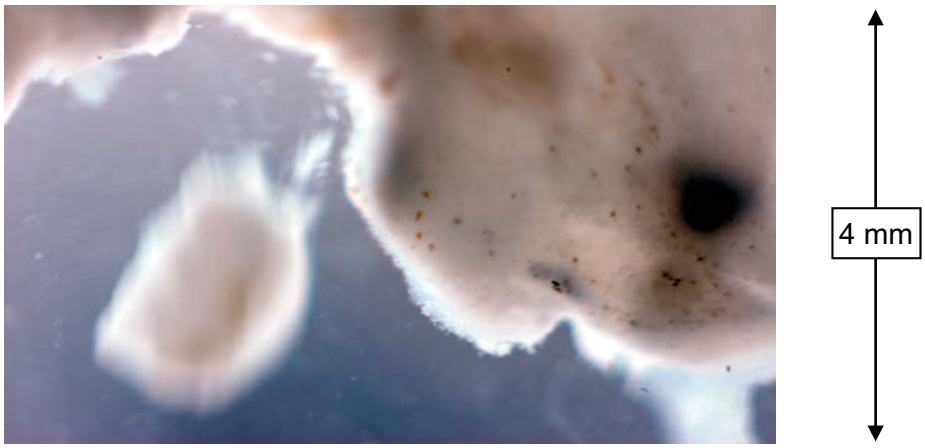

Figure A3-3. *An enlarged detail of the hanging gel. The whole picture is 4 mm high. Large and small black particles are clearly seen.*

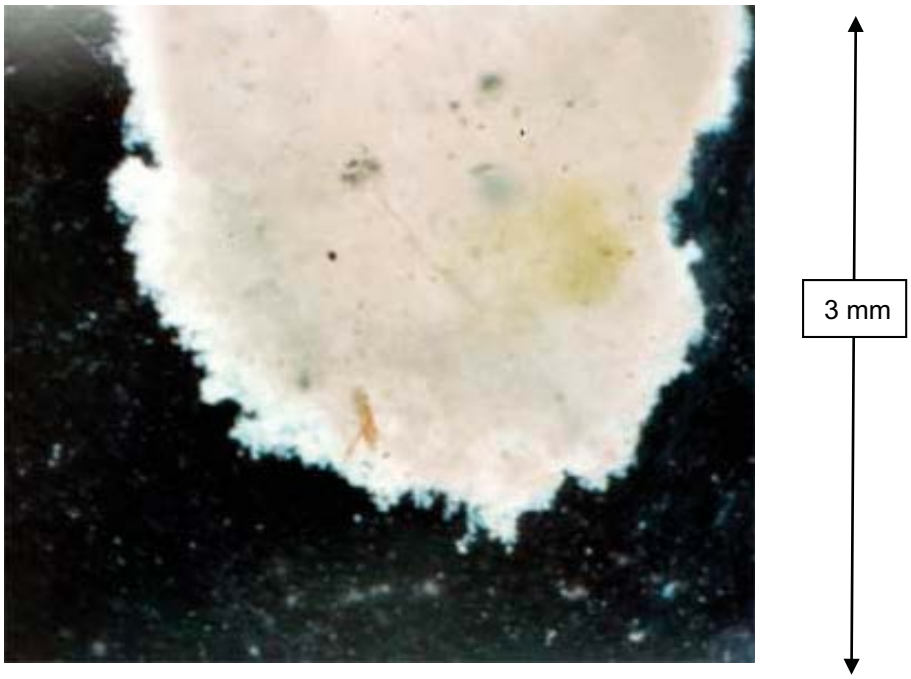

Figure A3-4. *An enlarged detail of the hanging gel. The whole picture is 3 mm high. Small dark particles are clearly identifiable.*

Figure A3-5 shows the release of wormlike agglomerates from a gel formed by the deionised-water washed MX-80 that dissolved the calcium sulphate and increased the relative content of detritus in the subsequently dried and ground bentonite.

Figure A3-6 shows a detail of the wormlike agglomerate. The accumulation of detritus on the upper left hand side of the agglomerate is clearly seen. Expansion was from NW to SE direction in this picture. After the experiment the water contained the following main cat-ions: [Na] = 0.42 mM. [Ca] = 0.02 mM, [Mg] = 0.12 mM.

Figure A3-7 shows an enlargement of a section of the still hanging gel with the gel/water interface. The accumulated dense rim of detritus has fallen away and the remaining detritus particles remain more ”evenly” distributed in the gel.

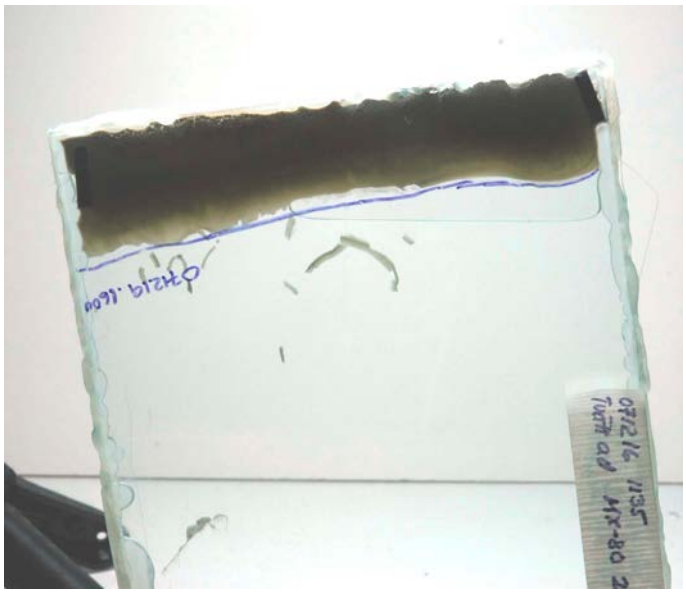

Figure A3-5. *Falling of worm like blobs hours after turning the slit upside down.*

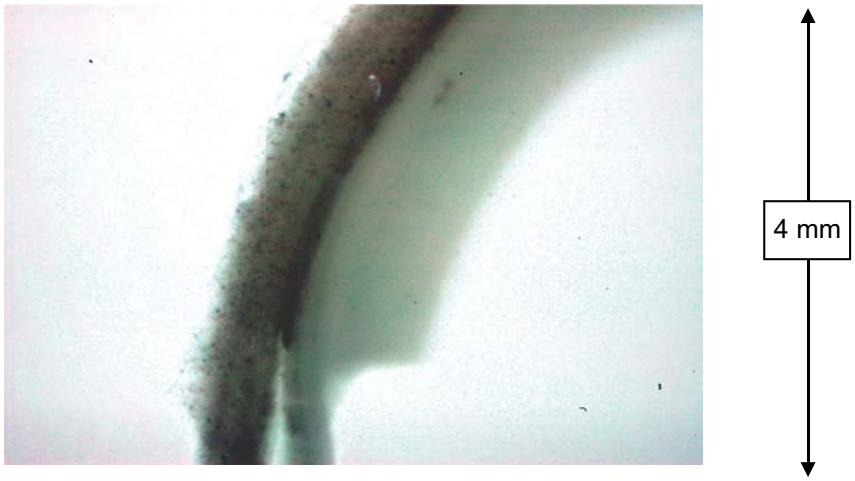

Figure A3-6. *Enlargement of worm like blob. Picture shows a 4 mm high section.*

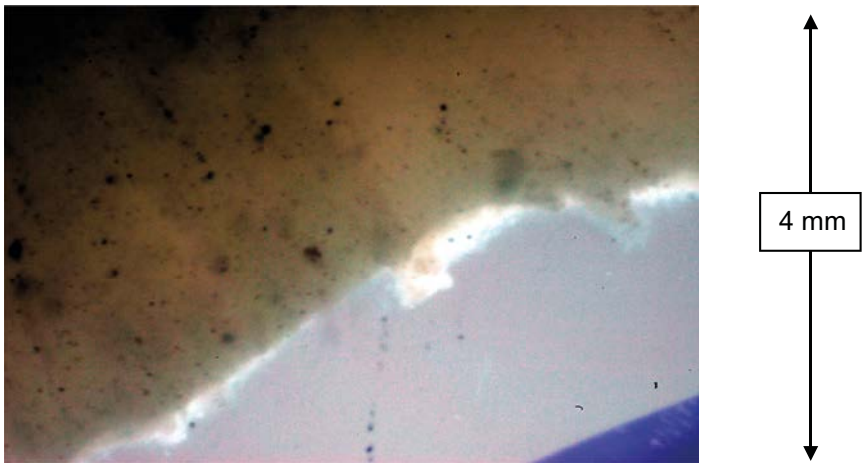

Figure A3-7. *Enlargement of a gel/water interface. Picture shows a 4 mm high section. Detritus material is clearly seen.*

Schatz et al. (2013) performed a number of experiments in which cylindrical compacted smectite tablets were allowed to expand into a water-filled slit between two transparent plastic plates. The smectite used was washed of detritus particles and was homoionic with either Na or Ca. The water in the 1 mm aperture slit flowed slowly and could erode the expanding gel. The slit was horizontal during the expansion. The expanded gel was essentially symmetrically radial during the entire expansion phase even when there was considerable erosion from the gel/water interface. The experiments were run for many hundreds of hours, some for up to 3 000 hours. De-ionized water and water with 0.83, 1.66, 4.0, 17, and 171 mM NaCl were used. At the end of some of the tests the equipment was turned 90° to see how gravity would influence the expanded gel. For the 171 and 17 mM waters the expanded gel did not change shape or release any particles even after a week or more. At 4 mM some limited sedimentation could be seen. In De-ionised water streams of small particles could be seen to be released. These rapidly sedimented. In 0.83 mM water release and sedimentation of agglomerates could also be seen.

Figure A3-8 shows the release of streams of particles in a vertical fracture. It is also seen that somewhat below the source the particles seem to form a denser phase, from which again streams of particles are released.

In some of the experiments it could be clearly seen that downstream of the expanded circular gel a several mm wide region was entirely transparent but then agglomerates formed and flowed downstream, as shown in Figure A3-9. This suggests that the invisible individual smectite particles, which are smaller than the wavelength of visible light are released from the rim need time to form large enough agglomerates to become visible.

A Canadian study by Vilks and Miller (2010) found similar effects caused by gravity.

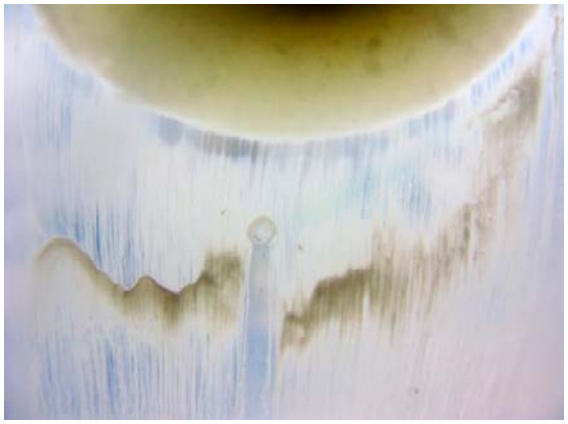

Figure A3-8. *Close-up picture of sedimenting agglomerates in de-ionised water. The cylindrical region is 2 cm in diameter. Figure 59 in Schatz et al. (2013).*

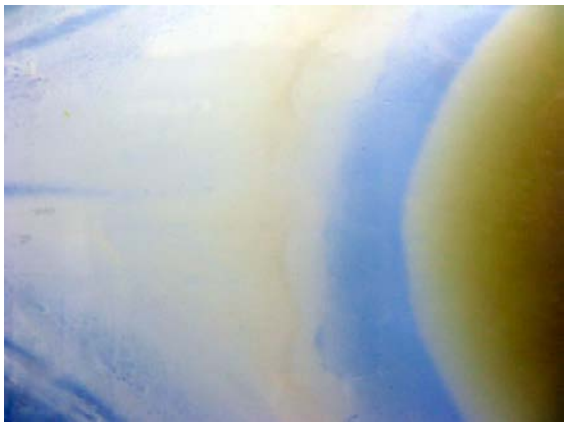

Figure A3-9. *Close-up picture of down-stream region from a 50/50 mix of Ca and Na smectite in de-ionised water. Flow is from right to left. Figure 45 in Schatz et al. (2013).*

A3.3 Interpretation of the experiments and conceptualisation of processes

The experiments and observations suggest that smectite in waters with ion concentrations below CCC can form flocs with low volume fraction of smectite. The flocs have a somewhat higher density than water and can be released from other flocs in a downward facing gravity field. The flocs are flexible and can penetrate narrow passages such as the openings in fine nets and reform after passage to larger flocs, which have more favourable surface to volume ratio for sedimentation. The flocs are clearly visible to the naked eye and range in size from a fraction of mm to several mm. In narrow slits they tend to form coin-like flocs but irregular shapes when they cannot any more find room in the slit aperture. Also in slits as narrow as one mm they sediment at a velocity that can be seen by the eye.

The following conceptual picture emerges. The smectite gel expands as described by the dynamic model and reaches a volume fraction that is near the co-volume fraction of one where typically ϕ is around 0.01 (Neretnieks et al. 2009). Up to this point the sheets are arranged in stacks with sheets in parallel. At this point the smectite sheets begin to have room to rotate without touching each other. The particles now can form a sol in which they diffuse further and further out into the water, unless restrained by gravity as it would be in an upward migration. Horizontally the sol would expand forever but upward the diffusion is restrained by gravity and a steady state concentration profile forms. This is typically seen in experiments in test tubes that stand vertically. Under some conditions the particles in the sol region can agglomerate to form a space filling complex 3D structure where edge to face bridges form. This may happen when the electrical charge at the edges is opposite to that of the flat faces of the particles. The faces of smectite particles have a negative charge due to isomorphic substitution of silicon for aluminium atoms and aluminium for ferrous iron or magnesium atoms in the smectite sheet, which can be visualised as a sandwich formed of two silicon oxide sheets with one aluminium oxide sheet between. On the faces water is in contact with the silicon oxide but at the edges water is also in contact with aluminium oxide. The aluminium oxide can be hydrated and can by hydrolysis be positively or negatively charged or neutral depending on the pH of the water and on which cations are present in the water. The charge of the face of the particle will be constantly negative over a very wide range of pH because the charge is dominated by the permanent charge due to the isomorphic substitution. When the edge charge is positive there will be face to edge attraction and agglomerates may form. There is evidence that the edges can have positive charges in the pH regions expected to exist, or form deep in crystalline rocks. See e.g. discussion in Birgersson et al. (2009, Section 5.4). However, it is still not clear why this happens because there are theoretical reasons that the negative charge of the surface should "spill over" the edge (Secor and Radke 1985).

The flocs are flexible and can be sheared, deformed by compression, dilated, pulled apart to form smaller flocs or grow and become larger. The agglomerated smectite, seen as a body or a fluid, has a somewhat higher density than water. We visualise the agglomerated mass to behave like a fluid, and call it "agglomerate fluid", AF, which is slightly denser than water. When AF is subject to a downward pulling gravity as if it were poured on top of the less dense water the system will become unstable. This is in analogy to the Rayleigh–Taylor instability. See e.g. en.wikipedia.org/wiki/Rayleigh–Taylor-instability. Streaks of the denser fluid will drop down into the lighter fluid in complex random patterns just as observed in the examples shown above.

We wish to explore how this conceptual picture can be used to estimate the rate of release of smectite from a compacted water saturated smectite mass (source) intersected by a vertical, water filled fracture. We neglect the presence of any detritus material in the smectite and consider only pure smectite clay. We consider a case where the pore water as well as the water in the fracture has an ion concentration below the CCC. The pH and other conditions are such that edge to face attraction may take place. The smectite expands in the fracture driven by the strong repulsive forces between the particles. At some distance r_R, from the centre of the source, the volume fraction of the gel/sol has reached the co-volume fraction at which the smectite particles can rotate sufficiently for edges to hit faces. Some smectite particles diffuse away as sol particles into the water but other agglomerate. The AF is lost by the Rayleigh–Taylor mechanism, which releases "streams" of different forms and mass into the fracture where they sediment downward. The streams can also break up to flocs. The small flocs sediment downwards with a velocity set by the terminal velocity of sphere-like particles in free water, some unimpeded by other flocs, some influenced by the presence of other flocs. The flocs can grow when joining other flocs and eventually may become as large as the fracture aperture.

They will then be influenced by not only the immediate water surrounding them but also by "wall friction". Small flocs sediment slower than large in free water because they have larger surface to volume ratios. Flocs that fill the space between the walls of the slit will be retarded also because of friction against the walls. One can speculate that the formation of the slower moving blobs that eventually touch the wall could be the cause of the secondary AF below the circular source in Figure A3-8. This secondary AF in turn, having a higher density than the water below, again starts to release small streams of blobs.

The rate of loss of smectite from the source will be set by the width of the horizontal extent of the AF and the smallest of the two rates below.

- Rate of agglomeration to flocs.
- Rate of release/sedimentation of flocs.

One can also speculate about the formation rate of flocs and AF as seen in Figure A3-9 where a transparent region is visible downstream (to the left) of the source. In the transparent region the colloidal size smectite particles, being smaller that the wavelength of visible light, makes the sol transparent. Further downstream agglomeration has made the particles larger and the fluid becomes opaque.

Another possible way of formation of AF may be that the original stacks of smectite sheets that make up the compacted smectite partly retain the stack configuration also when the gel has expanded considerably. The 1 nm thick 100–300 nm size coin-like smectite sheets are aligned in stacks in the compacted clay. The distance between the sheets at high compaction is less than 1 nm. There are many tens of sheets in each stack. The swollen expanded stacks then make up the AF. There is in this case no need to consider a rate of agglomerate formation, as these are the remainders of the original stacks. The volume fraction of smectite in such agglomerates can be larger or smaller than in "house of cards like" agglomerates with edge to face contact. It may be reminded that the ionic strength was assumed to be below the CCC, which implies that the stacks would expand forever if not restrained by downward facing gravity or by the formation of some 3D volume filling complex structure. There are observations that suggest that there are other arrangements that can form 3D coherent structures, see Birgersson et al. (2009, Section 5.4). Figure A3-10 shows the two different forms of agglomerates.

The width of the horizontal extent of the AF will in turn depend on how far horizontally the expansion of the gel reaches from the deposition hole before the AF is lost by sedimentation.

Figure A3-11 illustrates these processes. The source of compacted smectite expands out into the vertical fracture. In locations where the smectite particles are sufficiently distant from each other to be able to rotate they form three-dimensional agglomerates in water and the "suspension" behaves like a fluid. AF is denser than water and as it lies above the pure water below, agglomerates are released and sediment downward. The larger flocs, which have a smaller surface to mass ratio than the smaller, fall faster, catch up with and attach to the smaller flocs to form larger agglomerates, which move faster, etc. When the particles grow they fill out the aperture and become more coin-like to find room in the fracture. These also experience friction against the walls of the fracture and slow down.

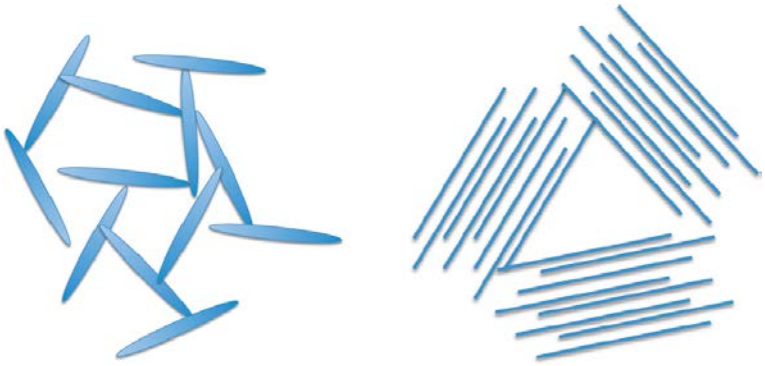

Figure A3-10. *Two different forms of agglomerates in the AF. At left, "house of cards" structure, at right, still expanding stacks.*

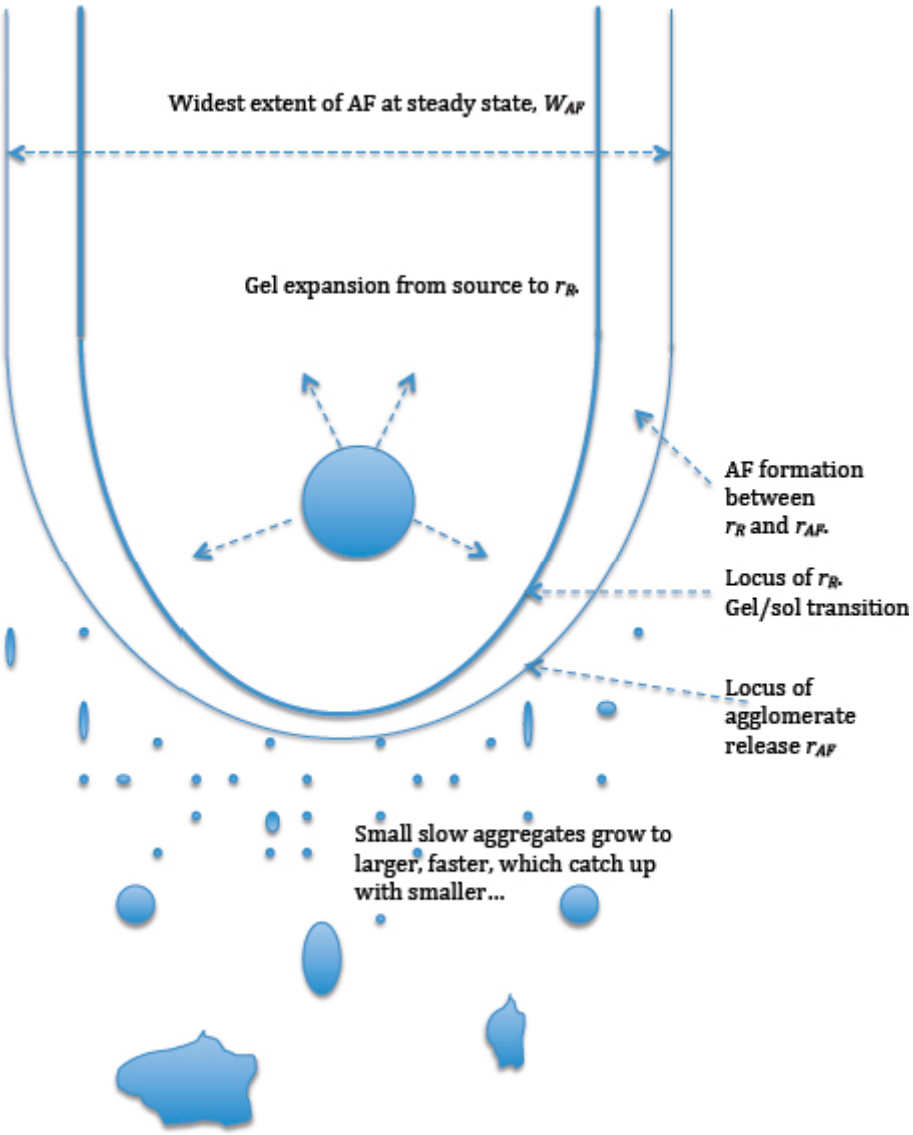

Figure A3-11. *Smectite gel expands in all directions in a vertical fracture and releases agglomerates, which sediment from a boundary at* r_{AF}.

The horizontal distance of $r_{AF}(x,y)$ stabilises at a locus-curve and eventually attains a maximum width W_{AF}. For lack of better information and for simplification in the subsequent modelling, the release rate of agglomerates downward is assumed to be constant per horizontal distance of the AF/water interface when steady state, SS, is reached. The overall rate of loss at SS of smectite from the source depends in a complex fashion on several of the local rates of gel expansion, agglomerate formation, initial rate of release of AF at the r_{AF} boundary and of what subsequently happens to the agglomerates that sediment down in the fracture. Some of the interrelated mechanisms are described below.

Starting from what happens in the lower regions of the fracture it is clear that if the mass rate of vertical transport of the grown larger agglomerates is faster than the release of the smaller particles at r_{AF} there will be no densification of the AF in the fracture below the source. If on the other hand the opposite were to happen then eventually the fracture would fill with the slowly expanding AF and might fill up all the way to r_{AF}, hindering release of new small agglomerates. The loss of smectite would then be set by the movement rate of the AF in the lower region of the fracture. However, if this happens it will lead to a horizontal growth of the AF and eventually stabilize at a maximum width W_{AF}.

A further complication in trying to quantitatively model these processes is that the rate of loss from the source (clay-filled deposition hole) is strongly influenced by distance to the rim r_R, which is unknown a-priory. The detailed, quantitative mechanisms and rates of AF formation as well as the quantitative mechanisms and rates of AF release and further fate in the fracture are not available. Therefore we approach the question of maximum release in a simplified way and try at least to do some bounding estimates of the rate of transport of AF in a sub-vertical slit.

A3.4 Mathematical model and some simulations of sedimentation loss

The task is approached by modelling on the one hand how fast particles smaller than the slit aperture sediment and on the other hand how fast larger agglomerates, when wall friction comes to play a role, sediment.

A3.4.1 Small spherical agglomerates

The terminal velocity of spheres v_{sph}, *when unimpeded by other particles* in the dilute fluid, is given by Stokes law (Bird et al. 2002, p 61)

$$v_{sph} = \frac{2}{9\mu_W} r_{sph}^2 \left(\varrho_{sph} - \varrho_W\right) g \qquad \text{(A3-1)}$$

r_{sph} is the radius, ϱ_{sph} the density of the sphere, ϱ_w the density of water, g the gravitation constant and μ_W the viscosity of water. ϱ_{sph} , is given by

$$\varrho_{sph} = \phi\, \varrho_{smec} + (1 - \phi)\, \varrho_w \qquad \text{(A3-2)}$$

Where ϕ is the volume fraction of smectite in the agglomerate. The density of smectite ϱ_{smec} = 2.7×10^3 kg/m^3. The volume fraction at which colloidal particles are released and could form agglomerates is expected to be around 1 %. This gives an agglomerate density (sphere) ϱ_{sph} = 1.017×10^3 kg/m^3. ϱ_{sph}–ϱ_W = 17 kg/m^3 and a smectite concentration in the agglomerate of $\phi\, \varrho_{smec}$ = 27 kg/m^3. The viscosity of water is 10^{-3} Pa × s and g = 9.8 m/s^2.

Neither the rate of release, the size nor the number of flocs per interfacial area of the AF/water interface is known. We need to find some way of estimating these quantities or at least to see how they affect the total rate of loss from the source. We define an entity that states how many particles are regularly released per interfacial area of the AF/water interface, the surface density i.e., number of spots per m^2 from which release occurs. For visualisation purposes the spots are arranged on a square grid with a distance $n_{rS,h} \times r_{sph}$ between their centres. $n_{rS,h}$ is the number of radii between the centres of the spots in the horizontal direction. In addition an entity that describes the frequency of release in terms of how far the previous agglomerate must have moved before a new one is released from that spot, expressed as number of radii of the, assumed, spherical floc $n_{rS,v} \times r_{sph}$. Similarly $n_{rS,v}$ defines the vertical distance between spot centres.

The number density of the spheres then is

$$\varrho_{\#} = \frac{1}{r_{sph}^3 n_{rS,v}\, n_{rS,h}^2} \qquad \text{(A3-3)}$$

The smallest numbers the n's can have is 2 when the particles would be in contact with each other in all directions.

An upper bound of the release rate of spherical particles into a fracture aperture δ is by spheres with a radius $r_{sph.max}$ = $\delta/2$ and new sphere released when the previous has fallen by one sphere diameter δ. Then the largest $\varrho_{\#,max} = \frac{1}{\delta^3}$.

The number flux of spheres is

$$J_{\#} = \varrho_{\#} v_{sph} \qquad \text{(A3-4)}$$

The mass flux of smectite by the spheres is

$$J_{smec} = J_{\#}\frac{4}{3}\pi r_{sph}^3 \phi\, \varrho_{smec} = \varrho_{\#} v_{sph}\, \frac{4}{3}\pi r_{sph}^3 \phi\, \varrho_{smec} \quad \text{(A3-5)}$$

For $r_{sph} = r_{sph.max} = \delta/2$

$$J_{smec} = \frac{\pi\delta^2}{108\mu_W}\left(\varrho_{sph} - \varrho_W\right) g \phi \varrho_{smec} \quad \text{(A3-6)}$$

The maximum rate of mass loss N_{smec} from a source that has expanded the gel/sol to a width W_{AF} is

$$N_{smec} = J_{sph} W_{AF} \delta = \frac{\pi\delta^3}{108\mu_W}\left(\varrho_{sph} - \varrho_W\right) g \phi \varrho_{smec} W_{AF} \quad \text{(A3-7)}$$

It is acknowledged that Stokes law does not account for the influence of nearby spheres on the velocity and that the above relations are poorly valid. In the section below we describe the movement of flocs, which can be conceived as agglomerates of smaller particles.

A3.4.2 Large coin-like agglomerates

Agglomerates larger than a sphere that would find room in the aperture of the slit will have a coin-like form. Friction forces against the water around the edges of the "coin" and friction against the wall of the slit will restrain the sedimentation velocity. For large agglomerates the wall friction will dominate over the friction against water at the outer side of the agglomerate. The viscosity of gel/sol at different volume fractions and ionic strengths has been measured. It is found that the viscosity increases from that of water up to about ten times that of water when the volume fraction increases from zero to about 1 %. Above 1 % the viscosity becomes very high (Liu 2011). It can be likened to a Bingham fluid/body, which will need a minimum shear force to start moving. When $\phi >$ ≈ 0.01 gravity is not strong enough to mobilize the Bingham fluid. In the transition region between gel and sol we conceive that AF may behave similarly as the gel/sol at 1 % volume fraction. The sedimentation velocity of a coin-like agglomerate with cross section area A_{agg} in a slit is obtained by a force balance between the gravity force and the wall friction neglecting the friction against the water surrounding the edge of the "coin".

We estimate the "coin" settling velocity by comparison with a fluid flowing in a vertical, narrow aperture slit, wide enough to be able to neglect any friction effects against the boundaries of the slit. The friction against the walls counteracts the gravity and a steady state flow velocity will be reached. In analogy our "coin" made up of the viscous fluid with viscosity μ_{agg}, the coin being large enough to be able to neglect friction between water and "coin", is subject to the gravity-buoyance force $(\varrho_{coin} - \varrho_W)g$ and restrained by the friction against the walls. The velocity of the "coin" is then obtained by the same expression as for any other fluid under the same circumstances (Bird et al. 2002, p 63)

$$v_{coin} = \frac{1}{12\mu_{agg}}\delta^2(\varrho_{coin} - \varrho_W)g \quad \text{(A3-8)}$$

It may be noted that the velocity is independent of the coin size. This is because the mass of the "coin" grows in the same way as the size of area in contact with surface where friction acts to retrain the movement.

A comparison can made with the settling velocity of spheres in Equation (A3-9)

$$v_{sph} = \frac{2}{9\mu_W}\delta^2\left(\frac{r_{sph}^2}{\delta^2}\right)\left(\varrho_{sph} - \varrho_W\right)g \quad \text{(A3-9)}$$

Considering that μ_{agg} is about 10 times larger than μ_W for "coins" with ≈ 1 % smectite we find that the velocities are comparable when $\frac{r_{sph}^2}{\delta^2}$ is about 9/240, which is when the *diameter* of the spherical agglomerate is about 40 % of the slit aperture. Then wall effects for the settling sphere can be expected to start to slow down the spheres. Thus when the small agglomerates join to form larger agglomerates the sedimentation velocity will increase up to this point but then become constant when the agglomerates start to touch the walls.

Figure A3-12 shows the settling velocity of coin-like agglomerates as well as for spheres as function of fracture aperture. The viscosity of the AF is taken to be 10 times that of water, which then gives practically the same velocity for both agglomerate shapes.

The velocity is given in m/day. For a 1 mm aperture the velocity is about 10 m/day and is of the order(s) of magnitude that are observed in the experiments with 1mm fractures and in free water discussed above.

The rate of mass loss for a 1.85 m wide source with 0.1 mm aperture fracture is shown in Figure A3-13 as function of agglomerate size using an agglomerate density of 1 017 kg/m^3 of which 27 kg/m^3 is smectite for two different particle number density factors *fr*. We use *fr* to denote the fraction of the maximum particle density that AF has, so . $\varrho_{\#} = fr\, \varrho_{\#,max}$

As seen, the results are very sensitive to particle size and number density. The vertical dashed line indicates at what particle size the sedimentation rate would be larger if the small particles agglomerated to large and sediment as "coins" subject to wall friction. Then the velocity becomes independent of coin diameter. The loss will be 0.08 and 0.008 kg smectite/m and year for *fr* equal to 0.1 and 0.01 respectively. For a 1 mm fracture the loss would be 100 times larger. If *fr* is near 1 the agglomerate would seem to fill the fracture and sediment as a wide "sheet". This has been observed in a 0.1 mm aperture fracture (Schatz and Akhanoba 2015).

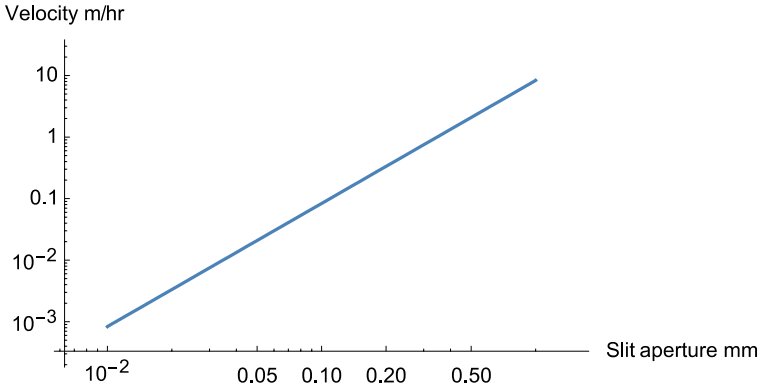

Figure A3-12. *Sedimentation velocity of large spheres, $d_{sph} = 0.4 \times \delta$ and large coin-like agglomerates with 1 % by volume smectite in a vertical slit vs. slit aperture.*

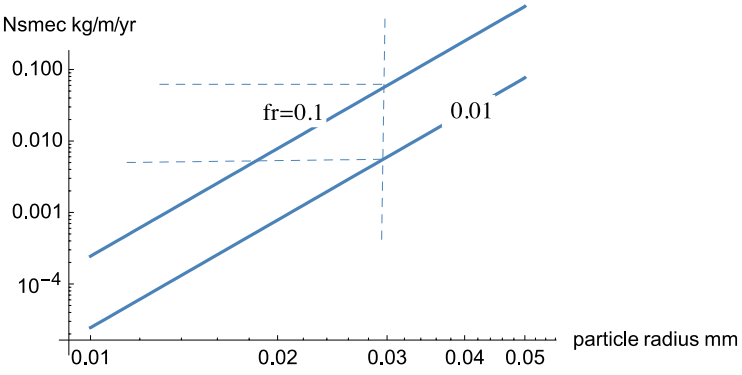

Figure A3-13. *Rate of mass loss vs. particle radius for two different fr-factors in a 0.1 mm aperture fracture.*

A3.5 Shearing off of agglomerates from gel interface

In this section we explore how the water seeping past the gel/sol interface could shear off particles from the expanding gel surface. The considered chemical conditions are such that the gel/sol is expansive at all volume fractions. The gel/sol viscosity increases very sharply as the volume fraction increases and the gel/sol does not *flow* as a fluid under the influence of typical hydraulic gradients expected at repository conditions when the volume fraction ϕ_R is above around 0.01. However, the gel is not cohesive as the vdW forces are always smaller than the repulsive DDL forces.

If the shear force on a small protuberance, smaller than the slit aperture, on the gels surface such as can be seen in Figures A3-3 and A3-4 can shear it off and carry it downstream, its presence will not noticeably slow down the water flowrate. If the agglomerate is larger than the slit aperture it would not be sheared off because its much higher viscosity than water would prevent this. As the gel is expansive new protuberances form and are released to the water much like they are seen to do in a gravitation field as shown in Figure A3-8. The small particles agglomerate to larger ones some distance downstream as is seen in Figure A3-9. A comparison is now made between the shear force by seeping water and that due to gravity. Gravity force was shown earlier to release particles and if the shear force is of comparable magnitude it suggests that shearing could contribute to gel/sol release and even be a mechanism that may shadow what can be done by the smectite particle diffusion in our rim model.

The shear stress of the water on the walls of the slit is

$$\sigma = \eta_w \frac{du}{dy} \approx \eta_w \frac{u}{\delta/2} \tag{A3-10}$$

The same stress also acts on the gel/water interface because the gel is stationary. For illustration we use a cubic protuberance with edge length d_p. Neglecting the pressure difference over the cube compared to the friction force F_s on the five sides of the cube exposed to shear with area 5 d_p^2 (the sixth side is attached) the shear force is

$$F_s = \sigma\, 5d_p^2 = \eta_w \frac{u\,2}{\delta} 5d_p^2 \tag{A3-11}$$

In a gravity field the particle is pulled down by a force that is

$$F_g = d_p^3(\rho_{agg} - \rho_w)g \tag{A3-12}$$

Figure A3-14 shows the two forces as function of particle size in a 1 mm aperture slit for two different water velocities. The agglomerate or gel particle has a smectite volume fraction 0.01 for which ρ_{agg} = 1 017 kg/m^3. The forces are comparable for velocities around 10^{-5} m/s. For higher velocities shear forces are larger and for lower velocities they are smaller. The lower bound of the particle size in the figures is 0.2 micrometres or 200 nm, which is the size (diameter) of the thin smectite particles. These results suggest that the release of smectite particles and agglomerates can be caused by shearing at higher velocities, in addition to particle diffusion in the sol region. It can even be a dominating effect. It also may explain the clear region seen in Figure A3-9. If the released particles are individual smectite sheets these are smaller than the wavelengths of visible light and the water then is still clear nearest the gel boundary. In the "steep" velocity gradient in the seeping water these particles rotate and contact each other and may agglomerate. This is seen a few mm from the gel surface but still do not cause the water that carries, the now opaque, slurry downstream to become noticeably more viscous. Admittedly this is a speculation. See Figure A3-9.

The above described phenomena, together with the experimental evidence, suggest that water velocity may not be slowed down as it would be if the sol region consisted of individual smectite particles, which by the co-volume effect, increases the viscosity of the gel/sol considerably. Also the volume fraction at which the release of particles commences, ϕ_R, can be larger than if it is determined by the individual smectite particle diffusion. These factors combined can lead to considerably larger release rates to the water in the rim zone.

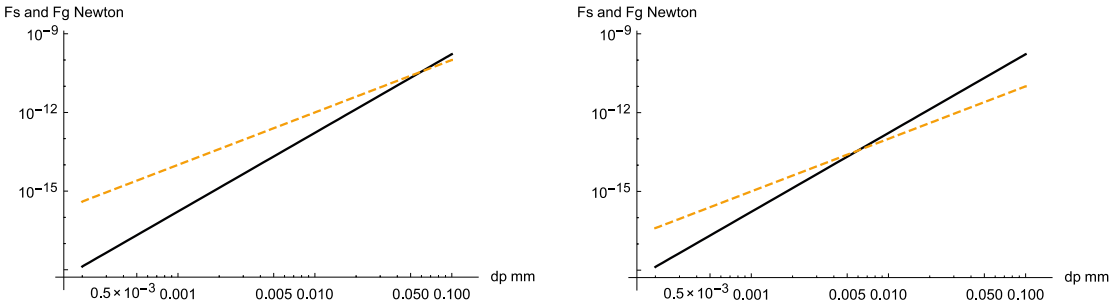

Figure A3-14. *Shear (dashed) and gravity (full) forces on particles with volume fraction 0.01 for a water velocity 10^{-4} m/s, left figure and 10^{-5} m/s, right figure.*

This is further underpinned by our modelling of Schatz et al. (2013) experiments where we found that when only smectite particle diffusion was considered, the release was underestimated by a factor 3-10. Invoking the above release mechanism with no viscosity increase of the water nearest the gel and adjusting the ϕ_R somewhat upward, the modelled and experimental rate of erosion and expansion of gel agreed quite well. However, it should be emphasized that we now have adjusted parameters in the original rim model, which is based on other mechanisms. It is therefore more a curve fitting exercise and not based on a model using independently determined parameter values, as is the case in our rim model. The above findings therefore cannot reliably be used for predictions under conditions that differ much from those in Schatz et al. (2013) experiments.

A3.6 Discussion and conclusions

For illustration purposes we make a very simple and crude estimation of the steady state loss due to sedimentation. This is done by comparing the width at which sedimentation loss is equal to the diameter of the expanding gel when steady state is reached.

The gel expansion can be modelled as a diffusion process. For a given distance to the rim r_R the steady state loss N_{SS} from a deposition hole can be approximated by (A3-13) (Appendix 1)

$$N_{SS} = D_{smec}\pi 2\, \varrho_{Smec}\delta \frac{\phi_i - \phi_R}{Ln[\frac{r_R}{r_i}]} \qquad \text{(A3-13)}$$

$D_{smec} = 10^{-9}$ m^2/s is the diffusion coefficient for the expanding gel (Neretnieks et al. 2009). ϱ_{Smec} is the smectite crystal density, $\phi_i = 0.5$ the volume fraction in the deposition hole with radius $r_i = 0.925$ m, and $\phi_R = 0.01$ is the volume fraction at the rim at radius r_R.

This can be compared to the sedimentation loss that would occur if $W_{AF} = 2r_R$ in Equation (A3-7). It is assumed that the small agglomerates have formed larger coin-like particles. The agglomerate density is taken to be the same as for the original spherical particles. At steady state the loss at the rim is equal to the loss from the deposition hole and

$$N_{PSS}(Eq.13) = N_{smec}(Eq.7) \qquad \text{(A3-14)}$$

Admittedly this is a rough approximation because (A3-13) describes radial expansion whereas (A3-14) describes linear transport. A plot of both expressions is shown in Figure A3-15 for aperture 0.1 mm as function of outer radius of the rim. They intersect at $r_R = 2.0$ m, for $fr = 0.01$. This means that the widest horizontal extent of the AF is 4.0 metres and that the SS loss is about 17 g/year in a 0.1 mm fracture. This is a crude estimate because when there is loss by sedimentation the expansion becomes asymmetric and not circular, as is the basis for (A3-13). For $fr = 0.1$ the radius is 1.07 m and the loss is about 150 g/year. In this case Equation (A3-13) is a very poor approximation for the loss at the rim. Nevertheless, the example shows that at high loss rates (large apertures) by sedimentation the width of the expansion will decrease and the locus at which sedimentation takes place approaches the diameter of the deposition hole. The width W_{AF} will be only somewhat larger than that of the deposition hole.

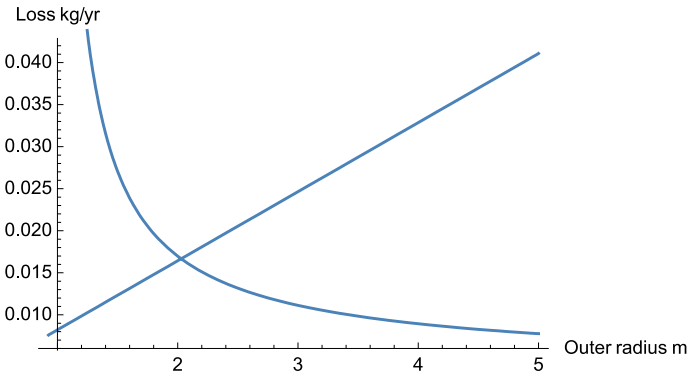

Figure A3-15. *Rate of loss from deposition hole N_{PSS} (curved line) and rate of loss by sedimentation N_{smec} (straight line) as function of the radius to the rim.*

Mean fracture apertures at repository depth are deemed to be less than 0.1 mm but their apertures vary. The sedimentation velocity is on the order of 10–100 m/year in a 0.1 mm aperture vertical fracture. Large fractures have an extent of 10–100 m or possibly more (Rhén et al. 2008). In such fractures the bottom would be reached in years. The transport can switch to other intersecting fractures in the fracture network unless they are horizontal. As the 0.1 mm fracture was taken to be one of the largest in the network it is likely that the network and the fracture would fill up and slow down or stop further loss from the source.

In conclusion: The smectite loss from a deposition hole by smectite agglomerates pulled by gravity is restrained by the rate of agglomerate transport in the fracture. In fractures smaller that 0.1 mm it is found to be less than some 10 to 100 grams per year from a deposition hole in a KBS-3 type repository that is intersected by a semi-vertical fracture. This is of the same order of magnitude as the loss by erosion in horizontal fractures (Appendix 1).

Shearing of agglomerates from the gel/water interface can contribute considerably to the release from the gel/water interface at very high seepage velocities. So far we have not succeeded in modelling this process quantitatively for use in a predictive model. However, as was found by comparing the shear force with the gravity force the release by shear is not expected to be larger than that caused by gravity.

The situation discussed considers purified smectites. These contain negligible amounts of larger non-smectite particles normally present in natural bentonites, which typically contain tens of percent of detritus material. It is expected that this material will be carried along by the expanding bentonite but will be released and left behind when the gel turns to sol. The detritus can then clog the narrower passages in the variable aperture fracture and it is expected that a filter will develop in the fracture that will prevent agglomerates or even individual smectite particles to pass. It was experimentally shown that a few mm thick detritus filter is sufficient to stop smectite transport (Richards and Neretnieks 2000). However this has as yet not been experimentally demonstrated to form in actual fractures.

A3.7 Acknowledgements

The research leading to these results has received funding from the European Atomic Energy Community's Seventh Framework Programme (FP7/2007-2011) under grant agreement n° 295487

Arkitektkopia AB, Bromma, 2017

SKB is tasked with managing Swedish nuclear and radioactive waste in a safe way.

skb.se